UNIVERSITE BRETAGNE LOIRE

UNIVERSITÉ DE NANTES

Thèse de Doctorat

Ning GUO

Mémoire présenté en vue de l'obtention du
grade de Docteur de l'Université de Nantes
sous le sceau de l'Université Bretagne Loire

École doctorale : Matière, Molécules, Matériaux en Pays de la Loire

Discipline : Chimie théorique, physique, analytique
Spécialité : Radiochimie
Unité de recherche : SUBATECH

Soutenue le 05/01/2017
Thèse N° :

Exploration des propriétés de l'astate aux degrés d'oxydation +I et –I en phase aqueuse

JURY

Président :	**Jean-Michel BOULER,** Professeur, Université de Nantes
Rapporteurs :	**Xiaolin HOU**, Professeur, University of Denmark **Thomas VERCOUTER**, Chercheur, Expert senior, CEA
Examinateurs :	**Jean-Michel BOULER,** Professeur, Université de Nantes **Julie CHAMPION**, Maitre assistant, IMT Atlantique **Gilles MONTAVON**, Directeur de recherche, CNRS **Cécile PERRIO,** Directeur de recherche, CNRS
Directeur de Thèse :	**Gilles MONTAVON**, Directeur de recherche, CNRS
Encadrant :	**Julie CHAMPION**, Maitre assistant, IMT Atlantique

Contents

Introduction générale

(Description de la thèse en français)

L'histoire connue du cancer débuta avec les Egyptiens; elle évolua très lentement au cours des siècles avec une précipitation des connaissances au 17ème siècle grâce entre autres, à la découverte du microscope en 1590 qui permit à la théorie cellulaire de se construire.[1] La découverte de la radioactivité par Becquerel en 1890 et la découverte en 1934 par Frédéric et Irène Joliot-Curie des isotopes radioactifs (radionucléides) produits artificiellement marque l'émergence d'une nouvelle discipline de la médecine centrée sur le traitement du cancer: la médecine nucléaire.[2] Le principe de la médecine nucléaire est d'injecter des isotopes radioactifs au patient et de cibler un organe ou une zone du corps dans le but de diagnostiquer ou de traiter des maladies.[3] La localisation ou la destruction sélective des cellules cancéreuses par un vecteur biologique couplé à un radionucléide est un concept simple et particulièrement attractif. Proposé par Ehrlich au début du 20e siècle, ce concept repose le plus souvent sur l'utilisation des propriétés de reconnaissance d'antigènes associés aux tumeurs cancéreuses par des anticorps.[4,5] Le concept de la radioimmunothérapie ciblée a ainsi été élaboré. Cette technique consiste à vectoriser, par l'intermédiaire d'un anticorps, un radionucléide émetteur alpha ou bêta permettant ainsi la destruction sélective des cellules tumorales.[6] La Thérapie Alpha Ciblée (TAC), liée à l'injection d'un émetteur alpha, est considérée pour traiter les plus petites tumeurs ou les maladies résiduelles après une chirurgie tumorale.[7] L'objectif de cette méthode est d'augmenter l'efficacité du traitement et de diminuer les dommages sur les tissus sains en même temps. Les résultats cliniques ont par ailleurs montré que cette technique ne présentait d'intérêt que dans le traitement de cellules cibles tumorales de petites tailles, facilement accessibles à l'anticorps radiomarqué ou de cibles plus volumineuses mais très radiosensibles comme les leucémies ou les lymphomes. Les traitements TAC demeurent actuellement du domaine de l'évaluation clinique et les divers exemples connus ou publiés montrent que ce concept de vectorisation peut encore être amélioré.

L'astate 211 est un candidat particulièrement intéressant pour la TAC

compte tenu de l'énergie des particules α qu'il émet et de sa période physique (7,2 h).[8] C'est un isotope dont la production demande un accélérateur pouvant fournir des particules α d'énergie moyenne (28 MeV). Malgré sa faible disponibilité, plusieurs études traitent du marquage de molécules organiques par At-211 pour des applications en médecine nucléaire.[9] Dans l'étape de radiomarquage, il est important de créer une liaison forte entre l'astate et les anticorps. Le marquage direct n'étant pas efficace, il est nécessaire d'utiliser des Agents Chélatants Bifonctionnels (ACB), devant assurer un double rôle : celui de former des complexes stables avec le radionucléide (éviter sa diffusion *in vivo* pouvant conduire à une radio toxicité) et celui d'assurer le couplage au vecteur. Des voies de marquage développées pour l'iode ont été appliquées à l'astate. La méthode la plus couramment utilisée est de réaliser des réactions de substitution nucléophile/électrophile pour former une liaison covalente entre At et un carbone d'un noyau aromatique. Cette méthode reste aujourd'hui limitée à des applications locales,[10] les applications par injection systémiques conduisant à une déshalogénation rapide du vecteur dans l'organisme. Ce résultat indique clairement la limite quant à la comparaison astate/iode. Bien qu'il soit clair que la plupart des propriétés chimiques des halogènes soient applicables, l'extrapolation des propriétés chimiques de l'astate à partir de son plus proche voisin, l'iode, n'est pas toujours observée. On parle alors de son caractère métallique.

Les voies de marquage spécifiques pour cet élément ne sont pas développées. En effet, pour permettre ce travail, il est important de connaître les espèces de l'astate « disponibles » dans le domaine Eh–pH de stabilité de l'eau, ou en d'autres termes les degrés d'oxydation de At, ainsi que leurs réactivités. Malheureusement, ces données restent limitées en raison de la faible disponibilité de At (production en cyclotron) et la manipulation de quantités non pondérables qui ne permettent pas l'utilisation d'outils spectroscopiques pouvant identifier sans ambiguïté la nature des espèces formées. Dans la littérature, les formes de l'astate proposées en phase aqueuse sont déduites en comparant leurs comportements dans des conditions données avec celui observé pour des composés supposés « modèles » ou « analogues ».

Ce travail de thèse a été réalisé dans le cadre du Labex IRON impliquant

entre autres, les équipes du laboratoire Subatech (UMR 6457) et du laboratoire Ceisam (UMR 6230). Il est motivé par l'installation à Nantes du cyclotron ARRONAX de haute énergie dédié à la médecine nucléaire et à la radiochimie. Il est réalisé en parallèle du projet vectorisation du Cancéropôle Grand Ouest. Face aux manques de connaissance de la chimie de l'astate, ce projet de thèse a pour objectif d'explorer la spéciation de l'astate dans des milieux (non) complexants aqueux. Les propriétés de réactivité de l'astate aux états d'oxydation +I et –I en solution aqueuse sont étudiées expérimentalement à l'aide de divers outils analytiques (appareil d'electromobilité, chromatographie ionique) couplés à un détecteur de radioactivité et de « méthodes radiochimiques » basées sur la technique d'extraction liquide/liquide permettant d'étudier de manière indirecte la formation des espèces.

Dans un premier chapitre, un exposé bibliographique portant sur la médecine nucléaire, la radiothérapie alpha et plus particulièrement les études publiées traitant de l'astate 211 sera exposé. L'astate appartient à la famille des halogènes et a, d'abord, été identifié dans les années 1940 par Dale R. Corson, Kenneth MacKenzie et Emilio Segrè.[11] Parmi ses 39 radioisotopes connus, At–211 est très intéressant comme candidat potentiel pour la TAC. Ensuite, les différentes méthodes de production de l'astate 211 seront présentées. Afin de surmonter les difficultés liées à l'utilisation de l'At–211 en TAC, les propriétés chimiques de base de l'At doivent être bien comprises. Les données fondamentales connues sur la chimie de At sont également présentées dans ce chapitre. Elles concernent (i) l'établissement du diagramme de Pourbaix de l'astate en milieu non complexant, (ii) les réactions entre $At(X)^+$ et les ligands complexants inorganiques et organiques à travers différentes méthodes et (iii) les études sur le comportement "At" en solution aqueuse étudié par electromigration. Sur la base de ces données, l'astate montre à la fois des propriétés en cohérence avec la tendance attendue dans la série des halogènes, mais aussi un caractère métallique très prononcé que l'on ne retrouve pas chez les autres halogènes plus légers. Par conséquent, l'objectif de ce travail est centré sur les analogies d'halogène et le caractère métallique de l'astate en solution aqueuse. Les questions/objectifs posés sont les suivants: est–ce bien l'espèce At^- qui existe en milieu réducteur ? At^+ existe de manière stable dans l'eau[12] et peut

former des complexes avec les autres halogénures (Br^-, Cl^-, I^-)[13,14]. Peut–on envisager l'existence d'espèce « exotiques » pouvant combiner trois atomes d'halogènes ? Enfin, une propriété des halogènes est de pouvoir faire des liaisons de « type halogène ». Une telle propriété est prédite également pour l'astate. Quelle méthode mettre en place pour pouvoir le montrer expérimentalement ? A chaque étape de la thèse, les résultats expérimentaux seront confrontés à des calculs théoriques dans un but de validation ou de prédiction.

En accord avec les propriétés chimiques des autres halogènes, et l'existence attendue de At^-, il avait été précédemment démontré par une méthode indirecte (chromatographie ionique) que l'astate pouvait exister sous une forme ionique chargée une fois négativement en milieu réducteur dans le domaine de pH acide.[15] Cependant, à ce jour, il n'existe aucune preuve directe (spectroscopique) de l'existence d'At^- en solution aqueuse. Un dispositif d'electromigration (fabriqué au laboratoire Subatech avec l'aide du service mécanique) a été mis au point à partir de l'appareil développé par Dreyer *et al.* dans la littérature.[16] Il a été utilisé pour étudier le comportement de l'astate dans un milieu réducteur sous un champ électrique homogène. La mobilité de l'astate, appelée mobilité (μ) peut ainsi être déterminée expérimentalement et extrapolée à force ionique nulle en utilisant le modèle Onsager–Fuoss (mobilité absolue, μ_0). Comme cela est indiqué dans la littérature pour les halogénures (F^-, Cl^-, Br^-, I^-), cette valeur dépend non seulement de la charge mais également du rayon ionique de l'espèce. C'est donc cette information que l'on souhaite obtenir. Les comportements de I^- et F^- ont été dans un premier temps mesurés en faisant varier des facteurs expérimentaux tels que le volume d'injection de l'échantillon, la tension appliquée pendant les expériences et la composition de l'électrolyte. Les valeurs suivantes de mobilité absolue $(-8,3 \pm 0,8) \times 10^{-4}$ $cm^2.V^{-1}.s^{-1}$ et $(-5,0 \pm 0,8) \times 10^{-4}$ $cm^2.V^{-1}.s^{-1}$ ont été déterminées pour, respectivement, I^- et F^-. Ces résultats permettent donc de valider notre appareil. Les effets de la température, de la force ionique, de la vitesse et de la permittivité de l'électrolyte sur l'application du modèle Onsager-Fuoss sont notamment discutés. En milieu acide réducteur, l'espèce de l'astate migre vers l'électrode positive confirmant l'existence d'une espèce anionique dans le milieu donné. L'étude réalisée en présence de I^- montre une mobilité légèrement inferieure pour l'astate en

comparaison de celle de l'iode. La mobilité absolue de l'espèce anionique de l'astate s'élève à (–8,3 ± 0,8) x 10^{-4} $cm^2.V^{-1}.s^{-1}$. Ces résultats sont tout à fait en accord avec des simulations récentes réalisées par dynamique moléculaire : les coefficients de diffusion d'At^- et I^-, qui peuvent être liés à des mobilités absolues, sont similaires avec une valeur légèrement plus petite pour At^- que I^-, avec un rapport de 0,94 ± 0,10.[17] On peut ainsi conclure que l'espèce en milieu acide réducteur correspond bien à At^-. Il s'agit d'autre part de la première valeur de mobilité absolue obtenue expérimentalement pour une espèce de l'astate. Ces résultats sont présentés dans le Chapitre 2 de ce document.

Comme démontré par les études antérieures de la littérature, At^+ peut former des espèces binaires avec des halogénures (X^-=Cl^-, Br^-, I^-) sous la forme de complexes 1 :1 et 1 :2 At :X^-.[13,14] Dans la littérature, une espèce ternaire composée de 3 halogènes différents a été identifiée, $BrICl^-$.[18] Il était ainsi intéressant d'explorer si l'astate peut aussi former une espèce trihalogénée, et plus particulièrement l'espèce $IAtBr^-$. Ainsi, dans le chapitre 3, une étude expérimentale pilotée par des calculs théoriques est proposée pour identifier une telle espèce. L'identification et la caractérisation des structures et des propriétés des nouveaux composés chimiques nécessitent habituellement d'utiliser un large éventail d'expériences complémentaires, parmi lesquelles les études spectroscopiques jouent un rôle majeur. Cependant, dans le cas de l'astate, les expériences sont restreintes en raison du caractère radioactif spécifique de l'At. Elle peut être encore plus compliquée si le domaine expérimental de l'espèce chimique est « petit » et complique donc sa recherche. C'est le cas du système étudié ici, ou en plus de l'espèce recherchée, il faut tenir compte de la formation des quatre complexes AtI, AtBr, AtI_2^- et $AtBr_2^-$. Dans ce chapitre, les calculs de mécanique quantique sont utilisés pour guider l'étude expérimentale en prédisant le domaine expérimental à cibler. L'analyse des données de compétition dans ce domaine indique qu'une espèce supplémentaire doit être considérée et que les points expérimentaux peuvent être bien décrits en considérant l'existence de l'espèce $IAtBr^-$. Cette dernière apparaît même être prédominante dans certaines conditions. La constante d'équilibre de formation du complexe associée s'élève à $10^{7,5 \pm 0,2}$, ce qui est en bon accord la valeur obtenue par la théorie de la fonctionnelle de la densité ($10^{6,9}$). Ce système

constitue non seulement le tout premier exemple d'une espèce trihalogéné ternaire qui implique l'élément astate, mais il est aussi caractérisé par des conditions où la première espèce trihalogénée déclarée prédominante en solution aqueuse peut exister. Je tiens à préciser que mes collègues Rémi Maurice (Subatech), Dumitru–Claudiu Sergentu (Subatech/Ceisam) et Nicolas Galland (Ceisam) ont été en charge de la partie de calcul théorique.

Les quatre halogènes plus légers que l'astate sont capables d'agir comme donneurs d'une liaison halogène avec la tendance suivante : F <Cl <Br <I, l'iode étant considéré comme formant les interactions les plus fortes.[19] La liaison halogène (XB) est communément appelée interactions intra– et intermoléculaires spécifiques impliquant un atome d'halogène. Dans une liaison halogène typique, un atome d'halogène fonctionne comme une espèce électrophile et interagit au niveau de ce que l'on appelle le «trou σ » avec un site nucléophile *via* une liaison faible non covalente. Habituellement, les acides de Lewis acceptent la densité électronique et les bases de Lewis sont des donneurs. En raison de l'emplacement de l'astate dans la famille des halogènes, qui est en dessous de l'iode, il est prédit que l'astate pourrait former une liaison halogène plus forte avec des bases de Lewis. Une méthode de compétition a été utilisée pour quantifier l'interaction entre AtI et 10 bases de Lewis différentes. En analysant les résultats expérimentaux obtenus par extraction liquide/liquide, les constantes de réaction entre AtI et les bases de Lewis dans le cyclohexane ont été déterminées. Une corrélation est trouvée par rapport à l'échelle de basicité de l'espèce I_2 établie par Laurence *et al.*,[20] les valeurs des constantes obtenues avec AtI augmentent avec la basicité de I_2. Ces résultats indiquent une liaison halogène entre AtI et les bases de Lewis. Ceci a été validé par des calculs de chimie quantique réalisés par mes collègues, Nicolas Galland et Rémi Maurice. En effet, les constantes d'interaction expérimentales apparaissent cohérentes avec celles calculées qui considèrent une liaison halogène avec l'atome d'astate de la molécule AtI. Il s'agit donc du premier travail expérimental qui montre, en complément des résultats théoriques, l'existence d'une liaison halogène avec At et que cette liaison est plus forte que celle faite avec l'iode et donc avec les autres halogènes.

Les travaux de ma thèse portant sur le comportement de l'astate aux

degrés d'oxydation (–I) et (+ I) en solution aqueuse ont conduits aux résultats suivants et sont présentés dans les trois chapitres suivants sous forme d'article:

1) l'étude de la mobilité de l'astate en milieu acide réducteur confirme l'existence de At^- et une première valeur de mobilité absolue est proposée et s'élève à $(-8,3 \pm 0,8) \times 10^{-4}$ $cm^2.V^{-1}.s^{-1}$;

2) l'astate peut interagir avec I^- et Br^- pour former une espèce mixte $IAtBr^-$. L'originalité du travail est que son domaine d'existence a pu être prédit de manière théorique. Il s'agit de la seule espèce contenant trois atomes d'halogène connue à ce jour qui peut prédominer en solution aqueuse. Son existence est intimement liée au caractère particulier de l'astate. La constante d'équilibre correspondante est de $10^{7,5 \pm 0,2}$, ce qui est en bon accord avec les calculs théoriques ($10^{6,9}$) ;

3) Une approche expérimentale est proposée, en complément de calculs théoriques, pour mettre en évidence que At peut former une liaison halogène avec des bases de Lewis, et que la liaison halogène est la plus forte connue à ce jour. Il s'agit d'un travail inédit qui est rendu possible par la présence d'ARRONAX et le travail main dans la main réalisé entre expérimentateurs et théoriciens.

References

(1) Hajdu, S. I. *Cancer* **2011**, *117* (5), 1097.

(2) Mould, R. F. *A century of X-rays and radioactivity in medicine: with emphasis on photographic records of the early years*; CRC Press, 1993.

(3) Zimmermann, R. *La médecine nucléaire: La radioactivité au service du diagnostic et de la thérapie*; EDP sciences, 2012.

(4) Ehrlich, P.; Herta, C. A.; Shigas, K. *Ztschr f Physiol Chem* **1904**, *61*, 379.

(5) Bloomer, W. D.; Lipsztein, R.; Dalton, J. F. *Cancer* **1985**, *55* (S9), 2229.

(6) Hoefnagel, C. A. *Eur. J. Nucl. Med.* **1991**, *18* (6), 408.

(7) McDevitt, M.; Sgouros, G.; Finn, R. *Eur. J. Nucl. Med.* **1998**, *25* (9), 1342.

(8) Allen, B. J. *Australas. Radiol.* **1999**, *43* (4), 480.

(9) Wilbur, D. S. *J. Nucl. Med.* **2001**, *42* (10), 1516.

(10) Zalutsky, M.; Reardon, D. *J. Nucl. Med.* **2008**, *49* (1), 30.

(11) Corson, D. R.; MacKenzie, K. R.; Segre, E. *Phys. Rev.* **1940**, *58* (8), 672.

(12) Champion, J.; Alliot, C.; Renault, E.; Mokili, B. M.; Chérel, M.; Galland, N.; Montavon, G. *J. Phys. Chem. A* **2010**, *114* (1), 576.

(13) Champion, J.; Seydou, M.; Sabatié-Gogova, A.; Renault, E.; Montavon, G.; Galland, N. *Phys. Chem. Chem. Phys.* **2011**, *13* (33), 14984.

(14) Ludwig, R.; Fischer, S.; Hussein, H.; Frind, M.; Dreyer, R. *J. Radioanal. Nucl. Chem. Artic.* **1989**, *134*, 141.

(15) Sabatié-Gogova, A.; Champion, J.; Huclier, S.; Michel, N.; Pottier, F.; Galland, N.; Asfari, Z.; Chérel, M.; Montavon, G. *Anal. Chim. Acta* **2012**, *721*, 182.

(16) Dreyer, I.; Dreyer, R.; Chalkin, V. A. *J. Radiochem. Radioanal. Lett.* **1978**, *35* (6), 257.

(17) Réal, F.; Severo Pereira Gomes, A.; Guerrero Mart??nez, Y. O.; Ayed, T.; Galland, N.; Masella, M.; Vallet, V. *J. Chem. Phys.* **2016**, *144* (12).

(18) Guidelli, R.; Pergola, F. *J. Inorg. Nucl. Chem.* **1969**, *31* (1964), 1373.

(19) Politzer, P.; Lane, P.; Concha, M. C.; Ma, Y.; Murray, J. S. *J. Mol. Model.* **2007**, *13* (2), 305.

(20) Laurence, C.; Graton, J.; Berthelot, M.; El Ghomari, M. J. *Chem. - A Eur. J.* **2011**, *17* (37), 10431.

Chapter 1. Literature survey

1.1. Nuclear medicine

Nuclear medicine specializes in using radiopharmaceuticals in order to diagnose and treat diseases. Radiopharmaceuticals are a group of pharmaceutical drugs containing radioactive substances. The history of nuclear medicine can be traced back to 1934 when Frédéric Joliot-Curie and Irène Joliot-Curie discovered artificial radioactivity, an event regarded as the most significant milestone in nuclear medicine.[1] In 1946, the first successful treatment of a patient with thyroid cancer using iodine-131 gained the public's recognition of nuclear medicine.[2] Although this first use of ^{131}I was in thyroid cancer therapy, its applications have since been expanded to imaging the thyroid gland, quantifying thyroid function and so on. Among the radionuclides that have been applied to nuclear medicine, technetium-99m, which was discovered in 1937 by C. Perrier and E. Segre, should be highlighted because it became the most utilized radionuclide for diagnosis.[3] Since then, diagnosis and therapy using radioactive substances have developed complementarily, with the objective of defining a more efficient way of diagnosing and curing complex diseases. The radionuclides that are of interest in nuclear medicine are displayed in Figure 1.1.[4]

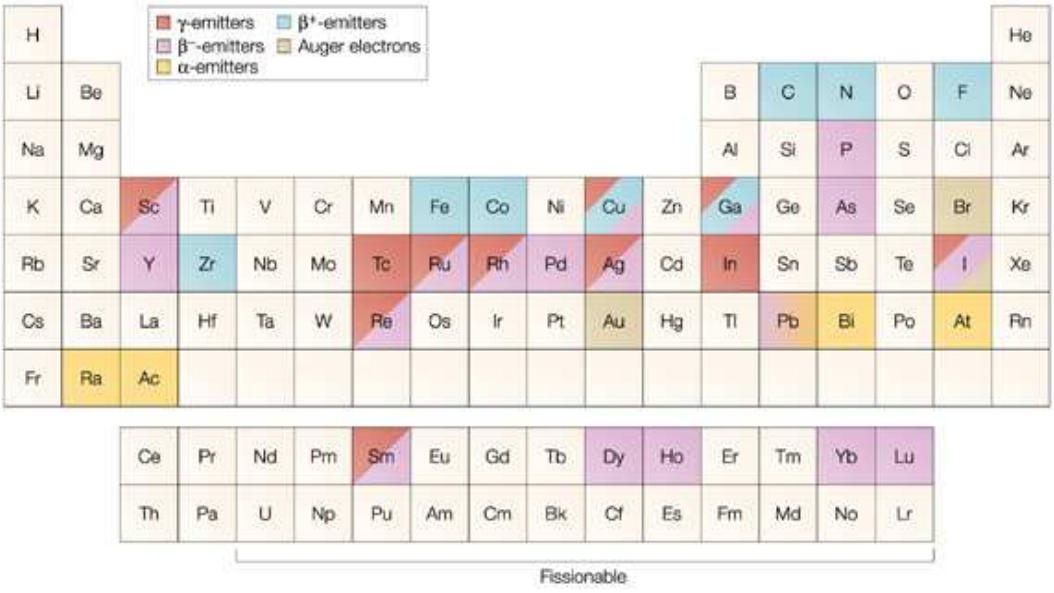

Figure 1.1. A representation of the periodic table, highlighting the elements of interest in nuclear medicine. The elements are color-coded by emission type.

1.1.1. Nuclear medicine diagnosis of cancers: imaging

In nuclear medical imaging, radiopharmaceuticals are injected or ingested internally. An external detector, such as a gamma camera, captures and forms images from the radiation emitted by the radiopharmaceuticals at the same time. Two major nuclear medical imaging techniques, Positron Emission Tomography (PET) and Single Photon Emission Computed Tomography (SPECT) have been developed as standard nuclear medicine services. Both PET and SPECT function by detecting gamma rays. Comparing these two methods, the SPECT scanner detects directly the gamma ray emitted by the tracers introduced inside the body while in PET, the tracers used emit positrons that are annihilated with the electrons a few millimeters away, causing two gamma photons to be emitted in opposite directions, which are detected by a PET scanner in time. Thus, PET can provide more information about the localization of a radiation event and has higher spatial resolution images than SPECT, which has an approximately 1 cm resolution.

The typical radioisotopes used for SPECT are presented in Table 1.1. Among them, ^{99m}Tc, which is a metastable nuclear isomer that emits gamma rays, is

widely used in SPECT applications. Attaching ^{99m}Tc to different kinds of pharmaceuticals enables it to be applied to different issues.

Table 1.1. Typical radioisotopes used for SPECT applications.

Radioisotope	Emission energy (keV)	Half-life	Application
^{99m}Tc	140	6 h	Bone scan; Myocardial perfusion scan; Sestamibi parathyroid scan; Brain scan; White cell scan
^{123}I	159	13 h	Neuroendocrine scan
^{131}I	971	8 d	Neurological tumor scan
^{111}In	171	67 h	White cell scan

Isotopes used in PET are typically those with a short half–life, such as ^{18}F (110 min), ^{11}C (20 min), ^{82}Rb (1.3 min), ^{13}N (10 min), ^{15}O (2 min) and ^{68}Ga (67 min), and ^{89}Zr (78 h). Among these, PET scanning with radioisotope fluorine-18 (^{18}F) fluorodeoxyglucose (FDG), named FDG-PET, is extensively used in clinical cancer imaging.[5] ^{18}F, with emission energy of 873 keV, delivers an effective radiation dose of 14 mSv when used in FDG for a PET scan. As a glucose analog, FDG can be taken up by glucose-using tissues, such as the brain, the liver, and most cancers. Thus, FDG-PET can be used for the imaging and diagnosis of cancers, particularly in Hodgkin's lymphoma, non–Hodgkin's lymphoma, and lung cancer.[5]

1.1.2. Nuclear medicine therapy for cancers: targeted radiation therapy

Since most cancers can be diagnosed by the imaging methods mentioned above, it is important to have an effective approach to treat these diseases. In nuclear medicine therapy, the radiation dose is administered internally. Thus, it is essential that it treats only the cancerous cells with a minimum exposure of the surrounding, healthy tissues. With this aim, targeted radiation therapy has been

developed in order to deliver the radiation precisely to tumor cells.

Targeted radiation therapy involves radiolabeled pharmaceuticals to deliver radiation selectively to tumors. The radioisotopes used are generally α-particle, β-particle or Auger-electron emitters. Based on modern medicine, cancer cells can be clearly distinguished from normal ones with the use of selective pharmaceuticals. In this case, antibodies from the immune system are regarded as the best candidates to carry radioisotopes to tumors. Antibodies can bind specifically to tumor-associated antigens, increasing the radiation delivered to the tumor cells and decreasing the radiation to normal tissues at the same time.

However, the selection of the radionuclide labeling on the biological vector is very important and should meet the following criteria: emission type, energy transfer, penetration range, and radioactive decay rate of the radionuclide. Regarding the emission type, labeling with α- and β-particle emitters has been of great interest.[4] A comparison between these two types of nuclide with respect to the mentioned criteria is illustrated in Table 1.2.

Table 1.2. α- and β-emitting nuclides and their general characteristics.

Emission type	α-particle emission	β-particle emission
Typical nuclides	^{213}Bi, ^{212}Bi, ^{211}At, ^{225}Ac, ^{149}Tb	^{90}Y, ^{131}I, ^{177}Lu, ^{186}Re, ^{212}Pb
Energy transfer	High linear energy transfer (LET), 4.0-8.0 MeV	Sparse energy transfer, 0.1-2.2 MeV
Penetration range	Short, 40-100 μm	Long, up to 600 μm
Half–life	Hours to several days	Microseconds to several hours

The β-particle emitters are appropriate for larger tumors due to their long penetration range and sparse scattering transfer. This long range is a

double-edged sword: it is advantageous when the targeted tumor is large enough to capture the sparse emission but when the tumor is smaller, it can lead to harmful radiation of normal tissues adjacent to it. Compared to β-particle emitters, the short penetration range α-emitting nuclides are ideal for the treatment of small tumors or residual diseases after surgery.

1.1.3. Radiolabeling

In nuclear medicine, a prerequisite is to fix the radionuclide to the biological vector. This step is firmly related to the basic chemistry of the desired radionuclide and is the most "instrumental" part as the goal is to attain an *in vivo* stable biological vector-radionuclide complex. Generally, there are two kinds of strategies employed in radiolabeling protocols:

1) The direct radiolabeling mechanism, which combines the radionuclide directly with a biological vector. For instance, ^{131}I, in the chemical form iodine monochloride, can be linked to phenyl rings corresponding to the terminal tyrosine groups of antibodies.[4,6]

2) The two-step radiolabeling mechanism, which involves a bifunctional chelating agent (BFC) as a connecter to combine the radionuclide and the biological vector. In this mechanism, the radionuclides with a so-called "metallic" character are commonly used to label biological vectors.[4,7] The mechanism scheme is shown in Figure 1.2. The chemical bond can be covalent for *e.g.* iodine, or coordinate for elements presenting a "metallic" character.

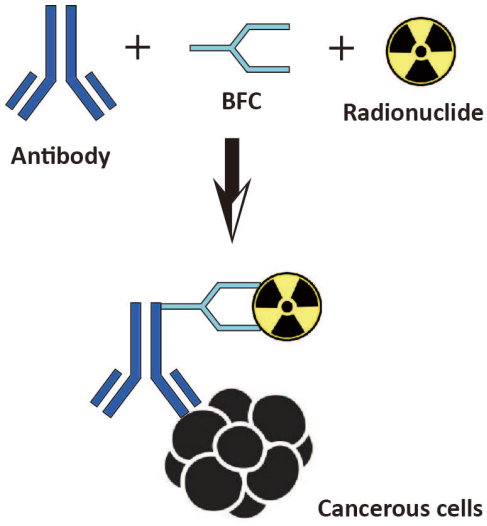

Figure 1.2. Two-step radiolabeling mechanism: an antibody fixed on a cancerous cell and linked to a radionuclide through a BFC.

1.1.4. Application of astatine-211 in nuclear medical therapy

As discussed in the previous part, radiolabeling involving α-particle emitters is now preferred for dealing with smaller tumors or the residual diseases after surgery. The few promising α-emitters, such as ^{212}Bi, ^{225}Ac, ^{213}Bi, ^{211}At, ^{223}Ra and ^{149}Tb, are displayed in Table 1.3.[8]

Among these α-emitting radionuclides, ^{211}At is considered to be a potential candidate for application in targeted alpha therapy (TAT) due to the following assets:[9–11]

1) At has a half-life of 7.21 h, which is long enough to complete the complicated labeling strategies.

2) At is a 100% α-particle emitter with energy between 5.9 and 7.5 MeV.

3) The LET_{mean} of its α-particles is close to the value needed to achieve the highest relative biological effectiveness of ionizing radiation.

4) The energy range of its α-particles corresponds to 55-80 μm, limiting the additional damage to adjacent healthy tissues.

5) The K-rays generated through the electron capture decay of ^{211}At to ^{211}Po

provide a valuable means for tracking ^{211}At in laboratory studies. The ^{211}At activity distribution can be imaged and quantified by planar and SPECT imaging.

Table 1.3. α-emitting radionuclides applied in nuclear medicine.

Potential candidates	Half-life	α-emission energy (MeV)	Advantages	Disadvantages
^{212}Bi	60.6 min	7.8	Production yield can be controlled	2.6 MeV γ-ray exposure
^{225}Ac	10 d	6 – 8.4	5 α-emissions	Immense α-particle recoil energy
^{213}Bi	45.6 min	6 – 8.4	Labeling reaction rapid and effective	Radiation damage to the biological vectors
^{211}At	7.21 h	6.8	Appropriate half-life	Production is facility-dependent
^{223}Ra	11.4	6	4 α-emissions	Gaseous product ^{219}Rn distributes *in vivo*
^{149}Tb	4.15 h	4	Weak specific irradiation	Decay products may deposit in bone mineral

1.1.4.1. Radiolabeling with astatine-211

Considering the cytotoxicity of ^{211}At, the stability of the ^{211}At-labeled biological vectors *in vivo* is a crucial issue.[12,13] To date, different types of bonds have been studied: At-C bonds, At-B bonds, and At-metal cation bonds. The labeling strategy is mainly based on those developed for iodine-labeled compounds.

a. At-C bonds

The direct electrophilic aromatic substitution (EAS) with At^+ was of wide interest. However, the ^{211}At-labeled complexes were shown to possess poor stability *in vivo* due to the rather weak bond strength between At and C atoms.[14] Therefore, it became clear that ^{211}At should be combined to biological vectors through BFCs rather than combined directly. Interesting compounds, such as astatobenzylguanidine (MABG, Figure 1.3a)[15] that binds selectively to neuroblastoma tumors, and succinimidyl astatobenzoate (SAB, Figure 1.3b)[16] that has been successfully linked to specific antibodies through the succinimidyl anchor, are achieved through EAS with $^{211}At^+$. The labeling of antibodies with SAB has been attempted clinically through the two-step radiolabeling mechanism: first ^{211}At is linked to the BFC and then the ^{211}At-BFC complex is connected to antibodies.[16,17]

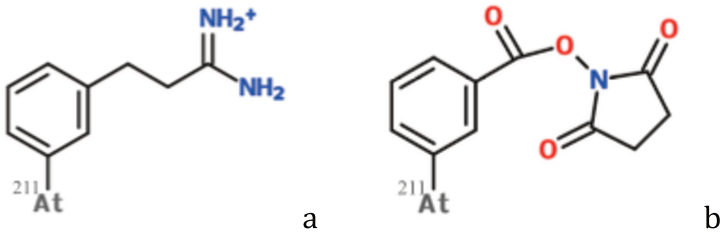

a b

Figure 1.3. Examples of ^{211}At-targeting agents synthesized through EAS using At^+: a. MABG; b. SAB.

The complexes synthesized through nucleophilic aromatic substitution (NAS) using At^- can be obtained *via* halogen exchange[18,19] or dediazoniation reactions[20,21]. Compounds such as ^{211}At-labeled methylene blue (Figure 1.4), which binds almost exclusively to melanoma tumors, are achieved through this approach.[24]

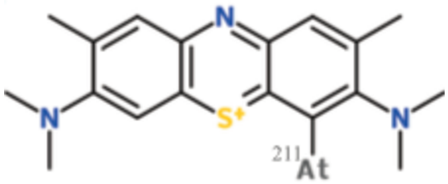

Figure 1.4. Example of ^{211}At-targeting agents synthesized through NAS using At^-: ^{211}At-labeled methylene blue.

b. At-B bonds

The antibody combining with ^{211}At-BFCs based on boron cluster derivatives turned out to be more advantageous than the classic ^{211}At-BFCs containing the At-C bond, as a result of the high affinity of ^{211}At for the B atom. Furthermore, the radiolabeling approach can be carried out in one step, since boron cages can be conjugated to antibodies beforehand. Wilbur *et al.* have synthesized many complexes using boron clusters as BFCs labeled with ^{211}At, such as [^{211}At]*nido*-carboranes (Figure 1.5a), [^{211}At]bis-*nido*-carboranes (Figure 1.5b) and [^{211}At][*closo*-decaborates]$^{2-}$ (Figure 1.5c), which are functionalized with various groups to strengthen the antibody conjugation.[22–24]

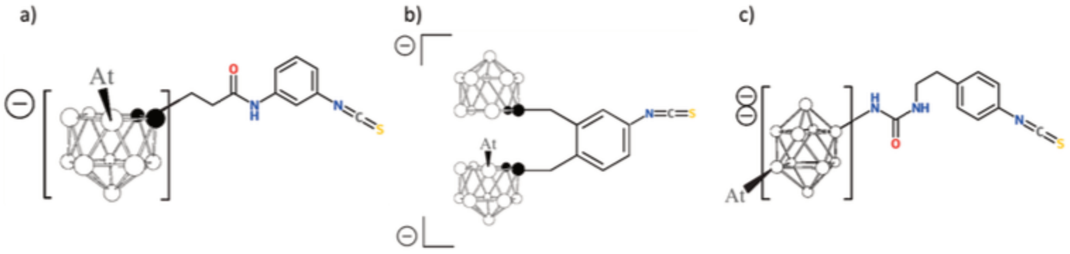

Figure 1.5. Examples of astatinated and functionalized boron clusters: a) a *nido*-carborane derivative, b) a bis-*nido*-carborane derivative and c) a *closo*-decaborate derivative. Filled circles represent C atoms while empty ones represent B atoms.

c. At-metal cation bonds

Another strategy is based on retaining ^{211}At in stable complexes. The idea is to complex astatide to metal cations, such as Rh (III) and Ir (III) chelated complexes.[25–27] These can then be used as a BFC (see Figure 1.6). According to the tendency in the halogen group, it was hypothesized that At$^-$ would also have the soft anion properties and the stronger interactions responding to the hard and soft acids and bases (HSAB) theory.[28,29]

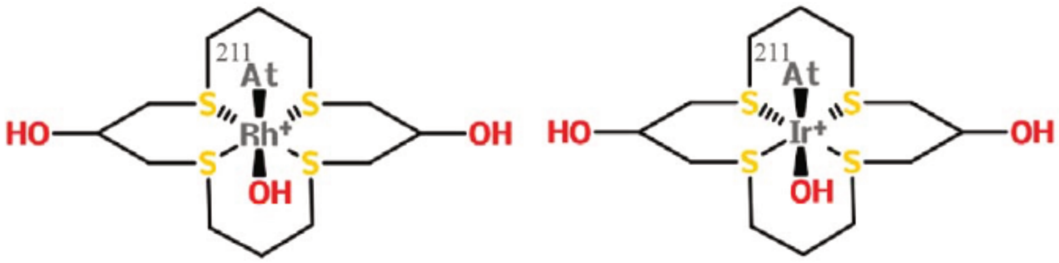

Figure 1.6. Examples of stable complexes with $^{211}At^-$ attached to Rh (III) and Ir (III) soft metal cations.

1.1.4.2. Summary

Different methodologies developed for iodine have been applied to astatine, considering both the At^+ and At^- species. Unfortunately, *in vivo* deastatination remains significant in some cases, notably when the biological vector is metabolized; astatobenzoate deastatination occurs *via* an unknown mechanism.[30] This shows that labeling with At is still limited and specific strategies should be developed. A pre-requisite is to know the basic properties of astatine, which have yet to be fully elucidated.

1.2. General properties of astatine

1.2.1. Astatine

Astatine, with the chemical symbol At and atomic number 85, belongs to the halogen group in the periodic table. It was isolated and identified by Dale R. Corson, Kenneth Ross MacKenzie, and Emilio Segrè through bombarding bismuth-209 with accelerated alpha particles in a cyclotron at the University of California, Berkeley in 1940.[31] They suggested the name “astatine”, which comes from the Greek astatos (αστατος) meaning "unstable", due to its radioactive properties, with the "-ine" suffix following the names of the four previously discovered halogens.[32] Since its discovery, 39 isotopes of astatine with the atomic masses of 191-229 have been experimentally identified and 37 more have been suggested on the basis of theoretical calculations.[33] No stable isotope

of astatine has been observed. Experimentally, five isotopes have been identified with half-lives exceeding 1 hour. Their atomic masses range from 207 to 211. Among these, the most stable one is astatine-210 with a half-life of 8.1 hours. Astatine is the rarest naturally-occurring element in the earth's crust, being the product of various heavier elements.[34] The total amount of astatine in the earth's crust is estimated at less than 1 gram at any given time.[35] Thus, it is difficult to collect from this source and the major route for obtaining astatine is through nuclear reactions (α, xn). Generally, the ^{211}At concentration is around 6×10^{-9} mol/L corresponding to 100 MBq/mL.

1.2.2. Astatine-211

Astatine-211 has a half–life of 7.21 hours and decays through a double-branched pathway (see Figure 1.7) producing one α particle per decay. The first route (42%) is by direct emission of 5.87 MeV α-particles to bismuth-207, which has a long half-life, and then decays to stable lead-207. The second route (58%) is by electron capture (EC) to polonium-211 with a half-life of 520 ms, which is immediately excited by the emission of 7.45 MeV α-particles to stable lead-207. The α-particles emitted by ^{211}At and ^{211}Po have a route in tissues of approximately 55 and 80 μm, respectively, with the mean high linear energy transfer (LET) of 97 keV/μm.[36] The second decay branch involves electron capture decay that emits polonium K-rays, which makes it convenient to track ^{211}At activity.[10]

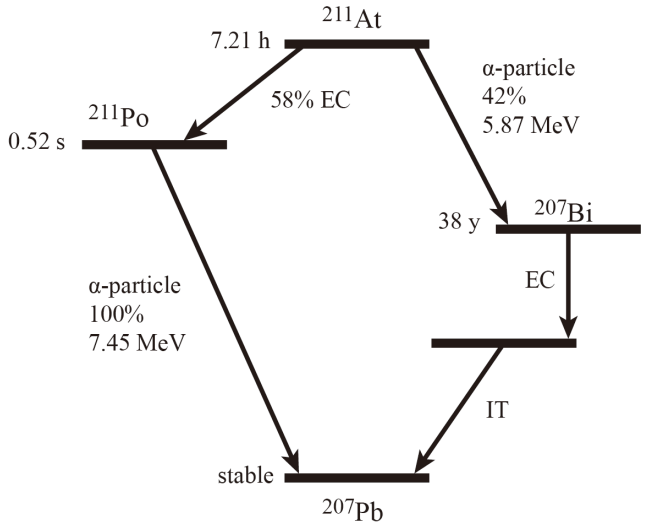

Figure 1.7. Scheme illustrating the double-branched decay of ^{211}At. IT: isomeric transition.

1.2.3. Production of astatine-211

It is possible to obtain ^{211}At *via* proton irradiation of thorium or uranium to yield radon-211, in turn decaying to ^{211}At. The drawbacks of this method are that it is not efficient and demands extensive separation procedures.[37] To date, the most commonly used method to produce ^{211}At is through bombarding a stable bismuth-209 target with energetic alpha particles (28 MeV). The factors limiting ^{211}At production by this method are:

1) The availability of suitable accelerator facilities. Although 36 cyclotrons are identified in the IAEA (International Atomic Energy Agency) report as having a characteristic α-particle beam to produce ^{211}At, only a few of them routinely produce ^{211}At, which has led to a commercial shortage.[38]

2) The prospect of melting the target. During the radiation, due to the poor thermal conductivity (7.97 $W \cdot K^{-1} \cdot m^{-1}$) and low melting point (272°C) of bismuth, it is important to provide adequate target cooling in order to minimize the loss of ^{211}At caused by volatilization.

3) The incident energy of the α-particle beam. The threshold for the ^{209}Bi(α, 2n)^{211}At reaction starts at around 21 MeV and decreases at about 30 MeV.

However, one cannot take advantage of the full breadth of the cross-section because the ^{209}Bi(α, 3n)^{210}At reaction occurs at about 29 MeV (see Figure 1.8).[39] ^{210}At, with a half-life of 8.3 h, is problematic in the production of ^{211}At. More than 99% of ^{210}At decays lead to the production of the 138.4-days α-particle emitter, ^{210}Po, which can be extremely toxic for bone marrow. In order to avoid the contamination of ^{210}At, the incident α-particle energy should be below the threshold for the ^{209}Bi(α, 3n)^{210}At reaction, *i.e.* less than 29 MeV.

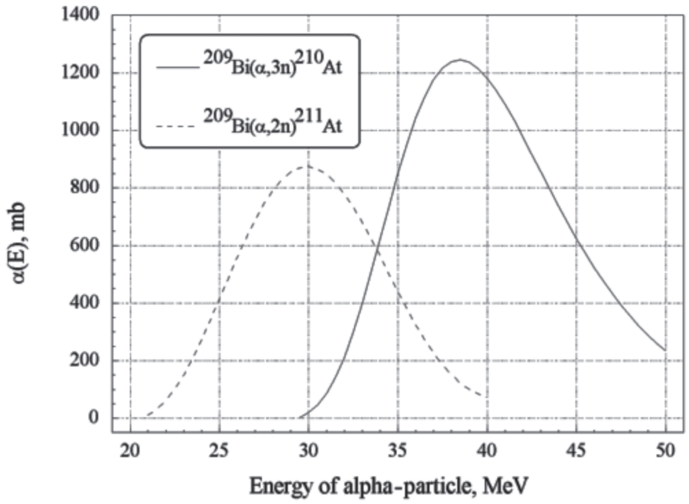

Figure 1.8. Fit of the cross-sections for ^{209}Bi(α, 2n)^{211}At and ^{209}Bi(α, 3n)^{210}At reactions.[39]

The quality of ^{211}At for medical use is influenced by not only the methods applied for the cyclotron irradiation but also the process to isolate ^{211}At from the bismuth target. Generally, there are two approaches for ^{211}At recovery – wet harvesting and dry distillation. In the former, the bismuth target is dissolved in concentrated acid, such as HNO_3 or $HClO_4$, and then astatine is extracted into an organic solvent, for example butyl or isopropyl ether.[40,41] Although this approach is useful when an oxidant state of ^{211}At is required, it is not ideal for processing a large amount of ^{211}At because it involves multiple radioactive manipulation steps. The commonly used approach to isolate ^{211}At from the bismuth target is dry distillation performed in a quartz vessel in the 650 – 800 °C range with a gentle flow of carrier gas – usually nitrogen or argon. The vaporized astatine is

condensed by promptly evacuating the system and reducing the pressure on the outlet side.[42,43]

In the present work, ^{211}At was produced *via* the ^{209}Bi(α, 2n)^{211}At nuclear reaction in the ARRONAX cyclotron in Nantes, France. The ^{209}Bi target was irradiated for two hours by an alpha external beam accelerated to 28 MeV (see Figure 1.9).[44] After irradiation of the target, a dry distillation method was used to isolate ^{211}At and then approximately 10 MBq of ^{211}At was recovered into 200 µL of chloroform.[42] The radionuclide purity of ^{211}At was verified by gamma–ray spectroscopy at 687 keV with a high purity germanium (HPGe) detector.

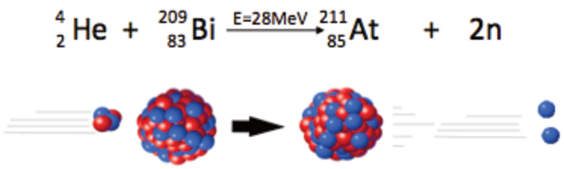

Figure 1.9. The reaction of ^{209}Bi(α, 2n)^{211}At.

1.3.The chemistry of astatine in aqueous solution

The chemical characteristics of astatine are generally predicted from its position in the periodic table. More precisely, it is located in the halogen group under iodine. From a chemist's point of view, it is complicated to investigate the chemistry of At because of the following problems:

1) Astatine is a rare element; it has neither a stable nor a long-lived isotope.

2) At is a kind of "invisible" element; a visible piece of astatine would immediately vaporize due to the heat generated by its intense radioactivity.[34]

3) At can only be worked with at ultra-trace concentration, typically less than 10^{-10} mol·L^{-1}.[45]

4) No spectroscopic tool can be applied to identify At reactivity/speciation at the molecular level.

All these difficulties explain why the chemistry of astatine is not well understood.

1.3.1. Speciation of astatine in a non-complexing aqueous solution

The primary information that a chemist needs is the Pourbaix diagram of an element, which indicates the predominant species as a function of both the pH and the redox potential (*E*). The Pourbaix diagram is notably of great importance in nuclear medicine in order to define the conditions for radiolabeling, *i.e.* the reaction yield will depend on the proportion of the species expected to react, *e.g.* At(–I) for nucleophilic and At(+I) for electrophilic substitution reactions.

In 2010, Champion *et al.* revisited the Pourbaix diagram of At, considering the discrepancies found in the literature. They evidenced that At species with an oxidation state of 0 cannot exist in aqueous solution, and proposed that At has three oxidation states in the range of water stability (E = –0.1 to +1.2 V *vs.* NHE, normal hydrogen electrode) and in the pH range 1.0 – 2.0.[46] Firstly, the species found in reductive acidic conditions was assumed to be At(–I), in accordance with the trend displayed by the lighter halogens. The existence of an anionic species with a charge of –I was shown in a complementary work by high performance anion exchange chromatography (HPAEC).[47]

With increasing redox potential, two other species were proposed with the oxidation states +I and +III corresponding to At^+ and AtO^+, respectively. These two stable cationic chemical forms show the more "metallic" character of At compared to the other halogens. In fact, only anionic and neutral species are observed for the other halogens (see Figure 1.11). When the pH increased to weak acidic aqueous, while remaining in oxidizing conditions, a neutral species was observed through dynamics experiments with ion-exchange resins.[48] Furthermore, the analysis of experimental data obtained by a competition method showed that the transformation of AtO^+ to this neutral species leads to the exchange of one proton, indicating the existence of AtO(OH). The hydrolysis thermodynamic constant of $10^{-1.9}$ was determined, which is in good agreement with that achieved by density functional theory (DFT) calculation.[48] When the pH increased to basic conditions, an anionic species appeared. This was shown by both ionic exchange[49] and electromobility experiments[50] whereas At^- was

expected based on the Pourbaix diagram of iodine. A recent work demonstrated that this species is most probably the second hydrolysis product of AtO^+, *i.e.* $AtO(OH)_2^-$, instead of At^-. Its formation can be quantified by the hydrolysis thermodynamic constant of $10^{-6.9}$, which is in agreement with the theoretical calculation.[51] Currently, the Pourbaix diagram can be displayed as Figure 1.10, which presents the "dual character" of At: on one hand, it follows the behavior of the lighter halogens with the presence of At^-; on the other hand, it can exist as a stable cation in the range of water stability like the metal-like elements.

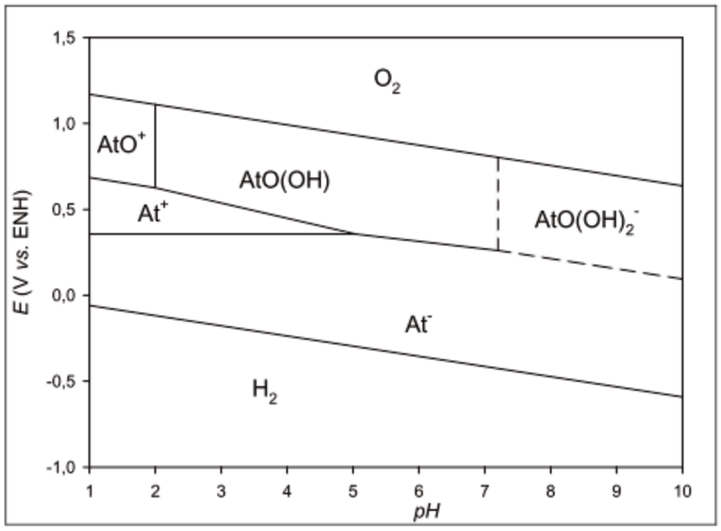

Figure 1.10. Pourbaix diagram of At in a non-complexing aqueous medium.[46,48,51]

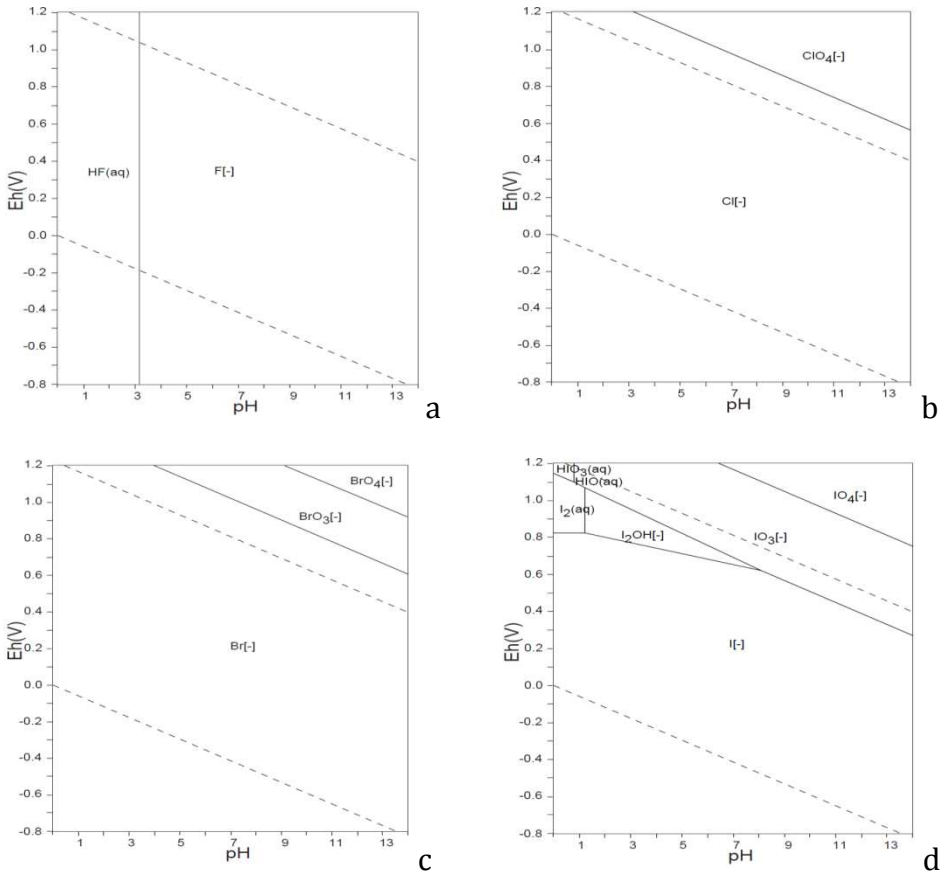

Figure 1.11. Pourbaix diagram of halogens in a non-complexing aqueous medium: a. F, b. Cl, c. Br, and d. I.

1.3.2. Speciation of astatine in aqueous solution in the presence of inorganic ligands

To reveal this "metallic" character experimentally, the reactions of astatine cations with complexing ligands have been studied in recent decades. Considering the specific radioactive properties of astatine mentioned above, it is a difficult task to identify the reaction and the species formed. Different indirect methods and assumptions based on the experimental outcomes have been used to study the reaction between astatine and complexing ligands. In the 1960s, Appleman investigated the reactions of astatine with the halogen ligands and proposed the existence of interhalogen species such as AtI, AtBr, AtI_2^-, $AtBr_2^-$, $AtCl_2^-$, $AtIBr^-$ and $AtICl^-$ from the solvent extraction behavior of astatine; the interrelated equilibrium constants were also provided.[52] Time-of-flight mass

spectrometry was used to identify the At species such as AtCl, AtBr and AtI, which was the first direct evidence of these species.[53] The research team of Dubna worked on At reactions in acid solution with a cation exchange method to obtain the equilibrium constants of AtCl and $AtCl_2^-$ formation.[54,55] Later, in the 1980s, the electromobility method was repeatedly applied to explore the reaction between astatine and halides (Cl^-, Br^-, I^-) or pseudo-halide (SCN^-) at different pH and ionic strength by Dreyer and coworkers.[56–60] All the related equilibrium constants are presented in Table 1.4.

Table 1.4. Overview of the reactions between At cationic species and inorganic ligands through different methods: electromigration (Elc) and the competition method in aqueous/organic (A/O) or aqueous/solid (A/S) systems.

Method	Medium	Equilibrium	Apparent constant
A/S[55]		$At(x)^+ + NO_3^- \rightleftharpoons At(x)(NO_3)$	$Log\beta_{1,NO_3^-} = 0.13$
	$H_2Cr_2O_7$ 0.1 M	$At(x)^+ + SO_4^{2-} \rightleftharpoons At(x)SO_4^-$	$Log\beta_{1,SO_4^{2-}} = 0.23$
		$At(x)^+ + 2SO_4^{2-} \rightleftharpoons At(x)(SO_4)_2^{3-}$	$Log\beta_{2,SO_4^{2-}} = 0.50$
	$HClO_4$ 1 M	$At(x)^+ + Cr_2O_7^{2-} \rightleftharpoons At(x)(Cr_2O_7)^-$	$Log\beta_{1,Cr_2O_7^{2-}} = 1.34$
A/S[55]	$HClO_4$ 0.3 M	$At(x)^+ + Cl^- \rightleftharpoons At(x)Cl$	$Log\beta_{1,Cl^-} = 3.10$
	$H_2Cr_2O_7$ 5×10^{-3} M		$Log\beta_{2,Cl^-} = 3.42$
	$HClO_4$ 0.5 M		$Log\beta_{1,Cl^-} = 3.20$
	$H_2Cr_2O_7$ 5×10^{-3} M	$At(x)^+ + 2Cl^- \rightleftharpoons At(x)Cl_2^-$	$Log\beta_{2,Cl^-} = 3.40$
A/S[54]	HNO_3 0.5 M		$Log\beta_{1,Cl^-} = 2.85$

	$H_2Cr_2O_7$ 5×10^{-3} M		$\text{Log}\beta_{2,Cl^-} = 5.40$
A/O[52]	$HClO_4$ 0.1 M		$\text{Log}K_{2,Br^-} = 2.50$
	HNO_3 0.5 M	$At(x)Br + Br^- \rightleftharpoons At(x)Br_2^-$	
Elc[58]	$K_2Cr_2O_7$ 0.5 M		$\text{Log}K_{2,Br^-} = 2.40$
	HNO_3 0.5 M	$At(x)SCN + SCN^- \rightleftharpoons At(x)SCN_2^-$	
Elc[56]	$K_2Cr_2O_7$ 0.5 M		$\text{Log}K_{2,SCN^-} = 2.60$
A/O[52]	$NaClO_4$ 0.8 M		$\text{Log}K_{2,I^-} = 3.30$
	HNO_3 0.5 M	$At(x)I + I^- \rightleftharpoons At(x)I_2^-$	
Elc[58]	$K_2Cr_2O_7$ 0.5 M		$\text{Log}K_{2,I^-} = 3.20$
	$HClO_4$ 0.01 M	$At(x)^+ + I^- \rightleftharpoons At(x)I$	$\text{Log}\beta_{1,I^-} = 6.17$
Elc[60]	$NaClO_4$ 0.04 M	$At(x)^+ + 2I^- \rightleftharpoons At(x)I_2^-$	$\text{Log}\beta_{2,I^-} = 9.42$
A/O[52]	$HClO_4$ 0.1 M	$At(x)I + Br^- \rightleftharpoons At(x)IBr^-$	$\text{Log}K = 2.08$
A/O[52]	$HClO_4$ 0.1 M	$At(x)I + Cl^- \rightleftharpoons At(x)ICl^-$	$\text{Log}K = 0.95$
	HNO_3 0.05 M		
Elc[59]	$K_2Cr_2O_7$ 0.005 M	$At(x)C(CN)_3 + C(CN)_3^- \rightleftharpoons At(x)(C(CN)_3)_2^-$	$\text{Log}K_2 = 2.83$

These results are based on the analysis of the outcomes of experiments and no spectroscopic data can confirm them. Comparing computational calculations and experimental outcomes can provide definitive evidence for the chemical form of the reaction product. This work was initially developed in the PhD thesis of

Champion.

She introduced competition experiments to study the distribution of a given At species in a biphasic system, in the presence of a complexing ligand.[45,61] The cationic forms of astatine, At^+ and AtO^+, were investigated. The reactions involving these At species with the complexing ligands can be described as:

$$At(x)^+ + mX^- \overset{\beta_{m,X^-}}{\longleftrightarrow} At(x)X_m^{1-m} \quad (1.1)$$

where $At(x)^+$ stands for At^+ or AtO^+, X for the ligand and $At(x)X_m^{1-m}$ for the reaction product formed with a 1:*m* stoichiometry.

The equilibrium constant β_{m,X^-} can be written as:

$$\beta_{m,X^-} = \frac{(At(x)X_m^{1-m})}{(At(x)^+)(X^-)^m} \quad (1.2)$$

where the data in parentheses represent the activity of the species at equilibrium.

Thus, the distribution of At between the aqueous and organic phases can be expressed as:

$$D = \frac{D_0}{1+\sum_m \beta_{m,X^-}(X^-)^m} \quad (1.3)$$

in which D_0 is the distribution coefficient in the absence of any complexing ligand.

With this strategy, the reactions of $At(x)^+$ species with some inorganic ligands such as Cl^-, Br^- and SCN^- were studied, involving the formation of both 1:1 and 1:2 complexes. The thermodynamic constants of these equilibria are summarized in Table 1.5. The complexation strength between $At(x)^+$ and the inorganic ligands increases in the order $Cl^- < Br^- < SCN^-$. Thus, the $At(x)^+$ species can be considered soft acids based on the HSAB theory.[45] Furthermore, the β_{m,X^-}-values obtained from the competition experiments are in good agreement with the theoretical calculation results.

Table 1.5. Thermodynamic constants of the equilibria considered for modeling astatine behavior in the presence of Cl^-, Br^-, and SCN^-.[45,61]

$At(x)^+$	At^+			AtO^+		
X^-	Cl^-	Br^-	SCN^-	Cl^-	Br^-	SCN^-
$Lg\beta_{1,X^-}$	1.9 ± 0.2	3.0 ± 0.2	3.8 ± 0.2	2.5 ± 0.2	2.7 ± 0.2	2.8 ± 0.2
$Lg\beta_{2,X^-}$	2.3 ± 0.1	4.1 ± 0.3	5.9 ± 0.3	3.0 ± 0.3	5.0 ± 0.2	5.3 ± 0.2

1.3.3. Interaction between astatine metal cations and organic ligands

The interactions between $At(x)^+$ and organic ligands, such as EDTA (ethylenediaminetetraacetic acid), DTPA (diethylenetriaminepentaacetic acid), tetramercaptocalix[4]arene and thiacalix[4]arenetetrasulfonate, have been investigated through electromigration, HPLC and competition methodologies.[61–64] As expected, these studies indicate the possibility of an interaction between $At(x)^+$ and organic molecules. However, ^{211}At-tetramercaptocalix[4]arene is unstable *in vivo* and cannot be applied to nuclear medicine.[64] At (I) and At (III) can form 1:1 and 1:2 complexes with thiacalix[4]arenetetrasulfonate; the associated equilibrium constants are detailed in the same work. It was also shown that the interaction strength for At (I) is slightly higher than for At (III).[61]

1.4. Motivations

In this work, the fundamental aspects of astatine chemistry are studied further using the approach initiated by J. Champion.[46] This combines both experimental and theoretical methods in order to identify At species. My work is mainly

focused on At (–I) and At (+I).

The At^- species is of interest for radiolabeling purposes. It can form ^{211}At-labeled molecules by the nucleophilic substitution reaction. It is therefore important to be aware of the dominant existence of this species. At^- is expected to exist in the whole pH range and for a wide range of *E* values as well, according to the Pourbaix diagram of the other halogens (F, Cl, Br and I). However, it was recently reported that another anionic species is thought to exist above pH 7, *i.e.* $AtO(OH)_2^-$, in weak oxidizing conditions.[51] Moreover, the existence of At^- has not yet been proved, and this is the starting point to "build" the Pourbaix diagram of At by Champion *et al.*. The first objective of this work is to use an electromigration device to derive the mobility at infinite dilution of the At species in acidic reducing conditions. This mobility can be compared with the trend expected to confirm the existence of At^-.

Revealing the interactions of At^+ with halides has been the subject of a certain number of research works. At^+ forms binary 1:1 and 1:2 stoichiometry complexes with Cl^-, Br^- and I^-.[45,60] It is expected to form species containing ternary halogens. However, only one form has been reported corresponding to $BrICl^-$.[65] Thus, the second objective of my work is to assess the possible existence of a ternary trihalogen species involving At, $IAtBr^-$. This is a challenging task as, besides the use of ultra-trace concentrations, a new species has to be identified among at least four others, *i.e.* AtBr, AtI, $AtBr_2^-$ and AtI_2^-. In this work, the originality of the approach is to predict the predominant domain in order to guide the experimental manipulation.

Thirdly, the halogen family is characterized by the possibility of forming halogen bonds. This is a specific non-covalent interaction between halogen atoms (Lewis acids) and Lewis bases. F, Cl, Br and I are capable of forming halogen bonds as halogen bond donors, with the trend of F < Cl < Br <I. Iodine is considered to form the strongest halogen bond.[66] Astatine certainly belongs to the halogen group and is assumed to form a stronger halogen bond than iodine, according to the former trend. This was recently predicted through theoretical calculations.[67,68] The challenge is to develop a methodology to show the

existence of such a bond by combining experimental and theoretical studies. The work will focus on AtI species whose domain of predominance can be deduced from the results of the previous part.

References

(1) Edwards, C. L. In *Seminars in nuclear medicine*; WB Saunders, 1979; Vol. 9, pp 186–189.

(2) Seidlin, S. M.; Marinelli, L. D.; Oshry, E. *J. Am. Med. Assoc.* **1946**, *132* (14), 838.

(3) Seaborg, G. T.; Segrè, E. *Phys. Rev.* **1939**, *55* (9), 808.

(4) Milenic, D. E.; Brady, E. D.; Brechbiel, M. W. *Nat. Rev. Drug Discov.* **2004**, *3* (6), 488.

(5) Rodriguez, E. A.; Wang, Y.; Crisp, J. L.; Vera, D. R.; Tsien, R. Y.; Ting, R. *Bioconjug. Chem.* **2016**, *27* (5), 1390.

(6) Hallaba, E.; El-Asrag, H.; Zeid, Y. A. *Int. J. Appl. Radiat. Isot.* **1970**, *21* (2), 107.

(7) Liu, S. *Adv. Drug Deliv. Rev.* **2008**, *60* (12), 1347.

(8) McDevitt, M.; Sgouros, G.; Finn, R. *Eur. J. Nucl. Med.* **1998**, *25* (9), 1342.

(9) Hall, E. J.; Giaccia, A. J. *Radiobiology for the Radiologist*, 6th ed.; Lippincott Williams & Wilkins, 2006.

(10) Johnson, E. L.; Turkington, T. G.; Jaszczak, R. J.; Gilland, D. R.; Vaidyanathan, G.; Greer, K. L.; Coleman, R. E.; Zalutsky, M. R. *Nucl. Med. Biol.* **1995**, *22* (1), 45.

(11) Turkington, T. G.; Zalutsky, M. R.; Jaszczak, R. J.; Garg, P. K.; Vaidyanathan, G.; Coleman, R. E. *Phys. Med. Biol.* **1993**, *38* (8), 1121.

(12) Garg, P. K.; Harrison, C. L.; Zalutsky, M. R. *Cancer Res.* **1990**, *50* (12), 3514.

(13) Lundh, C.; Lindencrona, U.; Schmitt, A.; Nilsson, M.; Forssell-Aronsson, E. *Cancer Biother. Radiopharm.* **2006**, *21* (6), 591.

(14) Vaughan, A. T. M.; Fremlin, J. H. *Int. J. Nucl. Med. Biol.* **1978**, *5* (6), 229.

(15) Vaidyanathan, G.; Affleck, D. J.; Alston, K. L.; Zhao, X.; Hens, M.; Hunter, D. H.; Babich, J.; Zalutsky, M. R. *Bioorg. Med. Chem.* **2007**, *15* (10), 3430.

(16) Narula, A. S.; Zalutsky, M. R. *Radiochim. Acta* **1989**, *47* (2–3), 131.

(17) Zalutsky, M.; Reardon, D. *J. Nucl. Med.* **2008**, *49* (1), 30.

(18) Norseyev, Y. V. *J. Radioanal. Nucl. Chem.* **1998**, *237*, 155.

(19) Ã, G. J. M.; Walte, A.; Sriyapureddy, S. R.; Grote, M.; Krull, D.; Korkmaz, Z.; Knapp, W. H. *Appl. Radiat. Isot.* **2010**, *68* (6), 1060.

(20) Wunderlich, G.; Fischer, S.; Dreyer, R.; Franke, W. G. *J. Radioanal. Nucl. Chem. Lett.* **1987**, *117* (4), 197.

(21) Visser, G. W. M.; Diemer, E. L. *Radiochem. Radioanal. Lett.* **1982**, *51* (3), 135.

(22) Wilbur, D. S.; Hamlin, D. K.; Chyan, M.-K.; Kegley, B. B.; Quinn, J.; Vessella, R. L. *Bioconjug. Chem.* **2004**, *15* (3), 601.

(23) Wilbur, D. S.; Chyan, M.-K.; Hamlin, D. K.; Kegley, B. B.; Risler, R.; Pathare, P. M.; Quinn, J.; Vessella, R. L.; Foulon, C.; Zalutsky, M.; Wedge, T. J.; Hawthorne, M. F. *Bioconjug. Chem.* **2004**, *15* (1), 203.

(24) Wilbur, D. S.; Chyan, M.-K.; Hamlin, D. K.; Vessella, R. L.; Wedge, T. J.; Hawthorne, M. F. *Bioconjug. Chem.* **2007**, *18* (4), 1226.

(25) Pruszyński, M.; Bilewicz, A.; Wąs, B.; Petelenz, B. *J. Radioanal. Nucl. Chem.* **2006**, *268* (1), 91.

(26) Pruszyński, M.; Bilewicz, A.; Zalutsky, M. R. *Bioconjug. Chem.* **2008**, *19* (4), 958.

(27) Pruszyński, M.; Łyczko, M.; Bilewicz, A.; Zalutsky, M. R. *Nucl. Med. Biol.* **2015**, *42* (5), 439.

(28) Pearson, R. G. *J. chem. Educ* **1968**, *45* (9), 581.

(29) Pearson, R. G. *J. chem. Educ* **1968**, *45* (10), 643.

(30) Ayed, T.; Pilmé, J.; Tézé, D.; Bassal, F.; Barbet, J.; Chérel, M.; Champion, J.; Maurice, R.; Montavon, G.; Galland, N. *Eur. J. Med. Chem.* **2016**, *116*, 156.

(31) Corson, D. R.; MacKenzie, K. R.; Segre, E. *Phys. Rev.* **1940**, *58* (8), 672.

(32) Davis, H. M.; Seaborg, G. T. *The Chemical Elements*, 2ed ed.; Science Service, 1964.

(33) Fry, C.; Thoennessen, M. *At. Data Nucl. Data Tables* **2013**, *99* (5), 497.

(34) Emsley, J. *Nature's Building Blocks: An A-Z Guide to the Elements*; 2011.

(35) Wiberg, E.; Wiberg, N. *Inorganic Chemistry*; Nils, W., Ed.; Academic Press, 2001.

(36) Vaidyanathan, G.; Zalutsky, M. R. *Curr. Radiopharm.* **2008**, *1* (3), 177.

(37) Berei, K.; Eberle, S. H.; Kirby, H. W.; Munzel, H.; Rossler, K.; Seidel, A.; Vasaros, L. *Handbook of inorganic chemistry-astatine*, 8th ed.; 1985.

(38) Zalutsky, M. R.; Pruszynski, M. *Curr. Radiopharm.* **2011**, *4* (3), 177.

(39) Morzenti, S.; Bonardi, M. L.; Groppi, F.; Zona, C.; Persico, E.; Menapace, E.; Alfassi, Z. B. *J. Radioanal. Nucl. Chem.* **2008**, *276* (3), 843.

(40) Yordanov, A. T.; Pozzi, O.; Carlin, S.; Akabani, G.; Wieland, B.; Zalutsky, M. R. *J. Radioanal. Nucl. Chem.* **2004**, *262* (3), 593.

(41) Roy, K.; Basu, S.; Ramaswami, A.; Nayak, D.; Lahiri, S. *Appl. Radiat. Isot.* **2004**, *60* (6), 793.

(42) Lindegren, S.; Bäck, T.; Jensen, H. J. *Appl. Radiat. Isot.* **2001**, *55* (2), 157.

(43) Zalutsky, M. R.; Zhao, X.; Alston, K. L.; Bigner, D. *J. Nucl. Med.* **2001**, *42* (10), 1508.

(44) Alliot, B. C.; Cherel, M.; Barbet, J.; Sauvage, T.; Montavon, G. *Radiochim. Acta* **2009**, *97*, 161.

(45) Champion, J.; Seydou, M.; Sabatié-Gogova, A.; Renault, E.; Montavon, G.; Galland, N. *Phys. Chem. Chem. Phys.* **2011**, *13* (33), 14984.

(46) Champion, J.; Alliot, C.; Renault, E.; Mokili, B. M.; Chérel, M.; Galland, N.; Montavon, G. *J. Phys. Chem. A* **2010**, *114* (1), 576.

(47) Sabatié-Gogova, A.; Champion, J.; Huclier, S.; Michel, N.; Pottier, F.; Galland, N.; Asfari, Z.; Chérel, M.; Montavon, G. *Anal. Chim. Acta* **2012**, *721*, 182.

(48) Champion, J.; Sabatié-Gogova, A.; Bassal, F.; Ayed, T.; Alliot, C.; Galland, N.; Montavon, G. *J. Phys. Chem. A* **2013**, *117* (9), 1983.

(49) Roessler, K.; Tornau, W.; Stoecklin, G. *J. Radioanal. Chem.* **1974**, *21*, 199.

(50) Dreyer, I.; Dreyer, R.; Chalkin, V. A. *J. Radiochem. Radioanal. Lett.* **1978**, *35* (6), 257.

(51) Sergentu, D. C.; Teze, D.; Sabatié-Gogova, A.; Alliot, C.; Guo, N.; Bassal, F.; Silva, I. Da; Deniaud, D.; Maurice, R.; Champion, J.; Galland, N.; Montavon, G. *Chem. - A Eur. J.* **2016**, *22* (9), 2964.

(52) Appelman, E. *J. Phys. Chem.* **1961**, 325.

(53) Appelman, E.; Sloth, E.; Studier, M. *Inorg. Chem.* **1966**, *5* (5), 766.

(54) Norseyev, Y. V.; Khalkin, V. A. *J. Inorg. Nucl. Chem.* **1968**, *351* (3), 3239.

(55) Tyung, D. K.; Dudova, I. V.; Khalkin, V. A. *Sov. Radiochem.* **1973**, *15* (4), 552.

(56) Dreyer, R.; Dreyer, I.; Pfeiffer, M.; Roesch, F. *J. Radiochem. Radioanal. Lett.* **1982**, *55* (4), 207.

(57) Dreyer, R.; Dreyer, I.; Fischer, S.; Hartmann, H.; Rosch, F. *Joural Radioanal. Nucl. Chem. Lett.* **1985**, *96* (3), 333.

(58) Dreyer, R.; Dreyer, I.; Rosch, F.; Beyer, G.-J. *J. Radiochem. Radioanal. Lett.* **1982**, *54* (3), 165.

(59) Fischer, S.; Dreyer, R.; Albrecht, S. *Joural Radioanal. Nucl. Chem. Lett.* **1987**,

117 (5), 275.

(60) Ludwig, R.; Fischer, S.; Hussein, H.; Frind, M.; Dreyer, R. *J. Radioanal. Nucl. Chem. Artic.* **1989**, *134*, 141.

(61) Champion, J.; Alliot, C.; Huclier, S.; Deniaud, D.; Asfari, Z.; Montavon, G. *Inorganica Chim. Acta* **2009**, *362* (8), 2654.

(62) Milesz, S.; Jovchev, M.; Schumann, D.; Khalkin, V. A.; Milanov, M. *Joural Radioanal. Nucl. Chem. Lett.* **1988**, *127* (3), 193.

(63) Milesz, S.; Norseyev, Y. V.; Szucs, Z.; Vasaros, L. *Joural Radioanal. Nucl. Chem. Lett.* **1989**, *137* (5), 365.

(64) Yordanov, A. T.; Deal, K.; Garmestani, K.; Kobayashi, H.; Herring, B.; Waldmann, T. A.; Brechbiel, M. W. *J. Label. Compd. Radiopharm.* **2000**, *43*, 1219.

(65) Guidelli, R.; Pergola, F. *J. Inorg. Nucl. Chem.* **1969**, *31* (1964), 1373.

(66) Politzer, P.; Lane, P.; Concha, M. C.; Ma, Y.; Murray, J. S. *J. Mol. Model.* **2007**, *13* (2), 305.

(67) Alkorta, I.; Blanco, F.; Solimannejad, M.; Elguero, J. *J. Phys. Chem. A* **2008**, *112* (43), 10856.

(68) Hill, J. G.; Hu, X. *Chem. - A Eur. J.* **2013**, *19* (11), 3620.

Chapter 2. First experimental evidence for the highest expected halide species in aqueous solution, At^-, by electromobility measurements

2.1. Abstract

At^- (astatide) is commonly expected to be the heaviest halide in the halogen group. However, there is no proof for the existence of this minus one charged species. Furthermore, investigations with astatine are restricted by its specific radioactive properties, which entail working at ultra-trace concentrations (typically less than 10^{-10} M). In this work, a homemade electromigration device is constructed and applied to obtain information about the charge/size ratio characterizing an ion in aqueous solution. An anionic At species is observed in reducing conditions. Moreover, we propose the first absolute mobility value for the At^- species: $(-8.3 \pm 0.8) \times 10^{-4}$ $cm^2V^{-1}s^{-1}$. This value appears close to that of I^- ($(-8.3 \pm 1.0) \times 10^{-4}$ $cm^2V^{-1}s^{-1}$), which is obtained through the same method. Since the theoretical calculation indicates the similar diffusion behavior for At^- and I^-, the similar absolute mobilities for the two ions obtained in this work confirm the existence of the At^- species.

2.2. Introduction

Astatine, element 85, is below iodine in the periodic table. One of its isotopes, At-211, is of great interest as a potential alpha-emitting therapeutic agent for nuclear medicine.[1] The specific radioactive properties of At-211 make it an effective candidate for targeted alpha therapy. A pre-requisite is to bind At-211 in a stable manner to a carrier-targeting agent.[2] Although this has triggered a

great deal of investigation, the basic physical and chemical properties of astatine are still poorly known.[3] The chemistry of At is commonly estimated as a heavier halogen analogue since there is no doubt that At belongs to the halogen group. However, compared to the lighter halogens, it also presents a metallic behavior.[4] From a chemist's point of view, it remains difficult to work on the chemistry of At in aqueous solution: on one hand, it does not have a long half-life radioactive isotope; on the other hand, it can only be worked with at ultra-trace concentrations (typically less than 10^{-10} M). Therefore, no spectroscopic tool can be used to identify the species of astatine at the molecular level. Thus, some indirect methods, such as competition,[4] high performance anion exchange chromatography (HPAEC) coupled to a gamma detector[5] and electromigration[6] have been proposed to investigate astatine species in non-complex and complex media.

Through the competition method combined with theoretical calculation, two At chemical forms have been revealed in oxidizing acid medium: At^+ and AtO^+ considering that At^- is the species that exists in reducing conditions. In the same work, the redox potential of At^-/At^+ and AtO^+/At^+ couples was determined with the respective values being 0.36 ± 0.01 and 0.74 ± 0.01 V *vs.* NHE (Normal Hydrogen Electrode).[4] The existence of At^- is assumed considering its location in the periodic table in the halogen group and an anionic species has been shown by different indirect methods.[5,7] However, no proof has been provided to identify the At^- species in aqueous solution. More recently, the charge of the At species in reducing acid medium was thought to be minus 1 by HPAEC coupled to a gamma detector, from analyzing the retention factor as a function of the ionic strength.[5] The objective of this work is to complete the current data by means of the electromigration method.

The mobility of an ion at infinite aqueous dilution, *i.e*. the absolute mobility, is a specific parameter of the ion, which depends on its size/charge ratio. It has been demonstrated that the absolute mobilities of lighter halides (F^-, Cl^-, Br^-, I^-) are related to their ionic radius.[8] Numerous conductance data of the halides (F^-, Cl^-, Br^-, I^-) can be found in the literature at 25 °C and infinite dilution but, to date, no critical evaluation has been performed. In addition, the mean values of the

absolute mobilities increase with the increase in ionic radius. The relationship between the absolute mobilities of the halides and their ionic radii has been reproduced through molecular dynamics simulation.[8] Recently, the diffusion coefficient of astatine was also calculated, giving a value of 1.88×10^{-5} cm^2s^{-1}, indicating a slight fall with respect to I^- (1.99×10^{-5} cm^2s^{-1}).[9] The measurement of the absolute mobility can thus be a value to verify the existence of At^-. Note that the term "At^-" will be used throughout this manuscript to indicate that At^- is the species expected in the studied medium, but proof is needed. However, to date, no experimental mobility of astatine at zero ionic strength has been given in the literature. In the 1970s and 1980s, Dreyer *et al.* found that the mobility of At species was quite distinct in different electrolytes and at different ionic strengths: $(-6.1 \pm 0.2) \times 10^{-4}$ $cm^2V^{-1}s^{-1}$ in 0.04 M KNO_3 and $(-7.4 \pm 0.2) \times 10^{-4}$ $cm^2V^{-1}s^{-1}$ in 0.05 M NaOH.[6,7,11,12] Nonetheless, these apparent mobility values cannot be extrapolated to zero ionic strength. In fact, they are reported without being corrected for electroosmosis. The previous investigations into the mobility of astatine are summarized in Table 2.1.

Table 2.1. Non-corrected apparent mobility of At (–I) in different media.

Ref	Medium	pH	E (V *vs.* NHE)	μ ($\times 10^{-4}$ $cm^2V^{-1}s^{-1}$)
7	0.04 M KNO_3	7	0.5	–6.1 ± 0.2
6	0.04 M KNO_3	7	0.5	–6.0
10	0.02 M $(NH_4)_2CO_3$, 0.015 M NH_4OH	–	–	–7.2 ± 0.2
12	0.05 M NaOH	~ 13	0.1	–7.4 ± 0.2
	0.1 M NaOH	~ 13	0.1	–7.2 ± 0.2

In this work, a homemade electromigration device was developed in order to: 1) identify the astatine species in a given reducing medium; 2) measure the mobility of At^- under experimental conditions eliminating the effect of electroosmosis; 3) obtain the absolute mobility of At^- through Onsager-Fuoss

treatment. Preliminary experiments were performed with I^- and F^- in order to validate the methodology.

2.3. Materials and methods

2.3.1. Materials

2.3.1.1. Chemicals

Commercially available sodium chloride, hydrochloric acid, magnesium chloride hexahydrate, sodium sulfite and sodium thiosulfate pentahydrate (Sigma-Aldrich) were used; all of these regents were of analytical grade. All solutions were prepared using Milli-Q water and all experiments were conducted at 22 ± 3 °C.

2.3.1.2. Radioactive sources

NaI-123, F-18DG and NaF-18

Iodine-123 ($T_{1/2}$ = 13.2 h) and fluorine-18 ($T_{1/2}$ = 109.8 min) were obtained commercially from IBA Molecular (Rennes, France). 18.5 MBq/mL of sodium iodide-123 was obtained in 1 mL of water with a radiochemical purity ≥ 95 %. Sodium fluoride-18 or fludeoxyglucose labeled with F-18 (F-18DG) were obtained in 0.50 mL of sodium chloride solution with an activity of 185 MBq/mL and a radiochemical purity ≥ 95 %.

Production of At-211

At-211 was produced by the ARRONAX cyclotron (Nantes, France) *via* the ^{209}Bi(α, 2*n*) ^{211}At reaction. The bismuth target was irradiated with an alpha external beam accelerated to 28 MeV for two hours.[13] A dry distillation method was used to isolate At-211 from the irradiated target, and then 10 MBq of At-211 was extracted into 200 µL of chloroform.[14] The radionuclide purity of At-211 was verified by gamma-ray spectroscopy with a high purity germanium (HPGe) detector.

Preparation of the samples

After reception of the At-211 source in chloroform (~ 50 MBq/mL), a few steps were carried out in order to obtain At in the desired medium. First, chloroform was vaporized under a stream of nitrogen. In this step, a Schott bottle containing 100 mL of 0.1 M Na_2SO_3 was used as the tail gas recovery facility to avoid the escape of astatine. Note that after this step, the recovery solution was checked by liquid scintillation counting, showing no activity loss with the nitrogen flow. Secondly, 500 µL of a 10^{-3} M Na_2SO_3 solution was added and heated to 100 °C for half an hour in a closed vessel to obtain At in the aqueous phase. Thirdly, the solution was left for 0.5 hour to cool down. Lastly, astatine was obtained in 500 µL of 10^{-3} M Na_2SO_3 solution (pH = 7.0 ± 0.1, E = 0.40 ± 0.03 V *vs*. NHE) and the main species turned into –I charge based on the previously established Poubaix diagram (E–pH) of astatine.[4,15,16]

The reducing medium for At electromobility measurement was composed of 0.1 M NaCl, 0.01 M HCl and 10^{-3} M $Na_2S_2O_3$ (pH = 2.0 ± 0.1, E = 0.40 ± 0.03 V *vs*. NHE). In order to use the Onsager-Fuoss treatment, which needs a symmetrical electrolyte, 10^{-3} M $MgCl_2$ was added to the medium.[17]

Astatine species were characterized by HPAEC coupled to a gamma detector using an eluent composed of 0.1 M NaCl, 0.01 M HCl and $10^{-3}/10^{-4}$ M $S_2O_3^{2-}/SO_3^{2-}$ with a flow rate of 350 µL/min through an AS20 column.[5] As shown in Figure 2.1, one peak was observed indicating the presence of one species. The retention time of the species in both the stock solution and the reducing medium applied in this work corresponded to that in the medium previously studied (0.1 M NaCl, 0.01 M HCl and $10^{-3}/10^{-4}$ M $S_2O_3^{2-}/SO_3^{2-}$ solution), in which the astatine species was thought to be At^-.[5]

An electrode (Inlab) freshly calibrated with standard pH buffers (pH 4.00 and 7.00, Merck) and a Pt combined redox electrode (Metrohm) calibrated with a redox buffer ($Fe(SCN)_6^{3-}/Fe(SCN)_6^{4-}$, 220 mV/Pt/SCE, Radiometer Analytical) were used to measure the pH and the potential of the electrolyte solution and the samples, respectively.

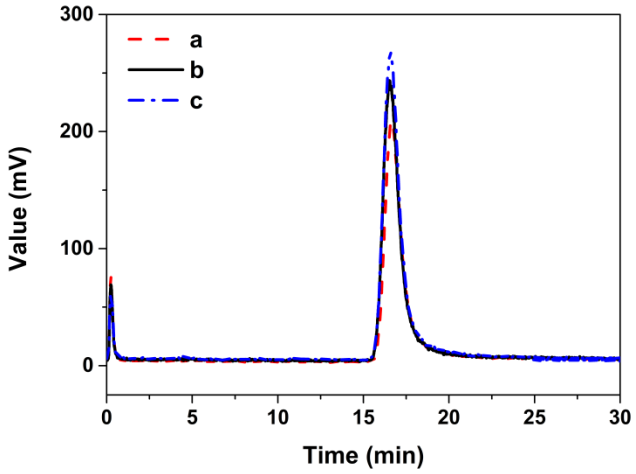

Figure 2.1. At species characterization with 350 µL/min of eluent containing 0.1 M NaCl, 0.01 M HCl and $10^{-3}/10^{-4}$ M $S_2O_3^{2-}/SO_3^{2-}$ on three samples: a. At in 0.1 M NaCl, 0.01 M HCl and $10^{-3}/10^{-4}$ M $S_2O_3^{2-}/SO_3^{2-}$; b. At in 0.1 M NaCl, 0.01 M HCl, 10^{-3} M $MgCl_2$ and 10^{-3} M $Na_2S_2O_3$; and c. At in 10^{-3} M Na_2SO_3.

2.3.2. Methods

2.3.2.1. Electromobility device

The device for measuring radioactive ion mobility in free electrolyte was developed by Milanov *et al.*[18] and similar equipment was built by ourselves to investigate the mobility of fluorine, iodine and astatine ions. The diagram of the device is shown in Figure 2.2. The sample is injected through the outlet 01 and migration takes place in the horizontal glass tube, which is 500 mm long with an inner diameter of 3 mm. The two electrolyte cells (b) and the migration tube are filled with electrolyte. A water bath system is used to maintain the temperature of the electrolyte in both the migration tube and the electrolyte cells. Additionally, a thermosensor (f) connected to a thermostat is inserted into the electrolyte to calibrate the temperature (25 ± 1°C). The hydrodynamic resistors (c, nitrocellulose membrane, 220 nm) are connected between the migration tube and the electrolyte cells to prevent the transfer of rotational and laminar flows from the cells into the tube. Furthermore, to hinder the liquid flow caused by hydrostatic pressure, electrolyte cells are linked by a PVC tube through the

bottom 07. Pt-electrodes (d) with protective glass cylinders (e) are inserted into the cells, and connected to the power supplies (HCP series, FuG Elektronik GmbH) providing a high voltage in the range of 125-2000 V. In this work, the voltage applied to the electromigration device was set at 445 ± 3 V. The voltage-measuring electrodes are inserted into the electrolyte through the outlets 02 to set the electric field intensity. The actual voltage applied in the migration tube is shown by a digital multimeter (Française d'Instrumentation). The electrolyte solution inside the electrolyte cells can be refreshed by pumping out near the Pt-electrodes through outlets 05 and in through outlets 06 with a 4-channel tubing pump (ISMATEC), in order to ensure the constancy of the electrolyte composition in the cells, especially the pH and ionic strength. A gamma ray detector (Raytest, controlled by the modified GITA STAR system) is employed to monitor the radioactivity along the migration tube back and forth at a fixed speed of 37 s per scan. The detector sensor is a BGO crystal with a photomultiplier tube that detects gamma and high beta radiation with a 15 mm tungsten collimator. For the online data recording, the computer program Elphi is used running under Windows. After each scan, the software reads the data from the detector. The detection system works with the following radionuclides: I-123 (E_γ = 159 keV, ~500 kBq), F-18 (E_γ = 511 keV, ~500 kBq) and At-211 (E_γ = 687 keV, ~500 kBq).

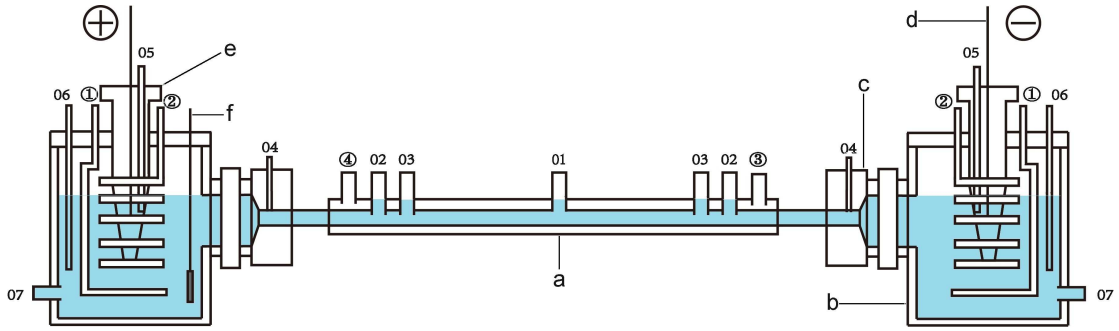

Figure 2.2. Diagram of the electromobility set-up. a. migration tube; b. electrolyte cells; c. hydrodynamic resistor; d. Pt-electrode; e. glass cylinder; f. thermosensor; 01. outlet for the injection of solution containing radioactive sample; 02. outlets used to insert the voltage-measuring electrodes; 03. outlets used to measure the temperature of the medium inside the migration tube with a thermometer probe; 04. outlet for filling the migration tube with the electrolyte; 05 and 06. outlets used to refresh the electrolyte in the cells; 07. outlets for the junction of the cells; ①,②,③,④. outlets for the water bath.

2.3.2.2. Data analysis

The data obtained by the Elphi software are the activity of the radionuclide recorded at each position inside the migration tube, reflecting its distribution in the electrolyte as a function of the distance at a given time.

Figure 2.3 shows this activity distribution in the migration tube after the injection of ~500 kBq I-123; the peak/species is located around the injection outlet, which is in the middle of the tube. The peaks obtained from different scans at different times visually show the movement of the species to the positive electrode in the electric field (Figure 2.3). Note that the small peak stuck in the middle of the tube corresponds to the activity remaining in the injection inlet, and this activity is not part of the data interpretation.

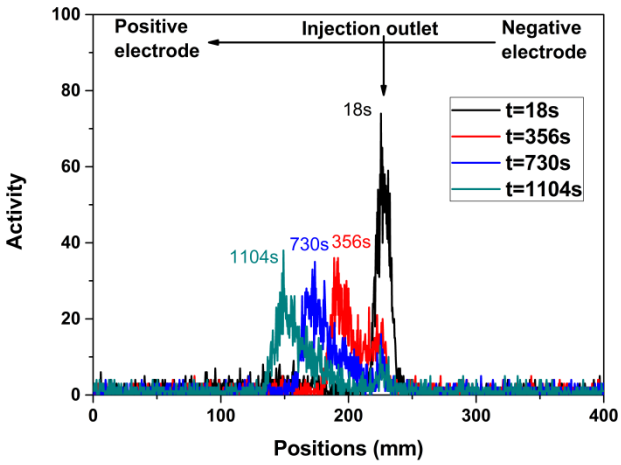

Figure 2.3. Activity of I-123 as a function of the position along the migration tube at different times: I-123 ~ 500 kBq (< 100 µL), *I* = 0.1 M (NaCl), *V* = 7.9 ± 0.1 V/cm, *T* = 25 ± 1 °C.

2.3.2.3. Effect of the electroosmosis

The migration of ions in the experiments is affected by the electroosmosis occurring in the glass electromigration tube of 3 mm inner diameter.[19] Electroosmosis is the motion of the liquid introduced by an applied potential across the tube. In order to quantify the effect of the electroosmosis flow, a neutral species (F-18DG) was introduced. Several experiments were carried out in different electrolytes by injecting ~500 kBq of F-18DG. As seen in Figure 2.4, the movement of the peak is weak but can be clearly observed, which demonstrates the presence of electroosmosis. Furthermore, the values of the electrolyte flow rate inside the migration tube for different samples are not constant (see Table 2.2). They can be positive or negative but are independent of the experimental factors, such as the electrolyte constituent, the ionic strength, pH, or the voltage applied. Thus, in our methodology, F-18DG always accompanied the X^- in order to determine precisely the electroosmosis effect occurring in a given experiment.

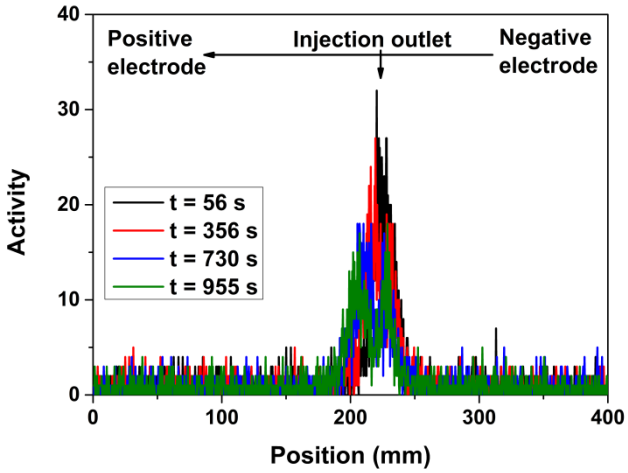

Figure 2.4. Activity of F-18DG as a function of the position along the migration tube at different times: F-18DG ~ 500 kBq (< 10 µL), *I* = 0.1 M (NaCl), *V* = 7.9 ± 0.1 V/cm, *T* = 25 ± 1 °C.

To avoid mixing the two different radionuclides in the same electrolyte, F-18DG was injected after most of the radio-ions (X^-) had moved away from the injection position. An example is given in Figure 2.5 with both I-123 and F-18DG.

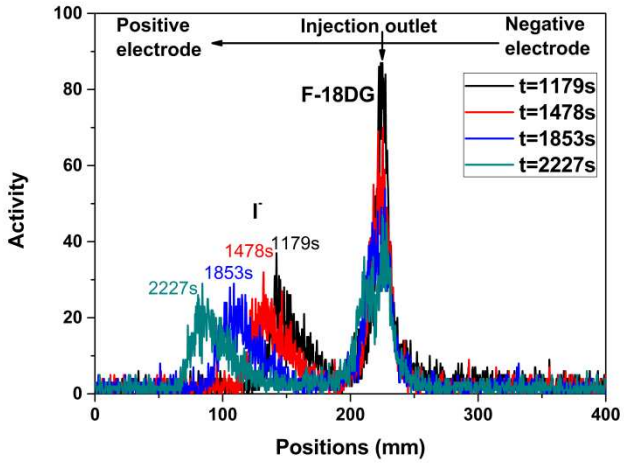

Figure 2.5. Activity of I-123 and F-18DG as a function of the position along the migration tube at different times: I-123 ~ 500 kBq (< 100 µL), F-18DG ~ 500 kBq (< 10 µL), *I* = 0.1 M (NaCl), *V* = 7.9 ± 0.1 V/cm, *T* = 25 ± 1 °C.

Table 2.2. Flow rates of electrolytes in the migration tube represented by F-18DG.

Medium	I (M)	V (V/cm)	μ ($\times 10^{-4}$ $cm^2V^{-1}s^{-1}$)
0.1 M NaCl	0.1	7.9 ± 0.1	−0.3 ± 0.0
pH = 7.0 ± 0.1			1.1 ± 0.1
E = 0.5 ± 0.3 V			−1.2 ± 0.1
			−0.1 ± 0.0
			−1.1 ± 0.1
			0.2 ± 0.0
			−0.3 ± 0.0
			−0.1 ± 0.0
			0.3 ± 0.0
		5.4 ± 0.1	0.4 ± 0.0
		10.3 ± 0.3	0.2 ± 0.0
0.1 M NaCl,	0.116	7.9 ± 0.1	−1.5 ± 0.1
0.01 M HCl,			−0.1 ± 0.0
10^{-3} M $Na_2S_2O_3$,			0.2 ± 0.0
and 10^{-3} M $MgCl_2$			0.4 ± 0.0
pH = 2.0 ± 0.1			0.5 ± 0.0
E = 0.4 ± 0.3 V			0.6 ± 0.0
			0.2 ± 0.0
			0.4 ± 0.0
			0.2 ± 0.0
			0.5 ± 0.0
			−0.1 ± 0.0

After exporting all the scan data to Origin 9.0, the distribution peak obtained for each scan can be approximated with a Gaussian equation in order to identify the maximum peak position (Figure 2.6):

$$f(k,\vec{p}) = p_1 exp\left[-\frac{(k-p_2)^2}{2p_3^2}\right] \quad (2.1)$$

where p_1 is the amplitude, p_2 the centroid of the distribution and p_3 the scatter

parameter. The scatter of the distribution is related to the resolution of the detection system; the full width at half maximum is expressed as FWHM = $2\sqrt{2Ln(2)p_3}$. $\vec{p}$ is the vector shorthand notation for the parameters p_1, p_2 and p_3.

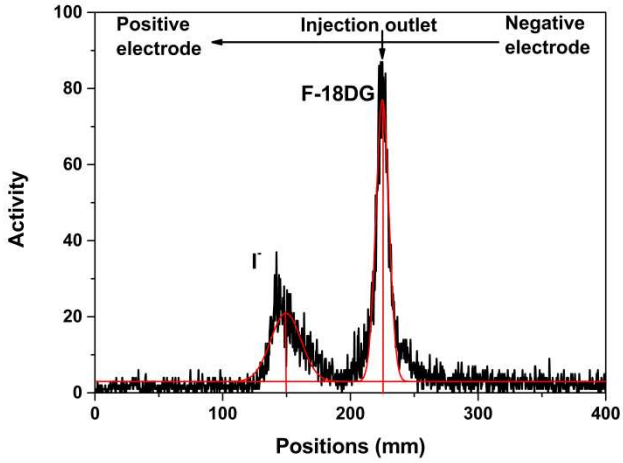

Figure 2.6. Example of Gaussian fitting of the peaks by Origin 9.0; the red line is the Gaussian fitting line.

Then the maximum peak position (P, mm) is plotted as a function of time (t, s) (Figure 2.7) in order to obtain the migration speed (v_a, cm/s) of X^- and F-18DG according to the following equation:

$$P = a + v_a \times 10 \times t \quad (2.2)$$

where a is the intercept of the line.

Finally, the velocity of X^- (v, cm/s) in the electrolyte is:

$$v = v_{a,X^-} - v_{a,F-18DG} \quad (2.3)$$

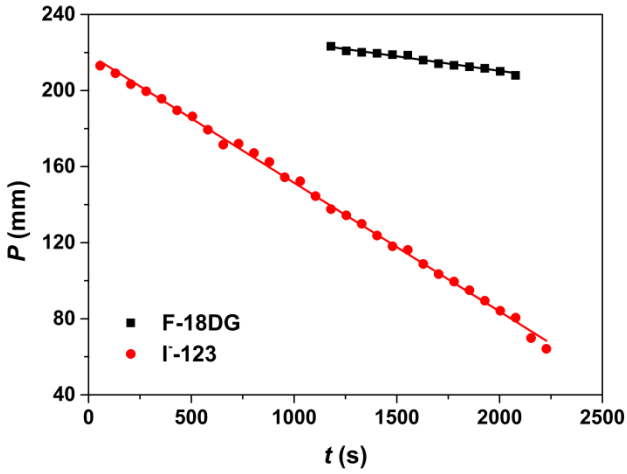

Figure 2.7. Example of data analysis: the position (*P*) as a function of *t* for I^--123 (circles) and F-18DG (squares). The lines are the fitting results using Equation (2.2).

Then the apparent mobility of X^- can be calculated by this equation:

$$\mu_{app} = \frac{v}{V/d} \quad (2.4)$$

where μ_{app} is the apparent mobility of the ion ($cm^2V^{-1}s^{-1}$), *V* is the voltage across the tube (V) and *d* is the distance between the two voltage-measuring electrodes (cm).

The weighted average and its associated uncertainty are calculated according to the following equations:

$$\bar{X} = \frac{\sum_{i=1}^{N}(\frac{X_i}{\sigma_i^2})}{\sum_{i=1}^{N}(\frac{1}{\sigma_i^2})} \quad (2.5)$$

$$\sigma_{\bar{X}} = \sqrt{\frac{1}{\sum_{i=1}^{N}(\frac{1}{\sigma_i^2})}} \quad (2.6)$$

where X_i represents the results obtained from each experiment and σ_i is the corresponding uncertainty; $\bar{X}$ represents the weighted average and $\sigma_{\bar{X}}$ is its associated uncertainty.

2.3.2.4. Onsager-Fuoss model

With the former steps, μ_{app} of X^- is obtained. Then the mobility of X^- in an infinitely dilute solution can be extrapolated from μ_{app} by the Onsager-Fuoss

model:[17,20]

$$\mu_{app} = \mu_0 - \left(\frac{e^3}{12\pi}\sqrt{\frac{N_A}{(\varepsilon kT)^3}}z\mu_0\sum_n C_n R^n + \frac{e^2}{F6\pi\eta}\sqrt{\frac{N_A}{\varepsilon kT}}|z|\right)\frac{\sqrt{I}}{1+\frac{Ba}{\sqrt{2}}\sqrt{I}} \quad (2.7)$$

where μ_{app} ($cm^2V^{-1}s^{-1}$) is the apparent mobility calculated by Equation (2.4), μ_0 is the absolute mobility of the ion ($cm^2V^{-1}s^{-1}$), e is the elementary charge (1.602×10^{-19} C), N_A is the Avogadro constant (6.022×10^{23} mol^{-1}), ε is the permittivity of the solution, k is the Boltzmann constant (1.381×10^{-23} $J{\cdot}K^{-1}$), T is the temperature (K), η is the viscosity of the solution, F is the Faraday constant (96485 C), and a is the parameter representing the distance of closest approach of ions, $B = \sqrt{\frac{2e^2N}{\varepsilon kT}}$, for an aqueous solution at 25 °C, $\frac{Ba}{\sqrt{2}} = 1.5$.[21] c_n is the nth number of a series, which is calculated by the formula $C_n = \frac{\prod_{i=0}^{n-1}(p-i)}{n!} \times \frac{-\sqrt{2}}{2}$ with $C_0 = \frac{1}{2}(2-\sqrt{2})$ and $p = 1/2$; only the first five terms of the series C_n ($n = 5$) will be taken into account.[17] $\boldsymbol{R}^n$ is the nth component of a vector $\boldsymbol{R}$, which is related to the ionic strength of the solution, the absolute mobility of the ion and the molar fraction of all the ions in the solution. $\boldsymbol{R}^n$ is determined by a recursion formula [17]:

$$r_j^n = (2H-1)_{ji}r_i^n \; ; \; r_j^0 = r_j \quad (2.8)$$

with h_{ji} the component of the matrix **H** calculated by the formula:

$$h_{ji} = \delta_{ji}\sum_i \Phi_i \frac{\omega_i}{\omega_i+\omega_j} + \Phi_i\frac{\omega_i}{\omega_i+\omega_j} \quad (2.9)$$

$\delta_{ji} = 1$ for $i = j$ and 0, otherwise, $\omega_i = \frac{\lambda_i^0}{\lambda_i^0+\lambda_j^0}$, and Φ_i is the ionic fraction expressed in concentration.

Effect of temperature (T) and ionic strength (I)

According to the Onsager-Fuoss equation, both the temperature (T) and the ionic strength (I) may affect the calculation using the Onsager-Fuoss model. We take the migration of iodide in NaCl solution as an example to study the effects of T and I. The apparent mobility of iodide as a function of I at 25 °C and as a function of T in 0.1 M NaCl solution were calculated using the Onsager-Fuoss model with the iodide μ_0 value of $(-7.964 \pm 0.008) \times 10^{-4}$ $cm^2V^{-1}s^{-1}$ (see ancillary data

section). The effect of I was significant. In order to keep the relative variation below 0.5 %, the ionic strength should be fixed with a deviation less than 0.01 M. Thus, a relatively large ionic strength equal to or greater than 0.1 M was used in the experimental work, for which such a 10 % deviation is not expected.

The experimental temperature of the electrolyte was maintained at 25 ± 1 °C. As calculated with the Onsager-Fuoss model, the relative variation of the apparent mobility between 24 and 26 °C is less than 0.5 %, which is acceptable. Thus, the effect of T deviation on calculations in our experimental conditions can be ignored.

Effect of permittivity (ε) and viscosity (η) of the electrolyte

The permittivity (ε) and viscosity (η) of the electrolyte are necessary parameters in the Onsager-Fuoss model. However, it is complicated to calculate ε and η for a mixed electrolyte. Thus, it is important to know their effects. For example, if the ionic strength (NaCl) varies in the range ± 0.1 M, the relative variation in ε and η is less than 2.2 % and 0.7 %, respectively. Accordingly, the variation in the apparent mobility of I^- calculated using the Onsager-Fuoss model is less than 0.3 % and 0.1 %, respectively. In this work, the deviation of the ionic strength was maintained far below 0.1 M, so the effect of the ε and η of the electrolyte can be ignored. In this case, the related ε and η of the mixed medium used in this work can be regarded as those of NaCl solution under the same ionic strength.

2.4. Results and discussion

2.4.1. Method validation

The electromigration method was first applied to the measurement of iodide mobility in order to validate it by comparing the experimental results with those of the literature. The mobility of I^- has been investigated by various methods in different electrolytes. Dreyer *et al.* obtained the value of -8.0×10^{-4} $cm^2V^{-1}s^{-1}$ in 0.04 M KNO_3 solution through the electromigration method.[6] With the same method, Milanov *et al.* studied the mobility of I^- in NaOH solution as a function of

the ionic strength in order to extrapolate the μ_0 to give a value of $(-8.15 \pm 0.20) \times 10^{-4}$ $cm^2V^{-1}s^{-1}$.[18] Since the effect of electroosmosis cannot be ignored, a coated capillary was used to investigate the mobility of iodide in a pH 3.5 solution and the value of -7.70×10^{-4} $cm^2V^{-1}s^{-1}$ was proposed considering an electroosmosis flow of 4×10^{-5} $cm^2V^{-1}s^{-1}$.[22] This result is lower than that evaluated from the literature data (see ancillary data).

2.4.1.1. I-123 and F-18DG system

Repeatability study

The behavior of iodide in 0.1 M NaCl solution with the electromigration device was studied with several samples. Iodide migration is reflected by the difference between the movement of I-123 and F-18DG. A dozen absolute mobility values of I^- extrapolated from experimental outcomes using the Onsager-Fuoss model are shown in Figure 2.8. The corresponding velocity and permittivity values are presented in Table 2.3. The average value of I^- μ_0 obtained was -8.3×10^{-4} $cm^2V^{-1}s^{-1}$ with a 2σ uncertainty of 1.0×10^{-4} $cm^2V^{-1}s^{-1}$, corresponding to a 95 % confidence interval. This value is in good agreement with the literature one ($(-7.964 \pm 0.008) \times 10^{-4}$ $cm^2V^{-1}s^{-1}$).

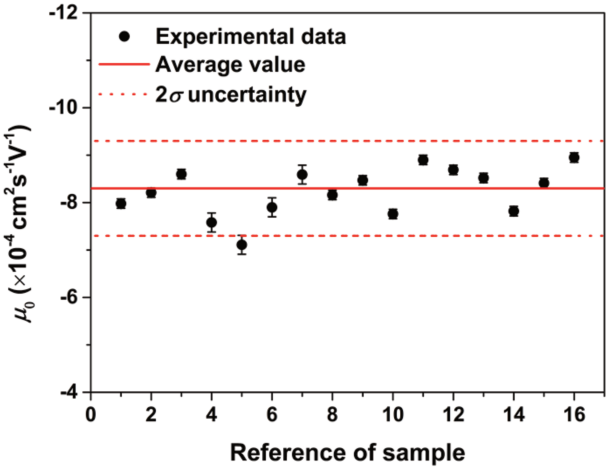

Figure 2.8. The absolute mobility (μ_0) of I^- extrapolated from the experimental outcomes as a function of the sample reference: the solid line corresponds to the average value of -8.3×10^{-4} $cm^2V^{-1}s^{-1}$ and the dashed lines represent the 2σ uncertainty interval.

Effect of injection volume

The sources of NaI-123 and F-18 (F-18DG or NaF-18) were commercially available with high voluminal activity at the reception time, *i.e.* 18.5 MBq/mL and 185 MBq/mL for I-123 and F-18 sources, respectively. The injection of these two isotopes can be managed with a tiny volume. In the case of At-211, the volume is constrained by the multistep manipulations to obtain At in the required solution. We were therefore interested to define the maximum injection volume to ensure that the migration behavior of At would not be affected by the injection manipulation.

The absolute mobility of iodide as a function of the injection volume is given in Figure 2.9 in which the solid and dashed lines represent the average μ_0 obtained previously in this work and the corresponding 2σ uncertainty range, respectively. The results clearly show that the μ_0 of I^- obtained through the electromigration method falls within the expected area when the injection volume is less than 100 µL. Consequently, the injection volume of all the samples should be restricted to below 100 µL.

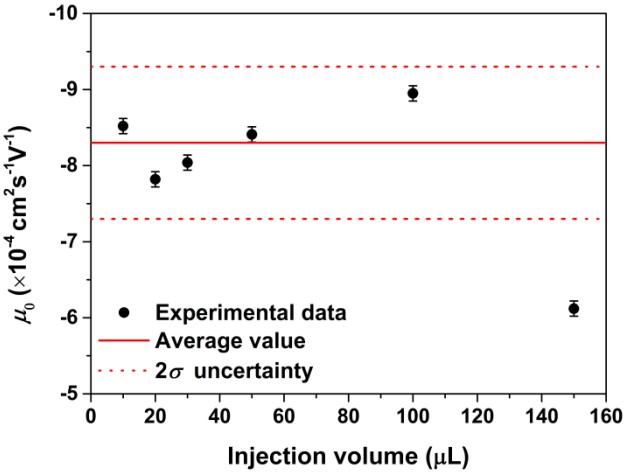

Figure 2.9. The absolute mobility (μ_0) of I^- extrapolated from the experimental outcomes as a function of the injection volume: the solid line is the average value of -8.3×10^{-4} cm^{2}V^{-1}s^{-1} and the dashed lines represent the 2σ uncertainty range.

Voltage effect

The effect of the voltage applied on the migration tube was also checked. Various values ranging from 5.5 to 10.5 V/cm were employed in the electromigration experiments. The absolute mobility of I^- determined as a function of voltage is shown in Figure 2.10. As expected, no significant effect was observed. The voltage applied in this work was 7.9 ± 0.1 V/cm.

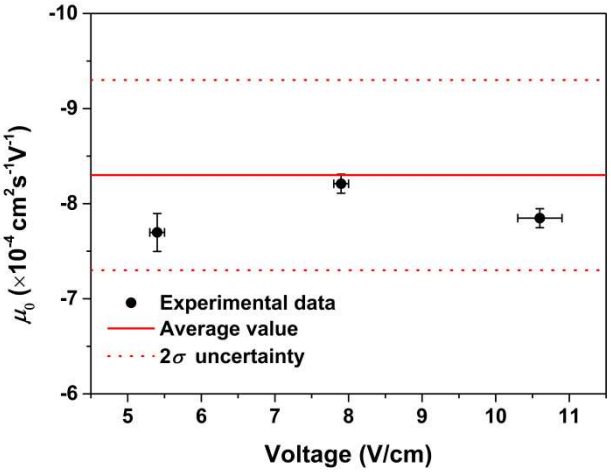

Figure 2.10. The absolute mobility (μ_0) of I^- extrapolated from the experimental outcomes as a function of the voltage: solid line is the average value of -8.3×10^{-4} $cm^2V^{-1}s^{-1}$ and the dashed lines represent the 2σ uncertainty range.

Simplification of the reducing medium parameters

The reducing medium used to obtain At^- species in this work was composed of 0.1 M NaCl, 0.01 M HCl, 10^{-3} M $Na_2S_2O_3$, and 10^{-3} M $MgCl_2$, with an ionic strength of 0.116 M. The corresponding parameters of this reducing medium, *i.e.* velocity and permittivity, are difficult to obtain, but are necessary when extrapolating the absolute mobility using the Onsager-Fuoss model. It would be easier to use the parameters of a 0.116 M NaCl solution. The migration behavior of I^- in this reducing medium was studied and simplified parameters were employed to extrapolate its absolute mobility. The average μ_0 of I^- calculated from the experimental outcomes in this condition was $(-7.9 \pm 0.4) \times 10^{-4}$ $cm^2V^{-1}s^{-1}$. This value is in reasonable agreement with the one obtained above in 0.1 M NaCl solution ($(-8.3 \pm 1.0) \times 10^{-4}$ $cm^2V^{-1}s^{-1}$), given the respective experimental

uncertainties. Therefore, the effects of velocity and permittivity were experimentally confirmed as not significant under the given experimental conditions and the parameters of the reducing medium could be simplified to those of a 0.116 M NaCl solution, which is shown in Table 2.3.

2.4.1.2. I-123 and F-18 system

The absolute mobility of X^- can also be obtained through the mobility differences between X^- and I^-, since the μ_0 of I^- has already been obtained experimentally. Furthermore, the electroosmosis effect can be corrected through the calculation of the difference between the X^- and I^- mobilities.

The electromigration of I-123 and F-18 was investigated at the same time in 0.1 M NaCl solution. I-123 was first injected into the migration tube and after it had moved away from the injection outlet, F-18 was added to the same electrolyte. The difference between the movements of the two anions was recorded. With time, the distance between the two different peaks that represent I-123 and F-18 increased; it can be directly calculated that F-18 moves slower than I-123 under the same experimental conditions. The difference in the absolute mobilities between F^- and I^- obtained was $(-2.4 \pm 1.0) \times 10^{-4}$ $cm^2V^{-1}s^{-1}$. Knowing the μ_0 of I^- ($(-8.3 \pm 1.0) \times 10^{-4}$ $cm^2V^{-1}s^{-1}$), the μ_0 of F^- can be calculated as $(-5.9 \pm 1.0) \times 10^{-4}$ $cm^2V^{-1}s^{-1}$, which is fairly similar to the evaluated values from the literature data, ($(-5.732 \pm 0.013) \times 10^{-4}$ $cm^2V^{-1}s^{-1}$).

In conclusion, the electromigration methodology can work well to investigate the absolute mobility of various anions in different electrolytes. However, there are still some requirements requiring attention: 1) The ionic strength of the electrolyte must be chosen carefully; if it is too small, its effect on the calculation with the Onsager-Fuoss model can be significant; if it is too large, the identification of the velocity and permittivity of the electrolyte can be complicated; 2) The injection volume of the sample needs to be less than 100 μL; 3) The "experimental" uncertainty, estimated from repeated experiments, is higher than the calculated absolute errors and is not expected to be below 10 %. Therefore, this electromigration method can be applied to study the absolute

mobility of At in optimized experimental conditions.

2.4.2. Investigation of At^- behavior with the electromigration method

To date, only a few studies have been carried out on the mobility of At^- using the electromigration method. Furthermore, the electroosmosis effect during the experiments was not discussed and the absolute mobility of At^- could not be defined. The non-corrected apparent mobilities of At^- in 0.05 M NaOH and 0.1 M NaOH solutions were determined as $(-7.4 \pm 0.2) \times 10^{-4}$ $cm^2V^{-1}s^{-1}$ and $(-7.2 \pm 0.2) \times 10^{-4}$ $cm^2V^{-1}s^{-1}$, respectively.[12] However, it was confirmed recently that in concentrated NaOH solution, $AtO(OH)_2^-$ is the predominant species instead of At^-.[15] Therefore, these mobilities cannot be attributed to "At^-". Both the mobilities of I^- and At^- were also investigated separately in 0.04 M KNO_3 solution, with non-corrected apparent values of -8.0×10^{-4} $cm^2V^{-1}s^{-1}$ and $(-6.1 \pm 0.2) \times 10^{-4}$ $cm^2V^{-1}s^{-1}$, respectively.[6] Knowing the average value of iodide absolute mobility is $(-7.964 \pm 0.008) \times 10^{-4}$ $cm^2V^{-1}s^{-1}$, the apparent mobility of I^- in 0.04 M KNO_3 can be calculated through the Onsager-Fuoss model, which gives -7.0×10^{-4} $cm^2V^{-1}s^{-1}$. As electroosmosis is the difference between the calculated and apparent mobility, it can be estimated as -1.0×10^{-4} $cm^2V^{-1}s^{-1}$. This value is within the range of those measured with our apparatus (Table 2.2) and evidences again that the electroosmosis flow significantly affects anion mobility. Thus, the apparent mobility of At^- in 0.04 M KNO_3 solution can be corrected for the electroosmosis effect, giving $(-5.1 \pm 0.2) \times 10^{-4}$ $cm^2V^{-1}s^{-1}$. Using the Onsager-Fuoss model, the μ_0 of At^- can be extrapolated to the value of $(-6.1 \pm 0.2) \times 10^{-4}$ $cm^2V^{-1}s^{-1}$. This value appears much lower than those found in the literature (about -8.7×10^{-4} $cm^2V^{-1}s^{-1}$, see the ancillary data section). Most importantly, the At species under the experimental conditions described in Table 2.1 is not thought to be "At^-", according to the Pourbaix diagram of astatine.[4,15,16] Therefore, the absolute mobility of At^- has not been experimentally defined and it is unclear whether At^- migrates faster or slower than I^-. To tackle this issue, two approaches were followed: the first aimed to extrapolate the μ_0 of At^- from experiments carried out in the presence of both "At^-" and F-18DG; the goal of the

second was to compare the behavior of At^- and I^- in the same electrolyte/experiment to define which has the larger μ_0.

2.4.2.1. At-211 and F-18DG system

At-211 stored in the stock solution was injected into the reducing medium (0.1 M NaCl, 0.01 M HCl, 10^{-3} M $Na_2S_2O_3$, and 10^{-3} M $MgCl_2$) followed by F-18DG used to measure the flow rate of electroosmosis. During these experiments, the peak representing At species moved towards the positive electrode, evidencing the anionic species of At. The experiments were carried out with two different sources of astatine in 7 samples. The apparent mobility of At species was corrected for the electroosmotic flow and the Onsager-Fuoss model was used to extrapolate the μ_0 with the relative parameters given in Table 2.3 and the tables in the ancillary data section. The μ_0 values for At species are displayed in Figure 2.11 and compared with those of I^-. The obtained values are coherent and fall within the 2σ uncertainty interval. The average value of μ_0 for At is $(-8.3 \pm 0.8) \times 10^{-4}$ $cm^2V^{-1}s^{-1}$. Compared to the μ_0 of I^- ($(-8.3 \pm 1.0) \times 10^{-4}$ $cm^2V^{-1}s^{-1}$), it is not possible to distinguish which one is larger. Therefore, a better way to compare the mobilities of At species and I^- is to inject both anions into the same electrolyte.

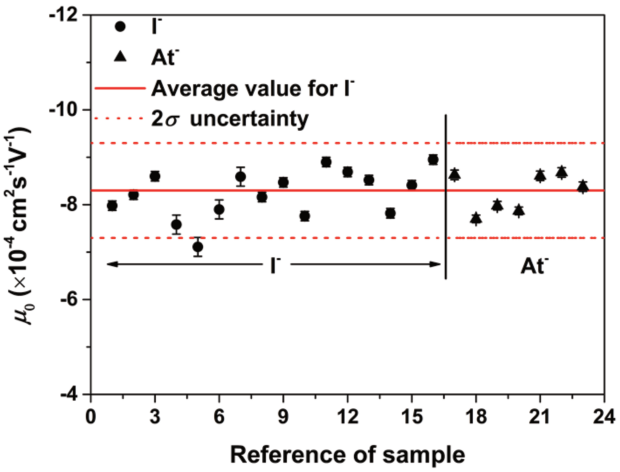

Figure 2.11. The absolute mobility (μ_0) of I^- (circles) and At^- (triangles) extrapolated from the experimental outcomes as a function of the sample reference: the solid line corresponds to the average value of -8.3×10^{-4} $cm^2V^{-1}s^{-1}$ and the dashed lines represent the 2σ uncertainty interval.

2.4.2.2. At-211 and I-123 system

As the μ_0 of I^- has been obtained, the At species absolute mobility can be calculated from the difference between the mobilities of At species and I^-. These were investigated using the same approach as described for the I^-/F^- system. I-123 was injected after At-211. From the decrease in the distance between the two peaks, which represent the two different anions, as a function of time, it is clear that At moves more slowly than I^-. Based on the experimental outcomes, the average difference between At and I^- absolute mobilities is $(0.3 \pm 0.4) \times 10^{-4}$ $cm^2V^{-1}s^{-1}$. The μ_0 of At^- is easily obtained with the value of $(-8.0 \pm 1.0) \times 10^{-4}$ $cm^2V^{-1}s^{-1}$, which agrees well with that obtained in the At-211/F-18DG system, $(-8.3 \pm 0.8) \times 10^{-4}$ $cm^2V^{-1}s^{-1}$.

The absolute mobilities of the halides obtained in this work and those extracted from the literature are displayed as a function of their ionic radius in Figure 2.12, based on the data in Table 2.4. A trend is clearly visible: for F^- to I^-, the larger the ionic radius, the higher the mobility. However, considering the experimental errors, the mobility appears to be rather similar for the two largest halides. The

experiment carried out in the presence of both I^- and "At^-" shows that "At^-" is slightly less mobile than I^-. In molecular dynamics simulations, similar results were obtained, *i.e.* the diffusion coefficients of At^- and I^-, which could be related to absolute mobilities, are similar with a slightly smaller value for At^- than I^-, with a ratio of 0.94 ± 0.10.[9] This theoretical approach corroborates the experimental results and one can conclude that the At species under the given conditions corresponds to At^-.

Table 2.3. Viscosity and permittivity of NaCl solution at different ionic strengths at 25 °C.

I (M)	ε[24]	η (mPa·s) [25]
0.10	77.34	0.89817
0.116	76.62	0.90287

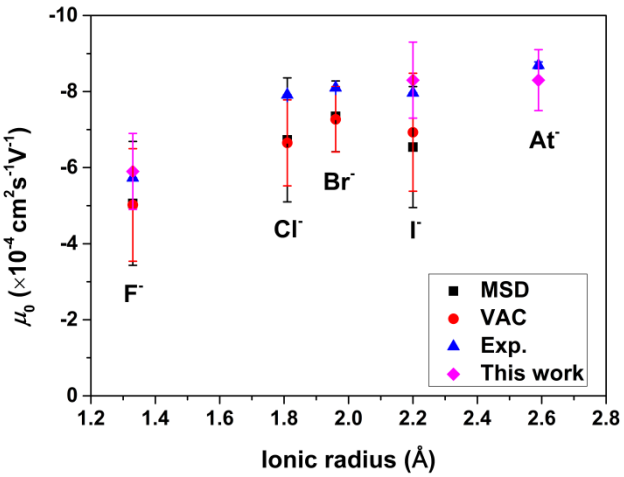

Figure 2.12. Absolute mobility of halides as a function of their ionic radius. MSD (squares) represents the mean square displacement calculation and VAC (circles) represents the velocity autocorrelation functions;[8] Exp. (triangles) represents the absolute mobilities, which are summarized in the table in the ancillary data section; the diamonds represent the experimental results from this work; and the ionic radii are from literature.[23]

Table 2.4. Absolute mobility at 25 °C and ionic radius of halides.

		μ_0 ($\times 10^{-4}$ $cm^2s^{-1}V^{-1}$)			
Halide	Ionic radius (Å)	*a* (MSD)[8]	*b* (VAC)[8]	*c* (Exp)	*d* (this work)
F^-	1.33[23]	–5.06±1.63	–5.02±1.48	–5.732±0.013	–5.9±1.0
Cl^-	1.81[23]	–6.73±1.63	–6.65±1.13	–7.9124±0.0020	–
Br^-	1.96[23]	–7.35±0.93	–7.27±0.86	–8.099±0.004	–
I^-	2.20[23]	–6.54±1.59	–6.93±1.55	–7.964±0.008	–8.3±1.0
At^-	2.59 ±0.09[26]	–	–	–8.69±0.09	–8.3±0.8

a and b are the computer simulations of the mobilities of the halides calculated from the mean square displacement (MSD) and the velocity autocorrelation functions (VAC), respectively; using the SPC/E model for water and ion - water parameters fitted to the binding energies of small clusters of ions.

c. Evaluated by the authors from the literature data.

2.5.Conclusion

The electromigration method, with the neutral molecular F-18DG measuring the effect of electroosmosis, was validated by investigating the mobility of iodide in different conditions with various effect factors. The absolute mobilities of I^- and F^- were extrapolated from the experimental results using the Onsager-Fuoss model. The values of μ_0 for I^- and F^- are $(-8.3 \pm 1.0) \times 10^{-4}$ $cm^2V^{-1}s^{-1}$ and $(-5.9 \pm 1.0) \times 10^{-4}$ $cm^2V^{-1}s^{-1}$, respectively, which are in good agreement with those in the literature. The same method was applied to explore the migration behavior of At in the given reducing medium, in which At^- is expected. The migration of astatine to the positive electrode under the experimental conditions provides direct evidence that the astatine species in the given reducing medium is minus charged. The μ_0 of At^- was obtained as $(-8.3 \pm 0.8) \times 10^{-4}$ $cm^2V^{-1}s^{-1}$. By comparing the migration behaviors of At^- and I^- in the same experimental conditions, it was confirmed that At^- has a smaller value of μ_0 than I^-. Furthermore, corresponding to the theoretical calculation, the similar values of

absolute mobilities between At^- and I^- indicated that At^- is the expected species in the given conditions. This work not only supplies the first experimental value of absolute mobility for At^-, but also evidences the existence of At^- in acid reducing aqueous solution. The μ_0 of At^- can provide important information to investigate the hydrogen bond between At^- and water.

References

(1) McDevitt, M.; Sgouros, G.; Finn, R. *Eur. J. Nucl. Med.* **1998**, *25* (9), 1342.

(2) Zalutsky, M.; Reardon, D. *J. Nucl. Med.* **2008**, *49* (1), 30.

(3) Wilbur, D. S. *Nat. Chem.* **2013**, *5* (3), 246.

(4) Champion, J.; Alliot, C.; Renault, E.; Mokili, B. M.; Chérel, M.; Galland, N.; Montavon, G. *J. Phys. Chem. A* **2010**, *114* (1), 576.

(5) Sabatié-Gogova, A.; Champion, J.; Huclier, S.; Michel, N.; Pottier, F.; Galland, N.; Asfari, Z.; Chérel, M.; Montavon, G. *Anal. Chim. Acta* **2012**, *721*, 182.

(6) Dreyer, I.; Dreyer, R.; Chalkin, V. A. *J. Radiochem. Radioanal. Lett.* **1978**, *35* (6), 257.

(7) Dreyer, I.; Dreyer, R.; Chalkin, V. A. *J. Radiochem. Radioanal. Lett.* **1978**, *36* (6), 389.

(8) Lee, S. H.; Rasaiah, J. C. *J. Phys. Chem.* **1996**, *100* (4), 1420.

(9) Réal, F.; Gomes, A. S. P.; Martínez, Y. O. G.; Ayed, T.; Galland, N.; Masella, M.; Vallet, V. *J. Chem. Phys.* **2016**, *144* (12).

(10) Dreyer, I.; Dreyer, R.; Chalkin, V. A.; M., M. *J. Radiochem. Radioanal. Lett.* **1979**, *40* (3), 145.

(11) Dreyer, R.; Dreyer, I.; Pfeiffer, M.; Roesch, F. *J. Radiochem. Radioanal. Lett.* **1982**, *55* (4), 207.

(12) Dreyer, R.; Dreyer, I.; Rosch, F.; Beyer, G.-J. *J. Radiochem. Radioanal. Lett.* **1982**, *54* (3), 165.

(13) Alliot, B. C.; Cherel, M.; Barbet, J.; Sauvage, T.; Montavon, G. *Radiochim. Acta* **2009**, *97*, 161.

(14) Lindegren, S.; Bäck, T.; Jensen, H. J. *Appl. Radiat. Isot.* **2001**, *55* (2), 157.

(15) Sergentu, D. C.; Teze, D.; Sabatié-Gogova, A.; Alliot, C.; Guo, N.; Bassal, F.; Silva, I. Da; Deniaud, D.; Maurice, R.; Champion, J.; Galland, N.; Montavon, G. *Chem. - A Eur. J.* **2016**, *22* (9), 2964.

(16) Champion, J.; Sabatié-Gogova, A.; Bassal, F.; Ayed, T.; Alliot, C.; Galland, N.; Montavon, G. *J. Phys. Chem. A* **2013**, *117* (9), 1983.

(17) Onsager, L.; Fuoss, R. M. *J. Phys. Chem.* **1932**, *36*, 2689.

(18) Milanov, M.; Doberenz, W.; Marinov, A.; Khalkin, V. A. *J. Radioanal. Nucl. Chem. Artic.* **1984**, *82* (1), 101.

(19) Mauerhofer, E.; Kling, O.; Rosch, F. *Radiochim. Acta* **2001**, *89*, 537.

(20) Aupiais, J. *J. Solution Chem.* **2011**, *40* (9), 1629.

(21) Jaros, M.; Vceláková, K.; Zuskova, I.; Gas, B. *Electrophoresis* **2002**, *23*, 2667.

(22) Mbuna, J.; Takayanagi, T.; Oshima, M.; Motomizu, S. *J. Chromatogr. A* **2004**, *1022* (1–2), 191.

(23) Shannon, R. D. *Acta Crystallogr. Sect. A* **1976**, *32* (5), 751.

(24) Marcus, Y. *J. Solution Chem.* **2013**, *42* (12), 2354.

(25) Mao, S.; Duan, Z. *Int. J. Thermophys.* **2009**, *30*, 1510.

(26) Chang, Z.; Li, J.; Dong, C. *J. Phys. Chem. A* **2010**, *114* (51), 13388.

Ancillary data

The absolute mobilities of the ions employed in the main text are evaluated from literatures. The procedures are detailed in the following part.

The mobilities of Cl^- and Br^- using electrophoretic system have already been evaluated in a previous paper.[1] The iodide mobility was determined from 13 independent values and 11 for fluoride ions. The uncertainty is in agreement with the expected precision of conductance measurements. For Na^+, the data obtained from some references ($\mu_0 > 5.2$) seem outside values when considering the intrinsic precision of conductance measurements. All other values (n = 26) agree with each other. For Mg^{2+}, one might have thought there would be no difficulty for this element. Unfortunately, this is not the case since there are two sets of statistically different data. The first gives a mean of 5.499 ± 0.003 and the second 5.531 ± 0.004 (see Figure c). The first set corresponds to the usual data recommended in the literature and is mainly based on the very precise determination performed by Shedlovsky *et al.*[2] This discrepancy has been carefully discussed by several authors because some recent determinations do not match the older ones.[3,4] It has been suggested that the original salt used by Shedlovsky may have been contaminated due to the particular mode of preparation (decomposition of a double ammonium magnesium chloride). The reference[5] was discarded because the association constant determined in this paper does not agree with those given by other independent techniques, leading to a probable underestimation. Other determinations are not mentioned because they were critically rejected by Miller and co-workers.[3] The excessive value obtained by Broadwater *et al*. was also rejected because the data show a concentration dependence that is not in agreement with either conductivity equation.[6] Based on criticisms made by several authors, only the second set of data was used to determine an un-weighted average, *i.e.* $\mu_0(Mg^{2+}, 25\ °C, 0)$ = 5.531 ± 0.004. This selected value is in close agreement with that "firmly" proposed by Bianchi and co-workers based on a thorough evaluation of older values.[4] It covers all recent values and is 0.7 % higher than those commonly proposed in the literature. A more conservative choice would be to accept all the

data and calculate a mean average: 5.515 ± 0.036. The reader is invited to choose between the recommended value and the conservative choice. For H^+, its conductance is well known. Conductance measurements are known to be precise, generally between 0.01 – 0.05 %. Based on the selected data in the table, we have determined an un-weighted mean with an associated uncertainty of 0.02 %.

For astatide, the source found in ref.[7] is not mentioned but very probably comes from the work of Dreyer and co-workers[8]. They have determined the electrophoretic mobility of several anions: Br^-, I^-, At^-, IO_3^-, IO_4^-, AtO_3^-, and AtO_4^-. The agreement is excellent for bromide (deviation –0.02 %), and good for iodide (dev. –2 %) and iodate (dev. –5 %) ions. However, the experimental value for astatide seems subject to caution for two reasons. First, the ionic radius of astatine is higher than for any other halide. This ion presents a low charge density and thus a structure breaker behavior, like for Br^-, I^-, and Cl^-, is expected. It is concluded that the electrophoretic mobility of astatide should be closer to that of bromide, *i.e.* about -8.0×10^{-4} $cm^2V^{-1}s^{-1}$, than that of the fluoride ion. Second, this assumption is supported by subsequent experiments performed by the same authors in sodium hydroxide by the electromigration method.[9] In 0.05 M NaOH, the authors found a mobility of $-7.3/-7.4 \times 10^{-4}$ $cm^2V^{-1}s^{-1}$ and about -7.8×10^{-4} $cm^2V^{-1}s^{-1}$ in 0.005 M NaOH. All values are in fair agreement and the weighted average is $-8.69 \pm 0.09 \times 10^{-4}$ $cm^2V^{-1}s^{-1}$, which seems consistent with the halide series but perhaps a little high. Therefore, the level P is assigned.

Table a. Selected electrophoretic mobilities of some anions. Data are given at zero ionic strength and 25 °C. Rejected data are in italic. R=reliable, P=provisional.

Ion	$-\mu_0 \times 10^4$ ($cm^2V^{-1}s^{-1}$)	Selected value	Q	Comment
Br^-		−8.099±0.004	R	Ref. 1
Cl^-		−7.9124±0.0020	R	Ref. 1
F^-	5.732,[10] 5.74,[11] 5.734,[12] 5.70,[13] 5.73±0.12,[14] 5.731(1),[14] 5.734,[15] 5.70,[16] 5.734,[17] 5.770,[18] 5.748±0.011[19] *5.64*,[13] *5.58±0.02*,[20]	−5.732±0.013	R	(1)Other source quoted in the publication.
I^-	7.96,[11] 7.960,[21] 7.978(2),[22] 7.978,[12] 7.955±0.004,[23] 7.942,[24] 7.939,[25] 7.966,[26] 7.958(3),[27] 7.975(3),[28] 7.977,[29] 7.974,[30] 7.970,[31] *8.000*,[15] *7.999*,[32] *7.99*,[16] *7.92*(1)[7]	−7.964±0.008	R	(1)Other source quoted in the publication. (2)Assuming $\mu_0(Cs^+)$= 7.964±0.011 (n=16 values selected from literature data). (3)Assuming $\mu_0(K^+)$= 7.622±0.006 (n=16 values selected from literature data).
At^-	8.76±0.24;8.36±0.25,8.67±0.25; 8.67±0.25[9] (2), 8.76±0.12[33] *6.0*[7] (1), *6.0*[8]	−8.69±0.09	P	(1) Other source quoted. (2) Extrapolation at I = 0, average data of 3 values using 3 different models (see text). Original data in sodium hydroxide 0.005 or 0.05 M.
$S_2O_3^{2-}$	8.81[34,35], 8.81[11], 9.001[36] (2), 8.996[36], 9.214[36] (3), 8.992[36] (4), 9.039±0.17[37], 8.80[16], 9.058[38], 8.799[7] (1), 8.712; 8.756; 8.81[39], 8.95[40] (5) *−109*[41] (1,5)	−8.91±0.08	R	(1)Other data quoted from the literature. (2)From water activity data. (3)Assuming $\mu_0(Sr^{2+})$ = 6.162±0.002 (n=10 values selected from literature data). (4)Assuming $\mu_0(Ba^{2+})$ = 6.595±0.002 (n=12 values selected from literature data). (5)Original conductance value ×1.066 due to the change in the definition of the resistance.

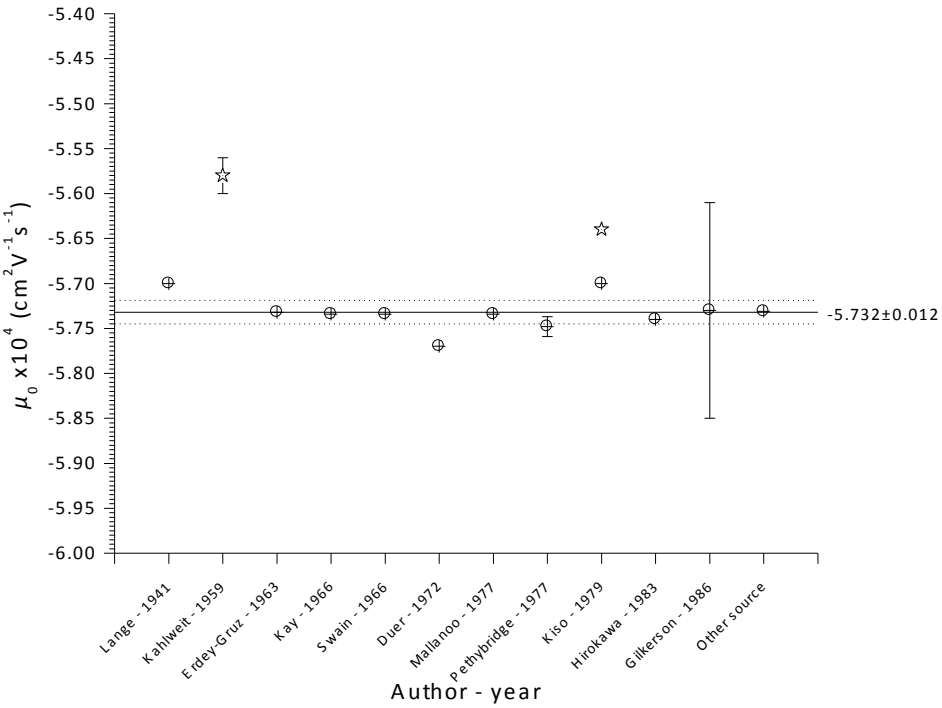

Fig. a: Literature data related to the absolute mobility of F^- ions at 25 °C and infinite dilution. (✯) Rejected values.

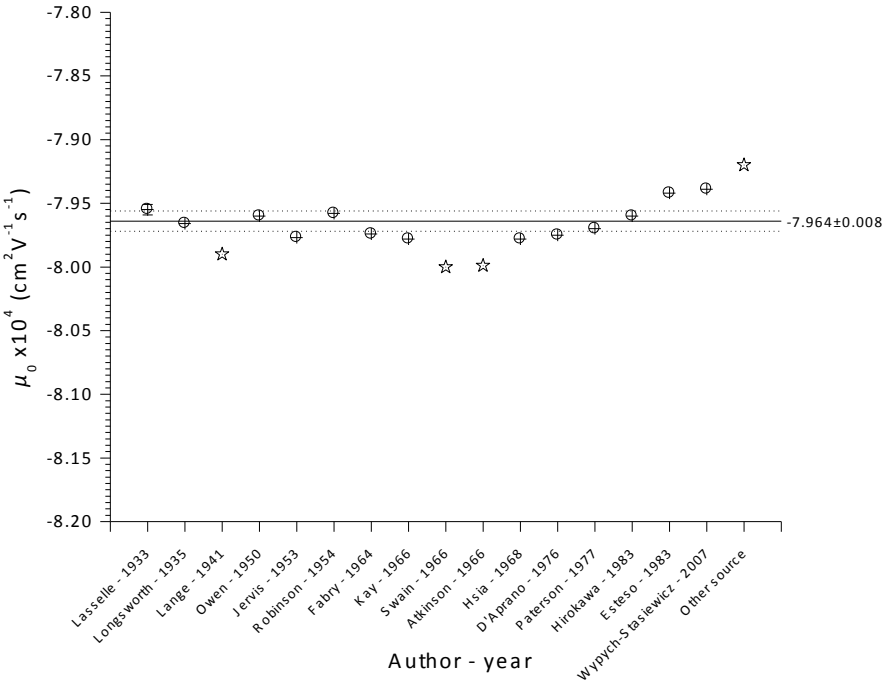

Fig. b: Literature data related to the absolute mobility of I^- ions at 25 °C and infinite dilution. (✯) Rejected values.

Table b. Selected electrophoretic mobilities of some cations. Data are given at zero ionic strength and 25 °C. Rejected data are in italic.

Ion	$\mu_0 \times 10^4$ ($cm^2V^{-1}s^{-1}$)	Selected value	Q	Comment
Na^+	5.190,[34] 5.196,[42] 5.198[(1)],[43,44] 5.198,[45] 5.194,[46] 5.190,[47] 5.193,[48] 5.193,[49] 5.203,[12] 5.191[(2)],[15] 5.193,[50] 5.190[(3)],[51] 5.194,[52] 5.200,[53] 5.193; 5.193,[54] 5.198,[19] 5.190[(4)],[55] 5.185; 5.180; 5.206; 5.207,[56] 5.194,[57] 5.19,[16] 5.2004,[58] 5.190±0.000[59] *5.108*,[60] *5.215*,[25] *5.212*; *5.210*,[61] *5.177*[56]	5.194±0.002	R	[(1)]Other source quoted in the publication. [(2)]Recalculation by replacing the original value $\mu_0(Cl^-) = -7.918$ by the value selected by this review $\mu_0(Cl^-) = -7.9124$. [(3)]Assuming $\mu_0(ClO_4^-) = -6.971 \pm 0.007$ (n=25 values selected from literature data). [(4)]Assuming the value $\mu_0(Li^+) = 4.010 \pm 0.002$ (n=17 values selected from literature data).
Mg^{2+}	5.528±0.002,[6+2] 5.537±0.005[(1)],[62] 5.508[(2)],[63] 5.524[(2)],[37] 5.535±0.005[(2)],[4] 5.533,[64] 5.526,[65] 5.530,[3] *5.499*,[57] *5.509*,[66+4] *6.01*,[16] *5.500*[(3)],[67,68] *5.544*,[69] *6.135*,[70] *5.4691*,[71] *5.493*,[34] *5.499*,[72] *5.499*,[2] *5.498*[(2)],[73] *5.496*,[74] *5.556±0.002*,[6] *5.356*[5]	5.531±0.004	R	[(1)]Two kinds of model have been used for the extrapolation at I = 0. [(2)]Other source quoted in the publication. [(3)]Assuming $\mu_0(Cl^-) = -7.9124$
H^+	36.239,[34] 36.256,[75] 36.268,[76] 36.235,[44] 36.259[(1)],[43,44] 36.245,[77] 36.246,[48] 36.265[(2)],[78] 36.254,[79] 36.235,[80] 36.265,[81] 36.257,[82] 36.264±0.05; 36.210,[83] 36.249,[84] 36.271[(3)][55], 36.233[16] *35.985*; *36.430*; *35.445*; *35.964*; *36.482*; *37.829*; *35.860*; *36.067*; *36.585*; *36.068*; *36.171*; *36.176*, *36.379*[(4)],[85] *36.295*,[86] *36.068±0.073*,[85] *36.295*,[87] *36.291*,[50] *37.19*,[88] *36.130*[89]	36.251±0.008	R	[(1)]Other source quoted in the publication. [(2)]Recalculation by the authors from literature data. [(3)] Assuming $\mu_0(Cl^-) = -7.9124$ [(4)]Compilation of several data from 1888 to 1931.

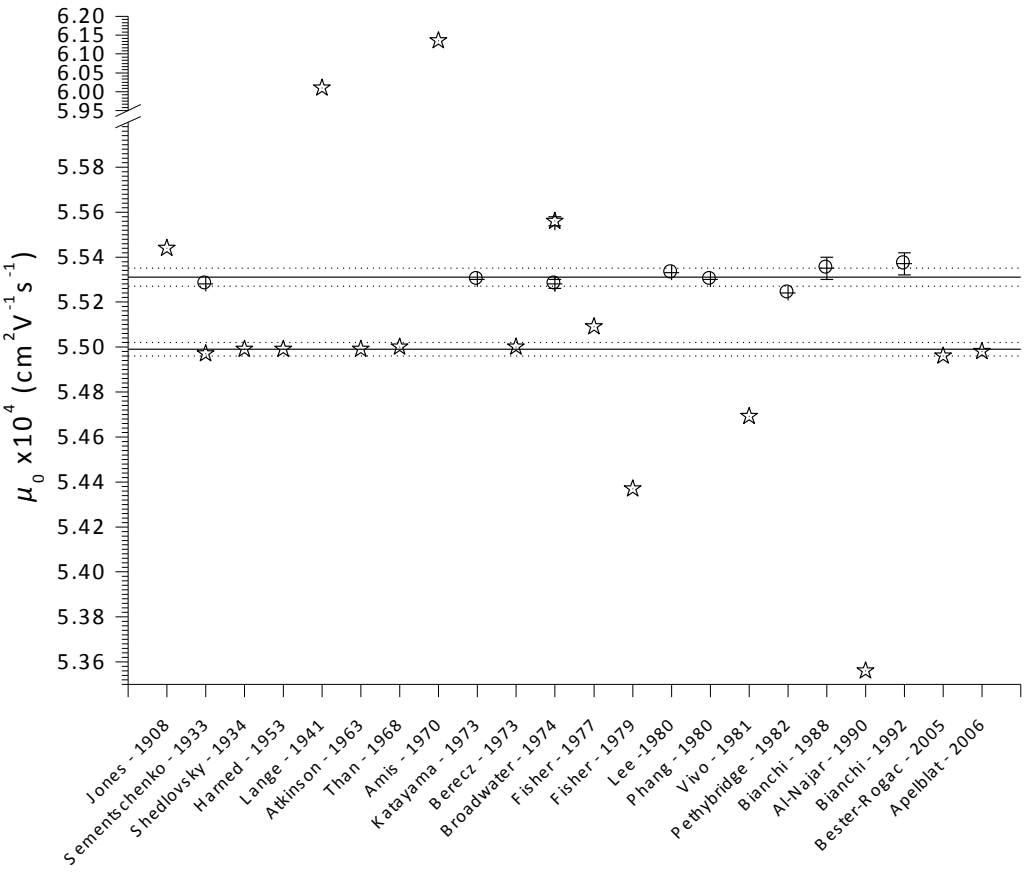

Fig. c: Literature data related to the absolute mobility of Mg^{2+} ions at 25 °C and infinite dilution. (✯) Rejected values.

References

(1) Aupiais, J. *J. Solution Chem.* **2011**, *40*, 1629-1644.

(2) Shedlovsky, T.; Brown, A. S. *J. Am. Chem. Soc.* **1934**, *56*, 1066-1071.

(3) Miller, D. G.; Rard, J. A.; Eppstein, L. B.; Albright, J. G. *J. Phys. Chem.* **1984**, *88*, 5739-5748.

(4) Bianchi, H.; Corti, H. R.; Fernandez-Prini, R. *J. Solution Chem.* **1988**, *17*, 1059-1065.

(5) Al-Najar, A. A.; Ibrahim, A. W. *Can. J. Chem.* **1990**, *68*, 770-773.

(6) Broadwater, T. L.; Evans, D. F. *J. Solution Chem.* **1974**, *3*, 757-769.

(7) Lucy, C. A. *J. Chromatogr. A* **1999**, *850*, 319-337.

(8) Dreyer, I.; Dreyer, R.; Chalkin, V. A. *Radiochem. Radioanal. Lett.* **1978**, *35*, 257-262.

(9) Dreyer, R.; Dreyer, I.; Rösch, F.; Beyer, G. J. *Radiochem. Radioanal. Lett.* **1982**, *54*, 165-176.

(10) Erdey-Gruz, T.; Majthenyi, L.; Kugler, E. *Acta Chim. Hung. Tomus* **1963**, *37*, 393-403.

(11) Hirokawa, T.; Nishino, M.; Aoki, N.; Kiso, Y.; Sawamoto, Y.; Yagi, T.; Akiyama, J.-I. *J. Chromatogr.* **1983**, *271*, D1-D106.

(12) Kay, R. L.; Evans, D. F. *J. Phys. Chem.* **1966**, *70*, 2325-2335.

(13) Kiso, Y.; Hirokawa, T. *Chem. Lett.* **1979**, 891-894.

(14) Gilkerson, W. R. *J. Solution Chem.* **1986**, *15*, 551-562.

(15) Swain, C. G.; Evans, D. F. *J. Am. Chem. Soc.* **1966**, *88*, 383-390.

(16) Lange, J. *Z. Phys. Chem. A* **1941**, *188*, 284-315.

(17) Mallanoo, T.; Stokes, R. H. *Aust. J. Chem.* **1977**, *30*, 1375-1377.

(18) Duer, W. C.; Robinson, R. A.; Bates, R. G. *J. Chem. Soc. Faraday Trans. I* **1972**, *68*, 716-722.

(19) Pethybridge, A. D.; Spiers, D. J. *J. Chem. Soc. Faraday Trans. I* **1977**, *73*,

768-775.

(20) Kahlweit, M. *Z. Phys. Chem. Neue Folge* **1959**, *21*, 436-437.

(21) Owen, B. B.; Zeldes, H. *J. Chem. Phys.* **1950**, *18*, 1083-1085.

(22) Hsia, K.-L.; Fuoss, R. M. *J. Am. Chem. Soc.* **1968**, *90*, 3055-3060.

(23) Lasselle, P. A.; Aston, J. G. *J. Am. Chem. Soc.* **1933**, *55*, 3067-3071.

(24) Esteso, M. A.; Liorente, M. L. *J. Chem. Eng. Data* **1983**, *28*, 337-338.

(25) Wypych-Stasiewicz, A.; Szejgis, A.; Chmielewska, A.; Bald, A. *J. Mol. Liq.* **2007**, *130*, 34-37.

(26) Longsworth, L. G. *J. Am. Chem. Soc.* **1935**, *57*, 1185-1191.

(27) Robinson, R. A.; Stokes, R. H. *J. Am. Chem. Soc.* **1954**, *76*, 1991-1994.

(28) D'Aprano, A.; Komiyama, J.; Fuoss, R. M. *J. Solution Chem.* **1976**, *5*, 279-295.

(29) Jervis, R. E.; Muir, D. R.; Butler, J. P.; Gordon, A. R. *J. Am. Chem. Soc.* **1953**, *75*, 2855-2858.

(30) Fabry, T. L.; Fuoss, R. M. *J. Phys. Chem.* **1964**, *68*, 974-976.

(31) Paterson, R.; Anderson, J.; Anderson, S. S.; Lutfullah. *J. Chem. Soc. Faraday Trans. I* **1977**, *73*, 1773-1788.

(32) Atkinson, G.; Mori, Y. *J. Phys. Chem.* **1966**, *45*, 4716-4718.

(33) Dreyer, R.; Dreyer, I.; Pfeiffer, M.; Rösch, F. *Radiochem. Radioanal. Lett.* **1982**, *55*, 207-214.

(34) Weast, R. C.; Astle, M. J.; Veyer, W. H.; CRC Press, Inc.: Boca Raton, 1988.

(35) Kaniansky, D.; Masar, M.; Marak, J.; Bodor, R. *J. Chromatogr. A* **1999**, *834*, 133-178.

(36) Pethybridge, A. D.; Taba, S. S. *Faraday Discus. Royal Soc. Chem.* **1978**, *64*, 274-284.

(37) Pethybridge, A. D.; Taba, S. S. *J. Chem. Soc. Faraday Trans. I* **1982**, *78*, 1331-1344.

(38) Denney, T. O.; Monk, C. B. *Trans. Faraday Soc.* **1951**, *47*, 992-998.

(39) Jellinek, K. *Z. Phys. Chem.* **1911**, *76*, 257-354.

(40) Holleman, A. F. *Rec. Trav. Chim.* **1895**, *14*, 71-81.

(41) Bredig, G. *Z. Phys. Chem.* **1894**, *13*, 191-288.

(42) Vlaev, L.; Tavlieva, M.; Barthel, J. *J. Solution Chem.* **2007**, *36*, 447-465.

(43) Harned, H. S.; Owen, B. B. *The physical chemistry of electrolytic solutions*, 3rd edition ed.; Reinhold: New York, 1958; Vol. 106, p 803.

(44) Robinson, R. A.; Stokes, R. H.; Butterworths Science Publications: London, 1959, pp 388-425.

(45) Darken, L. S.; Meier, H. F. *J. Am. Chem. Soc.* **1942**, *64*, 621-623.

(46) Shedlovsky, T. *J. Am. Chem. Soc.* **1932**, *54*, 1411-1428.

(47) Saxton, B.; Langer, T. W. *J. Am. Chem. Soc.* **1933**, *55*, 3638-3645.

(48) McInnes, D. A.; Shedlovsky, T.; Longsworth, L. G. *J. Am. Chem. Soc.* **1932**, *54*, 2758-2762.

(49) Cassford, G. E. *The temperature dependence of the conductance of single and mixed electrolytes in water*. University of Reading, Reading, 1983.

(50) Miller, D. G. *J. Phys. Chem.* **1966**, *70*, 2639-2659.

(51) D'Aprano, A. *J. Phys. Chem.* **1971**, *75*, 3290-3293.

(52) Gunning, H. E.; Gordon, A. R. *J. Phys. Chem.* **1942**, *10*, 126-131.

(53) Arevalo, A.; Vivo, A.; Esteso, M. A.; Llorente, M. L. *Anales Quim.* **1977**, *73*, 195-199.

(54) Monica, M. D.; Petrella, G.; Sacco, A.; Bufo, S. *Electrochim. Acta* **1979**, *24*, 1013-1017.

(55) Robinson, R. A.; Davies, C. W. *J. Chem. Soc.* **1937**, 574-577.

(56) Bury, R.; Justice, M. C.; Justice, J. C. *J. Chim. Phys.* **1970**, *67*, 2045-2053.

(57) Atkinson, G.; Petrucci, S. *J. Phys. Chem.* **1963**, *67*, 337-339.

(58) Vivo, A.; Esteso, M. A.; Llorente, M. L. *Anales Quim.* **1981**, *77*, 204-208.

(59) Beckers, J. L.; Verheggen, P. E. M.; Everaerts, F. M. *J. Chromatogr.* **1988**, *452*,

591-600.

(60) Li, N. C. C.; Brüll, W. *J. Am. Chem. Soc.* **1942**, *64*, 1635-1637.

(61) Kunze, R. W.; Fuoss, R. M. *J. Am. Chem. Soc.* **1963**, *67*, 911-913.

(62) Bianchi, H.; Corti, H. R.; Fernandez-Prini, R. *J. Solution Chem.* **1992**, *21*, 1107-1114.

(63) Sementschenko, W. K.; Serpinski, W. W. *Z. Phys. Chem. A* **1933**, *167*, 197-208.

(64) Lee, K.; Kay, R. L. *Aust. J. Chem.* **1980**, *33*, 1895-1902.

(65) Phang, S.; Stokes, R. H. *J. Solution Chem.* **1980**, *9*, 497-505.

(66) Fisher, F. H.; Fox, A. P. *J. Solution Chem.* **1977**, *6*, 641-650.

(67) Berecz, E.; Bader, I. *Acta Chim.* **1973**, *79*, 81-103.

(68) Than, A.; Amis, E. S. *Z. Physik. Chem. Neue Folge* **1968**, *58*, 196-205.

(69) Jones, H. C.; Jacobson, C. A. *Am. Chem. J.* **1908**, *40*, 355-410.

(70) Amis, E. S.; Casteel, J. F. *J. Electrochem. Soc.* **1970**, *117*, 213-218.

(71) Vivo, A.; Esteso, M. A.; Llorente, M. L.; Dominguez, B. *Anales Quim.* **1981**, *77*, 209-213.

(72) Harned, H. S.; Polestra, F. M. *J. Am. Chem. Soc.* **1953**, *75*, 4168-4169.

(73) Apelblat, A.; Manzurola, E.; Orekhova, Z. *J. Solution Chem.* **2006**, *35*, 879-888.

(74) Bester-Rogac, M.; Babic, V.; Perger, T. M.; Neueder, R.; J., B. *J. Mol. Liq.* **2005**, *118*, 111-118.

(75) McInnes, D. A. *The principles of electrochemistry*; Reinhold Publishing Corp.: New York, 1939, p 342.

(76) Kraus, C. A.; Parker, H. C. *J. Am. Chem. Soc.* **1922**, *44*, 2429-2449.

(77) Strong, L. E. *J. Chem. Eng. Data* **1980**, *25*, 104-106.

(78) Strong, L. E.; Pethybridge, A. D. *J. Solution Chem.* **1987**, *16*, 841-855.

(79) Hertz, H. G. *Ber. Bunsenges. Phys. Chem.* **1980**, *84*, 622-629.

(80) Vlaev, L.; Tavlieva, M.; Bester-Rogac, M. *J. Solution Chem.* **2007**, *36*, 171-192.

(81) Owen, B. B.; Sweeton, F. H. *J. Am. Chem. Soc.* **1941**, *63*, 2811-2817.

(82) King, F.; Spiro, M. *J. Solution Chem.* **1983**, *12*, 65-81.

(83) Parker, H. C. *J. Am. Chem. Soc.* **1923**, *45*, 2017-2033.

(84) Strong, L. E. *J. Chem. Eng. Data* **1980**, *25*, 104-106.

(85) Jeffery, G. H.; Vogel, A. I. *J. Chem. Soc.* **1932**, 400-415.

(86) Carman, P. C. *J. Phys. Chem.* **1969**, *73*, 1095-1105.

(87) Stokes, J. M. *J. Am. Chem. Soc.* **1961**, *65*, 1242-1247.

(88) Hlasko, M.; Salit, A. *Bulletin International de l'Académie Polonaise des Siences et des Lettres. Classe des Sciences Mathématiques et Naturelles Série A: Sciences Mathématiques* **1935**, 189-200.

(89) Jeffery, G. H.; Vogel, A. I. *J. Chem. Soc.* **1931**, 1715-1729.

Chapter 3. The heaviest possible ternary trihalogen species, IAtBr−, evidenced in aqueous solution: an experimental performance driven by computations

3.1. Abstract

Evidencing new chemical species in solution is particularly challenging when one works at ultra-trace concentrations, as it is likely to happen with radioelements such as astatine (*Z*=85). In this work, quantum mechanical calculations were used to predict the tiny experimental domain in which it is possible to detect the presence of an exotic ternary trihalogen anion, $IAtBr^-$, and thus to guide a series of experiments. By analyzing the outcomes of competition experiments, we show that $IAtBr^-$ exists and can even predominate in aqueous solution. The equilibrium constant associated to the $At^+ + I^- + Br^- \rightleftharpoons IAtBr^-$ reaction is determined to be $10^{7.5\pm0.2}$, which is in fair agreement with the density functional theory predicted one ($10^{6.9}$). This system not only constitutes the very first example of a ternary trihalogen species that involves the astatine element, but is also the first trihalogen species reported to predominate in solution. Also, we show that the oxidation number of At is zero in this species, as in the other molecules and anions that At^+ can form with Cl^-, Br^- and I^- ligands.

3.2. Main article

Evidencing and characterizing the structures and properties of new chemical compounds usually requires to perform a wide range of complementary experiments, among which spectroscopy ones play a major role. However, in

some particular cases, one can only work with quantities of matter that prohibit the use of such golden experiments. This is typically the case with the astatine (At, Z=85) element, which is artificially produced with the help of cyclotron facilities[1,2]. Things can even become more complicated if only a tiny experimental domain admits the occurrence of the speculated chemical species in sufficient quantity. In this work, we demonstrate that quantum mechanical calculations can *a priori* guide the experimental study by predicting the experimental domain to be targeted. For this, the expected amounts of the chemical species to be evidenced should be sufficient to result in sizeable changes on the scrutinized "macroscopic" property (here the distribution coefficient of At in biphasic systems). Following this original approach, we show that it becomes possible to identify exotic species that may not have been evidenced otherwise.

It is of fundamental interest for chemists to characterize the chemical species that involve the At element, since some of its compounds may not have any analogue. Indeed, due to relativistic effects, the behavior of At may be very different to its nearest halogen, iodine. For instance, the Pourbaix diagram(E–pH) of astatine involves cationic species such as At^+ and AtO^+,[3,4,5] while the one of iodine only involves anionic or neutral species. Of course, in some cases, At and I behave in a similar way. Since the ternary trihalogen $BrICl^-$ species has been characterized in solution by means of voltametric studies,[6] and its photodissociation behavior in the gas phase studied by means of pump-probe experiments,[7] we hypothesized that the $IAtBr^-$ analogue would form in solution. This work aimed at evidencing the realness of this formation, notably though the determination of the equilibrium constant (K) associated to the following reaction:

$$At^+ + I^- + Br^- \rightleftharpoons IAtBr^- \quad (3.1)$$

However, the presence of the I^- and Br^- ions can lead to the formation of binary dihalogen molecules and binary trihalogen anions that would compete with the formation of the targeted ternary trihalogen species. These formations are associated with the following reactions:

$$At^+ + X^- \rightleftharpoons AtX \quad (3.2)$$

$$At^+ + 2X^- \rightleftharpoons AtX_2^- \quad (3.3)$$

corresponding equilibrium constants associated with the involvement of one or two X^- units, respectively. Note that K notations are used for the formations of ternary complexes and β ones for the formations of binary 1:1 and 1:2 ones. Experimental values for the β_{1,X^-} and β_{2,X^-} constants are available in the literature, based on competition (X = Br)[8] or electromigration (X = I)[9] methods.

Table 3.1. Thermodynamic constants at zero ionic strength for the reactions of the At^+ cation with Br^- and I^- ligands (from the literature).

X^-	Br^-	I^- [a]
Log β_{1,X^-}	3.0 ± 0.2[8]	6.0[9]
Log β_{2,X^-}	4.1 ± 0.3[8]	9.2[9]

[a] Extrapolated from the values at 0.5 M ionic strength (6.2 and 9.4, respectively) to zero ionic strength through a truncated Davies equation[10].

Quantum mechanical calculations can be used as a cost-effective tool for assessing the stability of $IAtBr^-$ with respect to the other dihalogen and trihalogen species of interest. To accurately predict equilibrium constants by means of relativistic density functional theory (DFT), one can make use of ligand-exchange reactions in order to take profit of error cancellations.[3,5,8,11] Since experimental Log β_{2,X^-} values are available for X = Br and X = I, we consider here the following reaction:

$$\frac{1}{2}AtBr_2^- + \frac{1}{2}AtI_2^- \rightleftharpoons IAtBr^- \quad (3.4)$$

The computation of the associated equilibrium constant, K_1, readily leads to the Log K value of interest as follows:

$$\text{Log } K = \frac{1}{2}\text{Log } \beta_{2,Br^-} + \frac{1}{2}\text{Log } \beta_{2,I^-} + \text{Log } K_1 \quad (3.5)$$

The B3LYP exchange-correlation functional[12] was used, solvation free energies

were estimated by means of a conductor-like polarizable continuum model (CPCM),[13] and other computational details that typically lead to accurate complexation constants in the field of astatine chemistry were chosen[3,5,8,11] (see Supporting Information for more details and ref 11 for an extensive benchmark). A Log K_1 value of 0.2 was computed, leading to a predicted Log K value of 6.9. Using the latter combined with the equilibrium constants reported in Table 3.1, we can elaborate a predictive speciation diagram of At in aqueous phase with the presence of both the I^- and Br^- anions (see Figure 3.1). It becomes clear from this prediction that a predominance domain does exist for the $IAtBr^-$ species, but that it should be rather small. Indeed, according to the theoretical prediction, $IAtBr^-$ could be a predominant species when the concentrations of I^- is within the $\sim 10^{-4}$ to $\sim 10^{-2}$ M range meanwhile the Br^- one is within the ~0.1 to ~1 M one (see Figure 3.1). This severely restricts the experimental domain to be covered. Additional experimental constraints may further be considered.

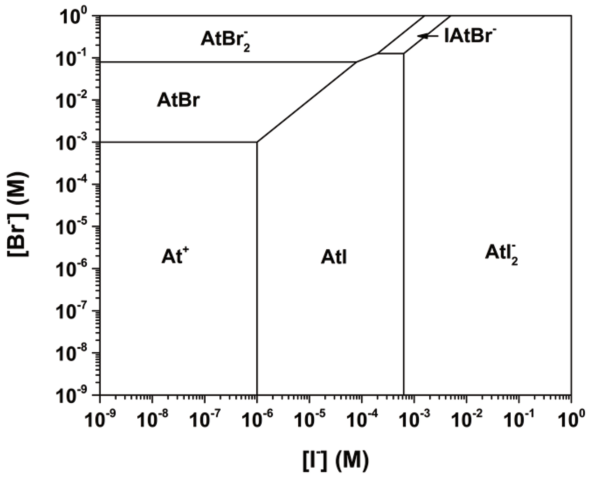

Figure 3.1. Predicted speciation diagram of At as a function of the initial concentrations of both the Br^- and I^- anions, based on the parameters displayed in Table 3.1 and the DFT predicted Log K value.

A competition method was used to experimentally investigate the speciation of At in the aqueous phase. In this work, we consider the distribution coefficient (D) between two liquid phases, one aqueous and the other organic (the solvent being the toluene).[14] Although a change in the D value arising from a change in

experimental conditions must indicate a change in speciation, an apparent constant *D* value may hide some composition changes in each phase. Therefore, one must find conditions that lead to sizeable changes in *D* to evidence new species. Simulations of the distribution coefficient as a function of the initial I^- concentration at fixed Br^- concentrations were conducted (see Figure 3.2). Four Br^- concentrations were considered, the largest value corresponding to the limit of validity of the truncated Davies equation, and the smallest one being out of the predicted predominance domain of $IAtBr^-$. We then select experimental conditions for which significant deviations appear between the model curves obtained by only considering the binary species (dash lines) and the ones obtained by also considering the ternary anion (solid lines). Therefore, we have retained the 0.1 and 0.05 M initial concentrations for the Br^- ligand, and we vary the I^- one between 5×10^{-5} and 2.5×10^{-4} M (*i.e.* we start near the beginning of the expected deviation and we end close to the maximum of it).

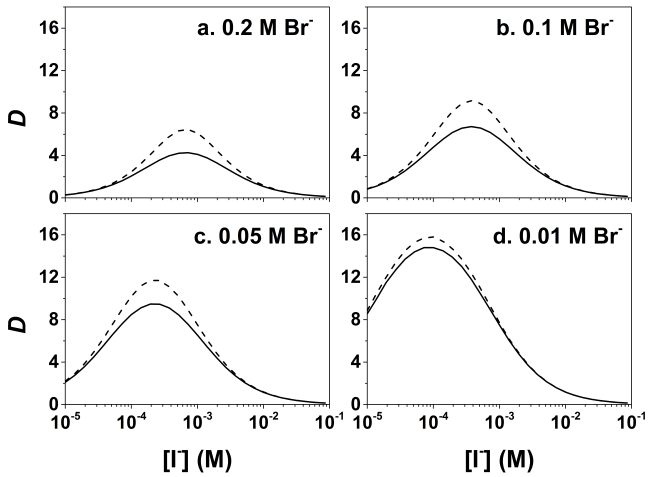

Figure 3.2. Simulation curves of the biphasic system: distribution coefficient (*D*) of astatine as a function of the I^- initial concentration at fixed Br^- concentrations (a.: 0.2 M, b.: 0.1 M, c.: 0.05 M, d.: 0.01 M), based on the parameters displayed in Table 3.1 and the DFT predicted Log *K* value. Dash lines correspond to the simulations that only deal with the binary 1:1 and 1:2 species, while solid lines are used for the simulations that also account for the formation of the $IAtBr^-$ species in the aqueous phase.

Prior to study ternary media that *a priori* include At^+, I^- and Br^- ions, we start by revisiting the binary At^+/Br^- and At^+/I^- systems to get accurate and consistent (with the same experimental procedure) values of the β_{1,X^-} and β_{2,X^-} constants. The aqueous phase consists in 0.1 M of $HClO_4$ (pH≈1, *E*≈0.6V), in which At^+ is the astatine dominant species, in the absence of complexing agent, according to its Pourbaix diagram.[3,4,5] The modeling of the At^+/Br^- system with adjustable $\text{Log}\,\beta_{1,Br^-}$ and $\text{Log}\,\beta_{2,Br^-}$ parameters (see Supporting Information) leads to the values displayed in Table 3.2. These values are in a good agreement with the previously published data.[8] Table 3.2 also gives the thermodynamic constants associated with the At^+/I^- binary system, which were derived from the modeling of the At distribution coefficient as a function of I^- concentration (see Figure 3.3). The experimental data shows no signature of any speciation change when the initial I^- concentration is below 10^{-8} M. The increase of *D* value between 10^{-8} and 10^{-5} M implies the formation of a new species that is extracted in toluene, and a plateau is reached between 10^{-5} and 10^{-3} M. The *D* value then decreases, which suggests the formation of another species that is not extracted in toluene. The experimental data are successfully modeled by considering the formation of 1:1 and 1:2 complexes, and the determined thermodynamic constants are found to be in good agreement with the electromigration data.[9]

Table 3.2. Thermodynamic constants at zero ionic strength for the reactions of the At^+ cation with Br^- and I^- ligands (this work).

X^-	Br^-	I^-
$\text{Log}\,\beta_{1,X^-}$	2.7 ± 0.2	6.1± 0.2
$\text{Log}\,\beta_{2,X^-}$	3.8 ± 0.3	8.8± 0.2

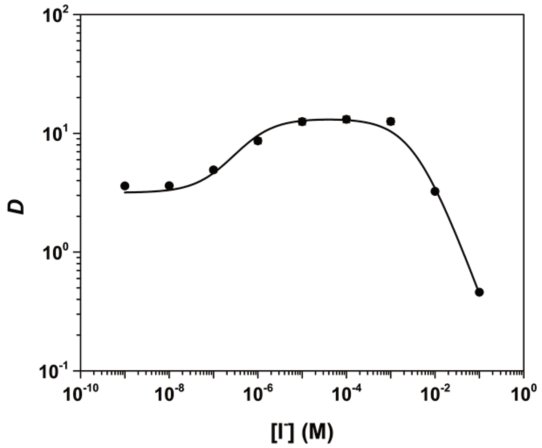

Figure 3.3. At^+/I^- binary system: distribution coefficient as a function of the initial I^- concentration. The model curve obtained with the $\mathrm{Log}\,\beta_{1,I^-}$ and $\mathrm{Log}\,\beta_{2,I^-}$ values reported in Table 3.2 is displayed in solid line.

We now continue by analysing the data obtained for the ternary $At^+/I^-/Br^-$ system. As shown in Figure 3.4, the *D* value increases with the I^- concentration for both the 0.05 and 0.1 M initial Br^- concentrations. First, we tried to model the data by only considering binary 1:1 and 1:2 species with the parameter values that are given in Table 3.2. As can be seen, the model curves (a for 0.05 M of Br^- and c for 0.1 M of Br^-) cannot explain at all the experimental data. Therefore, the formation of at least another species must be considered. Following the previous prediction, we then further consider the formation of the $IAtBr^-$ species via reaction 1. As can be seen in Figure 3.4 (curve b for 0.05 M of Br^- and curve d for 0.1 M of Br^-), a Log *K* value of 7.5 leads to a satisfactory modelling of the experimental data. Furthermore, the fairly good agreement between the experimental value of Log *K* (7.5 ± 0.2) and the theoretical one (6.9) prompt us to confirm the existence of the $IAtBr^-$ species. The introduction of the $IAtBr^-$ species in the model leads to an effective decrease in the estimated AtI population (see Figure 3.7). Since this species can be extracted in toluene, contrary to the anionic $IAtBr^-$ one, the formation of the $IAtBr^-$ species translates in Figure 3.4 in a decrease in the modelled distribution coefficient.

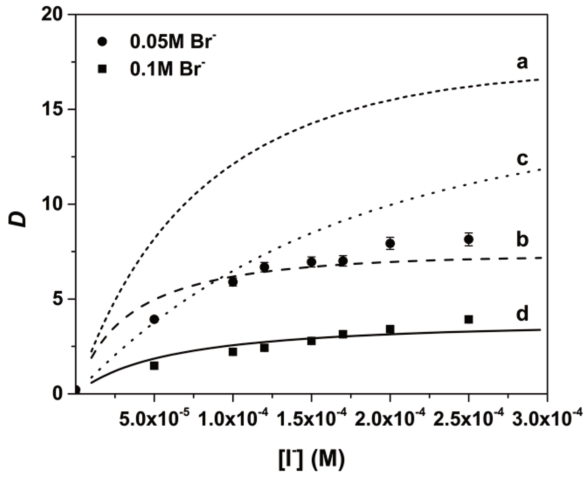

Figure 3.4. $At^+/I^-/Br^-$ ternary system: distribution coefficient as a function of the initial I^- concentration for two initial Br^- concentrations (0.05 M of Br^-, circles, and 0.1 M of Br^-, squares). The model curves obtained with only the values presented in Table 3.2 are displayed in short dash line (a. 0.05 M of Br^-) and dot line (c. 0.1 M of Br^-), and the ones obtained by further considering a Log *K* value of 7.5 are displayed in dash line (b. 0.05 M of Br^-) and solid line (d. 0.1 M of Br^-).

Having experimentally determined the Log *K* value, we can now build the At speciation diagram as a function of both the initial concentrations of I^- and Br^- (see Figure 3.5). The $IAtBr^-$ species can actually predominate for concentrations of I^- around 10^{-5}–10^{-2} M and Br^- around 0.1–1 M. This species, being the heaviest possible ternary trihalogen one, deserves some more attention from a chemical point of view. Of course, no structural information can be experimentally obtained on this species. Therefore, we discuss its relativistic DFT structure. All the structures of the trihalogen species considered in this work, *i.e.* $AtBr_2^-$, AtI_2^-, and $IAtBr^-$, are linear, the At atom being located in between the other two halogen ones. Therefore, the $IAtBr^-$ species is analogous to the ternary trihalogen $BrICl^-$ species, for which the heavier halogen, I, is located in between the two lighter ones.[7] The At–X distances are 2.91 Å ($AtBr_2^-$), 3.15 Å (AtI_2^-), and 2.92 and 3.14 Å ($IAtBr^-$) at the considered relativistic DFT level. One should stress that spin-orbit coupling must be taken into account for obtaining accurate geometries, At–X distances being affected by up to ~0.1 Å in

these systems. To determine the oxidation numbers (ONs) of At in these species, and also in the AtBr and AtI ones, as well as the ON of I in $BrICl^-$, we have estimated the number of valence *p* electrons of the heaviest halogen with complete active space configuration interaction (CASCI) calculations for which previously obtained complete active space self-consistent field (CASSCF) active orbitals were localized (see Supporting Information for more details). In all these species, more than 4.8 valence *p* electrons are obtained for the heaviest halogen, meaning that the actual wave function is much closer to the neutral limit for this halogen (5 *p* electrons) than to the first ionized one (4 *p* electrons). In other words, the ON of At in AtBr, AtI, $AtBr_2^-$, AtI_2^- and $IAtBr^-$ is zero (note that the ON of I in $BrICl^-$ is actually also zero), contrary to what was previously assumed for the AtI and AtI_2^- cases.[9] Since these species were formed from the At^+ moiety, one can consider that the formations of the molecules and ions considered in this work lead to a change in the At ON. This reveals that the wave functions in these species are not dominated by ionic configurations (of the forms $At^+ X^-$ and $X^- At^+ Y^-$, respectively), but rather by covalent ones (of the forms At–X and X–At Y^- and X^- At–Y, respectively). Note that, as expected, test calculations showed that the inclusion of spin-orbit coupling hardly affects the number of At *p* electrons, and thus, cannot change our conclusions on the At ON.

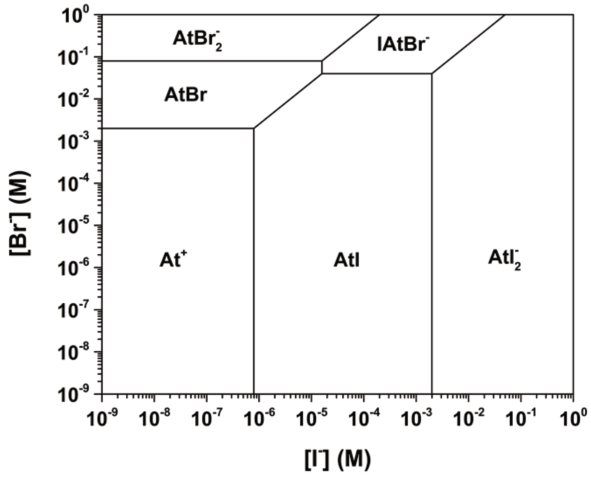

Figure 3.5. Experimental speciation diagram of At as a function of the initial concentrations of both the Br^- and I^- anions, based on the parameters displayed in Table 3.2 and the experimentally determined Log *K* value of 7.5.

In the present work, we have shown that adequate computational predictions can lead to the experimental discovery of an exotic chemical species, namely $IAtBr^-$. Of course, it is of high interest for chemists to know if other ternary trihalogen species that involve the At element can exist or even predominate in solution. Using the *in silico* methodology introduced in this work, we have assessed the possibility of forming the $IAtCl^-$ anion in the ternary $At^+/I^-/Cl^-$ case (see Supporting Information). Based on this prediction, we conclude that $IAtCl^-$ can be formed in solution. However, considering the extremely small-predicted domain of predominance, the experimental evidence of its existence may not be reachable in practice. Therefore, it is not yet confirmed if any other ternary trihalogen species involving At can predominate in solution.

Keywords: ternary trihalogen species • competition experiments • density functional theory • theoretical prediction • astatine

3.3.Support Information

3.3.1. Computational details

Gas-phase calculations were performed using the *NWChem* program package, v. 6.3 (patched by N. Govind).[15] Spin-orbit density functional theory (SO-DFT) calculations were performed to obtain the structures, energies, and vibrational frequencies of the binary 1:2 and ternary species of interest. The B3LYP exchange-correlation functional[12] was used owing its overall good behavior in reproducing equilibrium constants in the field of astatine chemistry.[8,11] Energy-consistent pseudo-potentials were used to mimic the role of core electrons and introduce implicitly scalar and spin-dependent relativistic effects, namely the ECP10MDF (Br),[16] ECP28MDF (I)[17] and ECP60MDF (At) ones[16]. Double-zeta basis sets with polarization and diffuse functions were used, in particular the aug-cc-pVDZ (Cl),[18] aug-cc-pVDZ-PP (Br) and aug-cc-pVDZ-PP-2c (I) ones,[16,17,19] plus a modified version[8] of the aug-cc-pVDZ-PP-2c basis set[16,19] for At, often referred to as 'mAVDZ'. Solvation free energies were computed with the *Gaussian 09* program package (revision A.02)[20] at the Hartree-Fock level, as the difference between the ground-state electronic energies that are obtained with and without the presence of a conductor-like polarizable continuum model (CPCM).[13] A key point in computing solvation energies is the definition of the cavity. The 1.2 α factor was used, together with the (united atom) UAHF cavity model[21] complemented with the 2.41 Å basic radius for At[8]. The scalar-relativistic (SR) versions of the ECP10MDF (Br), ECP28MDF (I) and ECP60MDF (At) energy consistent pseudo-potentials were used, together with the aug-cc-pVDZ (Cl),[18] aug-cc-pVDZ-PP (Br),[16] aug-cc-pVDZ-PP-2c (I)[17,19] and mAVDZ (At)[8] basis sets. The reaction constants were computed according to the following thermodynamic cycle:

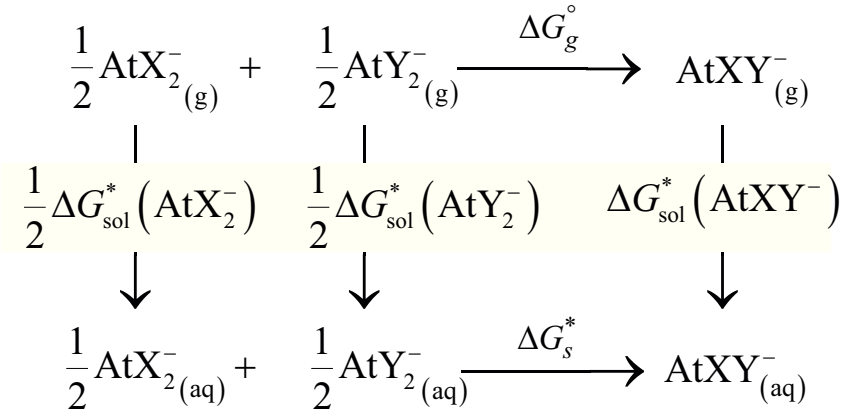

Additional gas-phase calculations were performed to determine the oxidation numbers (ONs) of the heaviest halogen in the astatine species of interest as well as in an iodine analogue. For this, we have performed single-point multiconfigurational calculations at DFT geometries obtained using the SR versions of the aforementioned pseudopotentials. The multiconfigurational calculations were performed with the MOLPRO program package.[22] Complete active space self-consistent field (CASSCF) calculations in which all the valence *p* electrons and orbitals define the active space were done. Aug-cc-pVTZ and aug-cc-pVTZ-PP basis sets[16–18] were used together with the previously mentioned SR pseudopotentials.[16,17] After CASSCF calculations, the orbitals were localized (Pipek-Medzey method) on each atom, and complete active space configuration interaction (CASCI) calcualtions were performed. The analysis of the occupation numbers gives the number of *p* electrons of the halogen under study, thus giving access to its ON (*e.g.* +I for ~4 or 0 for ~5 *p* electrons).

3.3.2. Materials and methods

3.3.2.1. Materials and production of At-211

Commercially available sodium iodide, sodium bromide, toluene and 70% perchloric acid were used (Sigma-Aldrich); all of these reagents were of analytical grade. All solutions were prepared using Milli-Q water and all experiments were conducted in air-conditioned laboratories (20±3 °C).

At-211 was produced *via* the $^{209}Bi(\alpha, 2n)^{211}At$ nuclear reaction in the ARRONAX

cyclotron at Nantes, France. Bismuth-209 targets were irradiated for two hours by alpha external beams accelerated to 28 MeV.[23] After irradiation of the target, a dry distillation method was used to isolate At-211 and then recover 10 MBq of At-211 into 200 µL of chloroform.[24] The radionuclide purity of At-211 was verified by gamma-ray spectroscopy with a high purity germanium (HPGe) detector. Astatine was recovered after back-extractions in 2 mL of 0.1 M NaOH solutions.

3.3.2.2. Competition method

At^+ was then obtained in 0.1 M $HClO_4$ solutions (pH≈1 and E≈0.6 V *vs.* NHE, the normal hydrogen electrode), in accordance with the established Pourbaix diagram of astatine.[3–5] The reaction constants between At^+ and the inorganic ligands (Br^- and I^-) were determined by the competition method proposed by Champion *et al.*.[8] The method consists in studying the distribution of At-211 between an aqueous phase and a toluene one as a function of the initial inorganic ligand concentrations present in the aqueous solution. The systems (4 mL of organic phase and 4 mL of aqueous phase were brought into contact in Pyrex tubes) were first equilibrated before At-211 (~1000 Bq) addition. After the addition of At^+, two hours of shaking were done to achieve distribution equilibrium of At(I) between the two phases. Then the two phases were separated, and an aliquot of both the aqueous and organic phases was withdrawn to derive the distribution coefficient D:

$$D = \frac{A_{org} \times V_{aq}}{A_{aq} \times V_{org}} \tag{3.6}$$

where V_{org} and V_{aq} represent given phase volumes, and A_{org} and A_{aq} are the astatine activities in the organic and aqueous phases at equilibrium, respectively. Uncertainties associated with D values were calculated according to the following equation:

$$\sigma_D = D \times \sqrt{\frac{\sigma^2_{A_{org}}}{A_{org}} + \frac{\sigma^2_{A_{aq}}}{A_{aq}} + \frac{\sigma^2_{V_{org}}}{V_{org}} + \frac{\sigma^2_{V_{aq}}}{V_{aq}}} \tag{3.7}$$

These activities were measured using liquid scintillation counting with a Packard 2550 TR/AB Liquid Scintillation analyzer with the Ultima Gold LLT scintillation liquid[8]. The quenching caused by the different solvents was considered to determine the At-211 activity (A) according to the following equation:

$$A = A_{\text{mes}} \times (8\times10^{-10}\times tSIE^3 - 2\times10^{-6}\times tSIE^2 + 0.0013\times tSIE + 0.7228) \quad (3.8)$$

with A_{mes} being the activity measured by liquid scintillation and $tSIE$ (transformed spectral index of the external standard) a parameter defined by the apparatus for counting efficiency determination.

Experiments were twice repeated with the same experimental conditions and the mean values are given together with uncertainties corresponding to a 95% confidence interval.

An electrode (Inlab) freshly calibrated with standard pH buffers (pH 4 and 7, Merck), and a Pt combined redox electrode (Metrohm) calibrated with a redox buffer ($Fe(SCN)_6^{3-}/Fe(SCN)_6^{4-}$, 220 mV/Pt/SCE, Radiometer Analytical), were used to measure the pH and the potential (E) of the aqueous phase of every sample at equilibrium. Since both the pH and E are here essentially controlled by the $HClO_4$ concentration, no significant deviation from the targeted 1 and 0.6 V values, respectively, was observed.

3.3.2.3. Determination of the stability constants

Considering the pK_a values of HBr (−8.8) and HI (−9.5),[25] dissolved NaBr and NaI salts produce the ionic Br^- and I^- species given the experimental conditions. These anionic species can form binary species with At^+ as follows:

$$At^+ + mX^- \rightleftharpoons AtX_m^{1-m} \quad (3.9)$$

with X^- corresponding to either Br^- or I^-, and where AtX_m^{1-m} are species formed with a 1:m stoichiometry. The associated equilibrium constant is given as:

$$\beta_{m,X} = \frac{[AtX_m^{1-m}]}{[At^+][X^-]^m} \quad (3.10)$$

where square brackets indicate the species concentrations at equilibrium.

The CHESS program was used to simulate the reaction equilibrium occurring in the biphasic system.[14] First, an input file containing the experimental conditions

(pH, *E* and temperature) is created, and the species distribution at equilibrium is calculated with the thermodynamic database introduced in CHESS, which contains (i) the distribution of At-211 between the aqueous and organic phases, (ii) the possible redox reactions involving At^+ in the given experimental conditions,[4] and (iii) the reactions describing the interaction between At^+ and the ligands.[8,9]

The equilibrium constants associated with the reactions were determined through the following steps:

1) The reaction parameters considered in the simulation with CHESS were adjusted to get the best "visual" agreement between the experimental data and the modeling data.

2) Based on the main equilibria, the expression of the At-211 distribution in the two phases as a function of the experimental conditions was obtained according to the following equations:

$$At^+ + Br^- \rightleftharpoons AtBr \qquad \beta_{1,\,Br^-} = \frac{[AtBr]}{[At^+]\times[Br^-]} \tag{3.11}$$

$$At^+ + 2Br^- \rightleftharpoons AtBr_2^- \qquad \beta_{2,\,Br^-} = \frac{[AtBr_2^-]}{[At^+]\times[Br^-]^2} \tag{3.12}$$

$$At^+ + I^- \rightleftharpoons AtI \qquad \beta_{1,\,I^-} = \frac{[AtI]}{[At^+]\times[I^-]} \tag{3.13}$$

$$At^+ + 2I^- \rightleftharpoons AtI_2^- \qquad \beta_{2,I^-} = \frac{[AtI_2^-]}{[At^+]\times[I^-]^2} \tag{3.14}$$

$$At^+ + I^- + Br^- \rightleftharpoons IAtBr^- \qquad K = \frac{[IAtBr^-]}{[At^+]\times[I^-]\times[Br^-]} \tag{3.15}$$

$$At^+ \rightleftharpoons \overline{At^+} \qquad D_0 = \frac{[At^+]_{org}}{[At^+]_{aq}} \tag{3.16}$$

$$AtI \rightleftharpoons \overline{AtI} \qquad D_1 = \frac{[AtI]_{org}}{[AtI]_{aq}} \tag{3.17}$$

From these constants, one can then obtain an expression for D:

$$D = \frac{D_0 + D_1 \times \beta_{1,I^-} \times [I^-]}{1 + \beta_{1,Br^-} \times [Br^-] + \beta_{2,Br^-} \times [Br^-]^2 + \beta_{1,I^-} \times [I^-] + \beta_{2,I^-} \times [I^-]^2 + K \times [I^-] \times [Br^-]} \tag{3.18}$$

Note that the extraction of the anionic species is neglected, and that the D_0 and D_1 parameters are the only adjustable parameters. Equation (3.18) was used to best fit the experimental data with Origin 9.0 by refining the parameter values of interest. The uncertainties associated with the parameter values were determined by the software.

3) The parameter values were then used in a final simulation with CHESS for validation.

4) All the equilibrium constants in the database were finally extrapolated to zero ionic strength using a truncated Davies equation.[10]

3.3.2.4. Determination of the reaction constants of the binary At^+/Br^- system

Figure 3.6 displays the astatine distribution coefficient as a function of the Br^- concentration. As can be seen in Figure 3.6, Br^- concentrations lower than 10^{-4} M does not affect D, which is thus controlled by the distribution of the At^+ species. For higher concentrations, D monotonously decreases due to the formation of binary 1:1 and 1:2 species. The modeling of this curve leads to the $\text{Log}\,\beta_{1,Br^-}$ and $\text{Log}\,\beta_{2,Br^-}$ values displayed in Table 3.2. These values are in a good agreement with the previously published data shown in Table 3.1.[8]

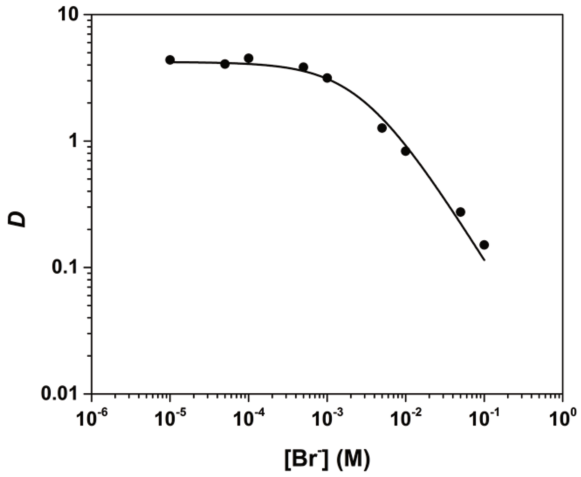

Figure 3.6. At^+/Br^- binary system: distribution coefficient as a function of the initial Br^- concentration. The model curve obtained with the Log β_{1,X^-} and Log β_{2,Br^-} values reported in Table 2 is displayed in solid line.

3.3.2.5. Speciation diagram of At under the probed experimental conditions

Speciation diagrams of astatine in the presence of Br^- at fixed concentrations, and as a function of the I^- concentration, are displayed in Figure 3.7. As can be seen, curves a (0.05 M Br^-) and c (0.1 M Br^-) are only based on the parameters displayed in Table 3.2, *i.e.* only the binary species are considered. In the range of probed I^- concentrations (5×10^{-5} to 2.5×10^{-4} M), the *D* value should largely increase according to the large increase of the AtI population (this species can be extracted in toluene). However, the experimental results displayed in Figure 3.4 shows that the *D* value only moderately increases under the experimental conditions, so that the formation of a new anionic species, $IAtBr^-$, was proposed to explain the data. When this formation is considered with a Log *K* value of 7.5, the dominant species under the probed experimental conditions is $IAtBr^-$, while the population of the AtI species is largely decreased (see curves b and d). Assuming that the anionic $IAtBr^-$ species is not extracted in toluene, one can understand that an increase of the $IAtBr^-$ population at the expanse of the AtI one, must lead to a reduction of the distribution coefficient, as was observed in

Figure 3.4.

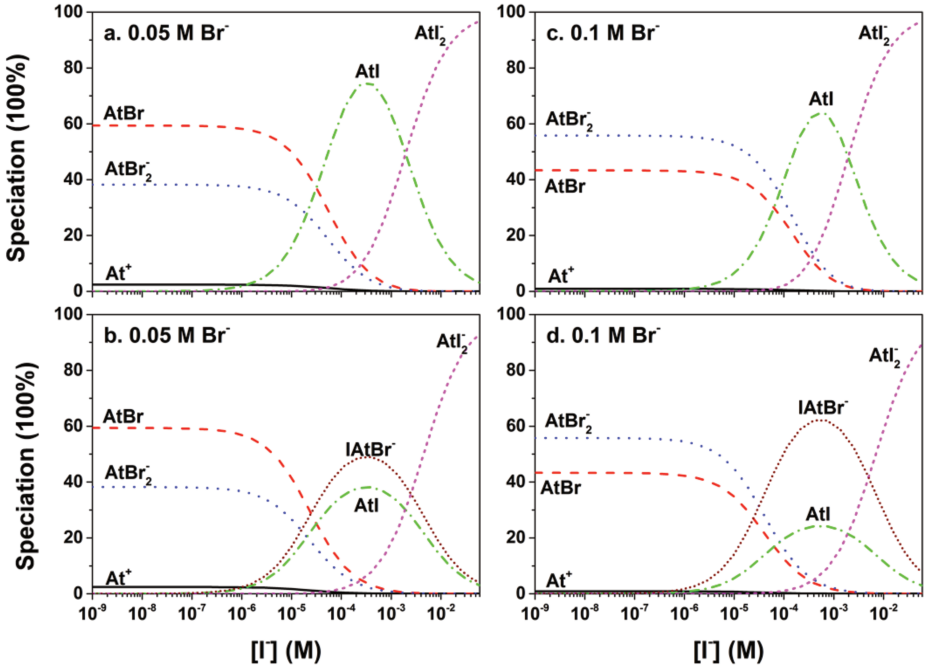

Figure 3.7. Speciation diagrams of At in the presence of Br^- at fixed concentrations, and as functions of the I^- concentration, obtained with the parameters displayed in Table 3.2 (a and c), and by further considering the experimental Log *K* value (b and d).

3.3.2.6. Discussion related to the $IAtCl^-$ species

In a similar way as what was done in the $IAtBr^-$ case, we used SO-DFT to assess the possibility to form $IAtCl^-$ in solution. Experimental values of the equilibrium constants associated with the formation of the binary 1:1 and 1:2 species are reported in Table 3.3. The equilibrium constant corresponding to the formation of the ternary $IAtCl^-$ species (K_2) was computed via the following ligand-exchange reaction:

$$\frac{1}{2}AtCl_2^- + \frac{1}{2}AtI_2^- \rightleftharpoons IAtCl^- \quad (3.19)$$

which readily leads to:

$$\text{Log } K' = \frac{1}{2}\text{Log } \beta_2(Cl^-) + \frac{1}{2}\text{Log } \beta_2(I^-) + \text{Log } K_2 \quad (3.20)$$

With similar computational details as before, we obtained a Log K_2 value of 0.4,

leading to a predicted Log *K'* value of 6.2. One should note that the At oxidation number in AtCl, $AtCl_2^-$ and $IAtCl^-$ is also predicted to be zero (the number of valence *p* electrons of At being larger than 4.7 in all these species).

Table 3.3. Thermodynamic constants available in the literature for the reaction of the At^+ cation with Cl^- and I^- ligands.

X^-	Cl^-	I^- *
Log β_{1,X^-}	1.9 ± 0.2[8]	6.0[9]
Log β_{2,X^-}	2.3 ± 0.1[8]	9.2[9]

* Extrapolated from the 0.5 M ionic strength (6.2 and 9.4, respectively) to zero ionic strength through a truncated Davies equation.[10]

The predicted speciation diagram of At in the presence of Cl^- and I^- ions is depicted in Figure 3.8. As can be seen, a very tiny domain where the ternary $IAtCl^-$ system should predominate is predicted. Therefore, even if we theoretically predict the formation of this species in solution, we did not attempt to experimentally evidence its occurrence due to the detection accuracy inherent to the experimental setup (competition method and analytical tools).

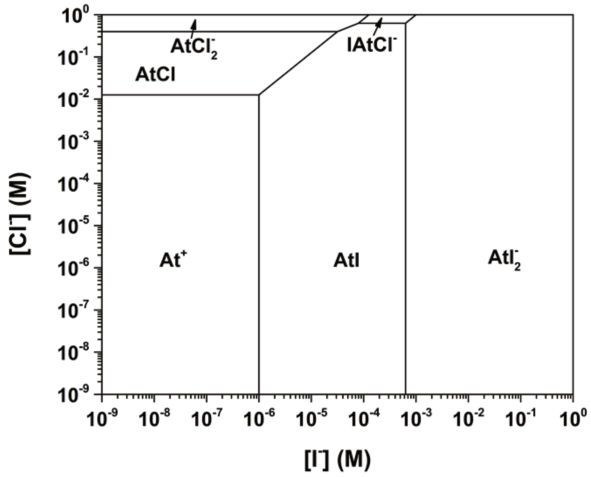

Figure 3.8. Predicted speciation diagram of At as a function of the initial concentrations of both the Cl^- and I^- anions, based on the parameters displayed in Table 3.3 and the DFT predicted Log K_2 value.

3.4. Ancillary section

3.4.1. Investigation of the $At^{+}/I^{-}/Br^{-}$ ternary system

Based on the theoretical calculation results, $IAtBr^{-}$ species might be predominant in a small specific area. In order to find this domain experimentally, the distribution coefficient (D) of astatine as a function of initial I^{-} concentration in the presence of four different initial Br^{-} concentrations (0.005 M, 0.01 M, 0.05 M and 0.1 M) was studied (Figure 3.9). When the Br^{-} concentrations are 0.005 M (a) and 0.01 M (b), the simulation (solid lines) with only considering the formation of binary species based on the parameters in Table 3.2 can explain the experimental results (squares). For Br^{-} concentrations of 0.05 M (c) and 0.1 M (d), the deviation between the simulation lines considering the formation of the binary species and the experimental data is noticeable, when the I^{-} concentration is between 10^{-5} and 10^{-4} M. Indeed, the experimental data are quite lower than the simulation lines in this area. This means that more details in this area need to be revealed and at least one more new species that cannot be extracted to toluene should be introduced. Based on this experimental attempt and the theoretical prediction, further experimental condition was studied for I^{-} concentration varying from 5×10^{-5} to 2.5×10^{-4} M in the presence of 0.05/0.1 M of Br^{-}. The results are given in Figure 3.4 in the main article.

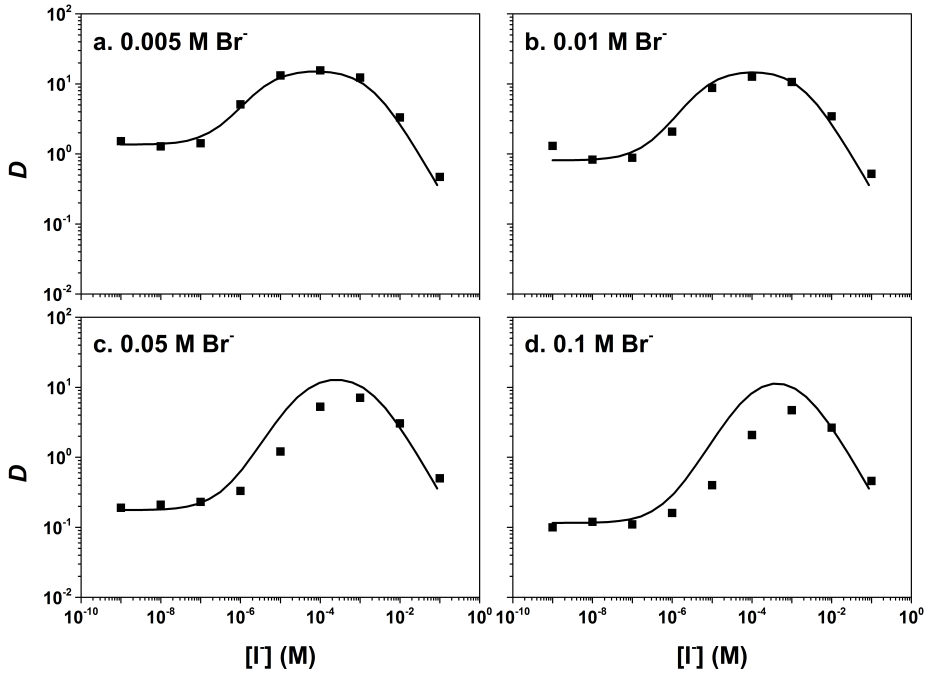

Figure 3.9. Distribution coefficient (*D*) of astatine as a function of the I^- initial concentration at fixed Br^- concentrations (a.: 0.005 M, b.: 0.01 M, c.: 0.05 M, d.: 0.1 M), based on the parameters displayed in Table 3.2. Solid lines correspond to the simulations that only deal with the binary 1:1 and 1:2 species.

3.4.2. Determination of the reaction constants of the binary At^+/Cl^- system

The binary system of At^+/Cl^- was also studied to give more information on the investigation of the $At^+/I^-/Cl^-$ ternary system. The distribution coefficient (*D*) of astatine as a function of Cl^- initial concentration is displayed in Figure 3.10. Cl^- concentrations lower than 10^{-3} M does not affect *D* value, which is caused by the distribution of the At^+ species. For higher concentrations, *D* decreases due to the formation of binary 1:1 and 1:2 species. The modeling of this curve with adjustable $Log\beta_{1,Cl^-}$ and $Log\beta_{2,Cl^-}$ parameters leads to the values displayed in Table 3.4, based on the following equations. The values obtained are in agreement with the previously published data shown in Table 3.4.[8]

$$At^+ + Cl^- \rightleftharpoons AtCl \qquad \beta_{1,\,Cl^-} = \frac{[AtCl]}{[At^+]\times[Cl^-]} \tag{3.21}$$

$$At^+ + 2Cl^- \rightleftharpoons AtCl_2^- \qquad \beta_{2,\,Cl^-} = \frac{[AtCl_2^-]}{[At^+]\times[Cl^-]^2} \tag{3.22}$$

$$At^+ \rightleftharpoons \overline{At^+} \qquad D_0 = \frac{[At^+]_{org}}{[At^+]_{aq}} \tag{3.23}$$

$$D = \frac{D_0}{1+\beta_{1,\,Cl^-}\times[Cl^-]+\beta_{2,\,Cl^-}\times[Cl^-]^2} \tag{3.24}$$

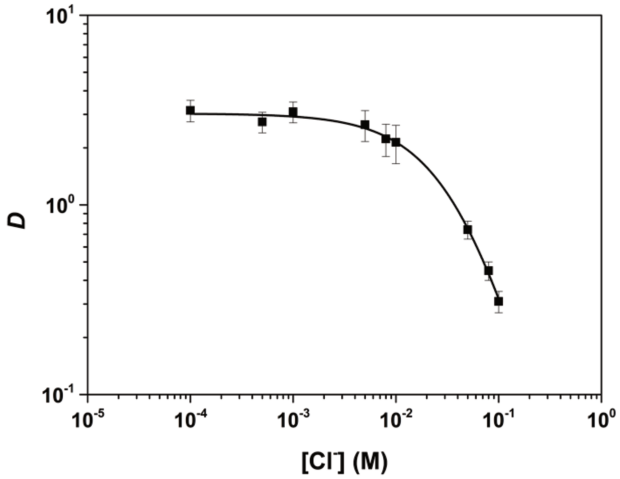

Figure 3.10. At^+/Cl^- binary system: distribution coefficient as a function of the initial Cl^- concentration. The model curve obtained with the $\mathrm{Log}\,\beta_{1,\,Cl^-}$ and $\mathrm{Log}\,\beta_{2,\,Cl^-}$ values reported in Table 3.4 is displayed in solid line.

Table 3.4. Thermodynamic constants at zero ionic strength for the reactions of the At^+ cation with Cl^- ligands at this work and the ones extracted from literature.

	This work	Literature
$\mathrm{Log}\,\beta_{1,\,Cl^-}$	1.6±0.3	1.9±0.2[8]
$\mathrm{Log}\,\beta_{2,\,Cl^-}$	2.4±0.2	2.3±0.1[8]

3.4.3. Investigation on the $At^+/I^-/Cl^-$ ternary system

According to the theoretical calculation, only a very tiny domain where the ternary $IAtCl^-$ system should predominate is predicted, which appears when the Cl^- concentration is larger than 0.8 M (Figure 3.8). However, the Davies equation, which was used to extrapolate the constants into zero ionic strength, has a limit of the ionic strength that should below 0.3 M.[10] For these reasons, it is difficult to identify the existence of $IAtCl^-$ species in the $At^+/I^-/Cl^-$ system. Some investigations on the $At^+/I^-/Cl^-$ ternary system with Cl^- concentration lower than 0.2 M were conducted.

The distribution coefficient of astatine as a function of initial I^- concentration in the presence of different Cl^- concentrations is displayed in Figure 3.11. The simulation considering with the binary 1:1 and 1:2 species (solid lines) could well explain the experimental data (squares), as seen in Figure 3.11. In addition, depending on the theoretical calculation, if we consider the formation of $IAtCl^-$ with the Log *K*' 6.2, the simulation lines can be displayed in Figure 3.11 (dash lines). This implies that under these experimental conditions, if new species like $IAtCl^-$ forms, it could not be directly identified through the variation of the *D* value.

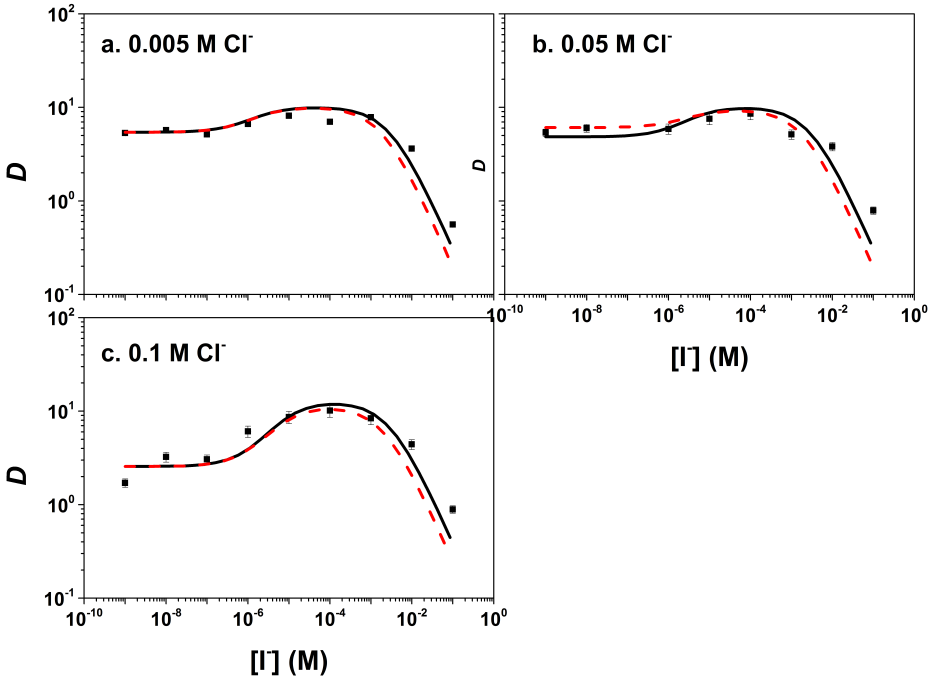

Figure 3.11. Distribution coefficient (*D*) of astatine as a function of the I^- initial concentration at fixed Cl^- concentrations (a.: 0.005 M, b.: 0.05 M, c.: 0.1 M), based on the parameters displayed in Table 3.2 and Table 3.4. Solid lines correspond to the simulations that only deal with the binary 1:1 and 1:2 species; dash lines correspond to simulations considering the $IAtCl^-$ species with the theoretical predicted Log *K*'.

3.5.Conclusion

1. Thermodynamic constants at zero ionic strength for the reactions of the At^+ cation with Br^-, I^- and Cl^- ligands were defined with the same experimental procedure; they are displayed in the following table:

X^-	Br^-	I^-	Cl^-
Log β_{1,X^-}	2.7 ± 0.2	6.1± 0.2	1.6±0.3
Log β_{2,X^-}	3.8 ± 0.3	8.8± 0.2	2.4±0.2

2. By analysing the data obtained for the ternary $At^+/I^-/Br^-$ system, the Log K for the formation of the $IAtBr^-$ species was defined as 7.5±0.2, which has a good agreement with the theoretical one (6.9).

$$At^+ + I^- + Br^- \rightleftharpoons IAtBr^-$$

3. The DFT structures of $AtBr_2^-$, AtI_2^-, and $IAtBr^-$ are linear, the At atom being located in between the other two halogen ones. With the CASCI calculation, the At oxidation number in AtBr, AtI, $AtBr_2^-$, AtI_2^- and $IAtBr^-$ is found as zero.

4. Through the computational prediction and the experimental attempt on the ternary $At^+/I^-/Cl^-$ system, it is difficult to give any conclusion on the existence of $IAtCl^-$ species.

References

(1) Zalutsky, M. R.; Pruszynski, M. *Curr. Radiopharm.* **2011**, *4* (3), 177.

(2) Wilbur, D. S. *Nat. Chem.* **2013**, *5* (3), 246.

(3) Sergentu, D. C.; Teze, D.; Sabatié-Gogova, A.; Alliot, C.; Guo, N.; Bassal, F.; Silva, I. Da; Deniaud, D.; Maurice, R.; Champion, J.; Galland, N.; Montavon, G. *Chem. - A Eur. J.* **2016**, *22* (9), 2964.

(4) Champion, J.; Alliot, C.; Renault, E.; Mokili, B. M.; Chérel, M.; Galland, N.; Montavon, G. *J. Phys. Chem. A* **2010**, *114* (1), 576.

(5) Champion, J.; Sabatié-Gogova, A.; Bassal, F.; Ayed, T.; Alliot, C.; Galland, N.; Montavon, G. *J. Phys. Chem. A* **2013**, *117* (9), 1983.

(6) Guidelli, R.; Pergola, F. *J. Inorg. Nucl. Chem.* **1969**, *31* (1964), 1373.

(7) Sanov, A.; Sanford, T.; Butler, L. J.; Vala, J.; Kosloff, R.; Lineberger, W. C. *J.Phys.Chem.* **1999**, *103*, 10244.

(8) Champion, J.; Seydou, M.; Sabatié-Gogova, A.; Renault, E.; Montavon, G.; Galland, N. *Phys. Chem. Chem. Phys.* **2011**, *13* (33), 14984.

(9) Ludwig, R.; Fischer, S.; Hussein, H.; Frind, M.; Dreyer, R. *J. Radioanal. Nucl. Chem. Artic.* **1989**, *134*, 141.

(10) Colston, B. J.; Robinson, V. J. *J. Environ. Radioact.* **1995**, *29* (2), 121.

(11) Sergentu, D.-C.; David, G.; Montavon, G.; Maurice, R.; Galland, N. *J. Comput. Chem.* **2016**, *37* (15), 1345.

(12) Stephens, P. J.; Devlin, F. J.; Chabalowski, C. F.; Frisch, M. J. *J. Phys. Chem.* **1994**, *98* (45), 11623.

(13) Cossi, M.; Rega, N.; Scalmani, G.; Barone, V. *J. Comput. Chem.* **2003**, *24* (6), 669.

(14) Champion, J.; Alliot, C.; Huclier, S.; Deniaud, D.; Asfari, Z.; Montavon, G. *Inorganica Chim. Acta* **2009**, *362* (8), 2654.

(15) Bylaska, E. J. *Pacific Northwest National Laboratory, Richland, Washington*. 2013, p 999.

(16) Peterson, K. A.; Figgen, D.; Goll, E.; Stoll, H.; Dolg, M. *J. Chem. Phys.* **2003**, *119* (21), 11113.

(17) Peterson, K. A.; Shepler, B. C.; Figgen, D.; Stoll, H. *J. Phys. Chem. A* **2006**, *110* (51), 13877.

(18) Woon, D. E.; Dunning, T. H. *J. Chem. Phys.* **1993**, *98* (2), 1358.

(19) Armbruster, M. K.; Klopper, W.; Weigend, F. *Phys. Chem. Chem. Phys.* **2006**, *8* (42), 4862.

(20) Frisch, M. J.; Trucks, G. W.; Schlegel, H. B.; Scuseria, G. E.; Robb, M. A.; Cheeseman, J. R.; Scalmani, G.; Barone, V.; Mennucci, B.; Petersson, G. A.; Nakatsuji, H.; Caricato, M.; Li, X.; Hratchian, H. P.; Izmaylov, A. F.; Bloino, J.; Zheng, G.; Sonnenberg, J. L.; Hada, M.; Ehara, M.; Toyota, K.; Fukuda, R.; Hasegawa, J.; Ishida, M.; Nakajima, T.; Honda, Y.; Kitao, O.; Nakai, H.; Vreven, T.; Montgomery Jr., J. A.; Peralta, J. E.; Ogliaro, F.; Bearpark, M.; Heyd, J. J.; Brothers, E.; Kudin, K. N.; Staroverov, V. N.; Kobayashi, R.; Normand, J.; Raghavachari, K.; Rendell, A.; Burant, J. C.; Iyengar, S. S.; Tomasi, J.; Cossi, M.; Rega, N.; Millam, J. M.; Klene, M.; Knox, J. E.; Cross, J. B.; Bakken, V.; Adamo, C.; Jaramillo, J.; Gomperts, R.; Stratmann, R. E.; Yazyev, O.; Austin, A. J.; Cammi, R.; Pomelli, C.; Ochterski, J. W.; Martin, R. L.; Morokuma, K.; Zakrzewski, V. G.; Voth, G. A.; Salvador, P.; Dannenberg, J. J.; Dapprich, S.; Daniels, A. D.; Farkas, Ö.; Foresman, J. B.; Ortiz, J. V; Cioslowski, J.; Fox, D. J. *Gaussian Inc Wallingford CT*. 2009, p Wallingford CT.

(21) Barone, V.; Cossi, M.; Tomasi, J. *J. Chem. Phys.* **1997**, *107* (8), 3210.

(22) Werner, H.-J.; Knowles, P. J.; Knizia, G.; Manby, F. R.; Schütz, M.; Others. .

(23) Alliot, B. C.; Cherel, M.; Barbet, J.; Sauvage, T.; Montavon, G. *Radiochim. Acta* **2009**, *97*, 161.

(24) Lindegren, S.; Bäck, T.; Jensen, H. J. *Appl. Radiat. Isot.* **2001**, *55* (2), 157.

(25) Trummal, A.; Lipping, L.; Kaljurand, I.; Koppel, I. A.; Leito, I. *J. Phys. Chem. A* **2016**, *120* (20), 3663.

Chapter 4. First halogen-bonded adducts involving At: At is a stronger halogen-bond donor than I

4.1. Abstract

Non-covalent interactions play an important role on a wide range of properties of many chemical systems. Among these interactions, halogen bonds form an important class of bonds. However, no halogen-bonded adduct with At has been reported so far. In this work, we evidence for the first time such systems and determine the ligand basicity scale with AtI as was done a few years ago for the I_2 case [Chem. Eur. J. **2011**, *17*, 10431-10444]. The complexation constants of a series of organic ligands with AtI are determined by means of competition experiments and the results are rationalized by relativistic quantum mechanical calculations. We find that AtI is a stronger XB donor than I_2 and that the At σ-hole in AtI corresponds to a more electrophilic site than I in the same system as well as in I_2. Therefore, we conclude that At is a stronger XB donor than I.

4.2. Introduction

Non-covalent interactions play an important role in the chemistry of a wide range of systems, in terms of structure, property and reactivity for instance. Therefore, they can be considered in the design of novel molecules and materials of desired properties. Among these, one may quote the hydrogen bonds and also halogen ones, of growing interest in the last few decades.[1,2] Unlike hydrogen bonds, halogen bonds are associated with electron donation to the halogen atom. Despite this fact, the halogen atom is part of the halogen-bond (XB) donor R-X. Moreover, these interactions are characterized by the directionality of the interaction with a near or perfect alignment between the halogen, the first

neighboring atom of R that is covalently bound to it, and the first neighboring atom of the electron-donating group (B). According to the recent definition given by IUPAC, "A halogen bond occurs when there is evidence of a net attractive interaction between an electrophilic region associated with a halogen atom in a molecular entity and a nucleophilic region in another, or the same, molecular entity".[3] A halogen bond (XB) is commonly represented by three dots, R-X···B. Note that in some cases, X can be covalently bonded to more than one group.[4,5] The electrophilic region associated with a halogen atom in R-X is the so-called "σ-hole", which is a region of space with a positive molecular electrostatic potential (MEP) that is perfectly of nearly centered on the R-X axis, as a consequence of the anisotropy of the electronic distribution. This region can interact favorably with electron rich sites, giving rise to halogen bonding.[6]

The F (to a lesser extent), Cl, Br and I elements can be involved in halogen bonds as XB donors.[7] Moreover, the XB strength scales with the polarizability of the XB donor atom: F < Cl < Br < I. The polarizability of astatine (At), the heaviest halogen, was computed to be higher than iodine.[8] Therefore, one can expect that At may be a stronger XB donor than I. Also, scalar relativistic calculations showed that the hypoastatous acid (HOAt) could form more stable X···N halogen bonds than its F, Cl, Br and I analogues.[9] One may also quote theoretical calculations focused on the reaction of the hypothetical diastatine compound with ammonia.[10] Even though these theoretical calculations give some clues on halogen bonds involving At, to date, no halogen-bonded adducts involving At have been reported. Therefore, it is crucial and timely to experimentally synthesize such systems.

To characterize the halogen bond strengths, the basicity scale with diiodine (pK_{BI2}) was proposed a few years ago.[11] It is identified "as the thermodynamic tendency of a substance to act as a halogen-bond acceptor and measure this property by the equilibrium constants of halogen-bond formation for a series of bases with a common reference acid, diiodine". The reaction between I_2 and a Lewis base is written as:

$$B + I_2 \rightleftharpoons B \cdots I - I$$

where I_2 is the considered Lewis acid, B is a Lewis base, and K_c is the related

equilibrium constant. The pK_{BI2} values used to define the basicity scale with diiodine can be thus obtained as:

$$pK_{BI_2} = \log(K_c/1\ \mathrm{L\ mol^{-1}})$$

This basicity scale was validated for dihalogen and interhalogen compounds, and is meant to be general.[11] Therefore, we aim at determining the basicity scale of a series of ligands with an astatine compound, with the aim of (i) checking the transferability of this scale to an astatine compound and (ii) comparing the interaction strengths with the ones that were previously obtained with diiodine.

However, At has no stable or long-live isotopes and it can only be produced in very small quantities of matter. Therefore, one can only work at ultra-trace At concentrations (typically below 10^{-10} M), which limits the experimental techniques that can be used to probe the nature of the species and the chemical bonds in them (no standard spectroscopy tool can be used at such low concentrations).[12] Also, one cannot envisage forming any XB donor that involves astatine at such concentrations, there is to date no experimental evidence that one can form the diastatine species. Therefore, among the diatomics that involve astatine, only heterodiatomic compounds can be envisaged. As shown in previous studies,[13,14] it is possible to form binary dihalogen compounds with astatine such as AtCl, AtBr and AtI in aqueous solution. Since we specifically want to compared the At and I XB donor abilities, we will thus focus here on the AtI XB donor.

As mentioned before, unlike with iodine, no spectroscopic tool can be used to probe astatine compounds. Competition methods can however be used to study speciation changes with astatine and also determine equilibrium constants.[12,13,15] In these approaches, the distribution coefficient (D) of astatine between two phases is tracked as a function of the initial concentrations of ligand(s). In this case, a change in the D value arising from a change in the experimental conditions must indicate a change in speciation. In this work, the competition between two liquid phases, an organic one and an aqueous one, is used to explore the interaction between AtI and a series of Lewis bases. Modeling is then used to determine the corresponding equilibrium constants in the organic phase. Also, in order to get further insight on the differences between the AtI and I_2

cases, these systems are studied by means of quantum mechanical calculations.

4.3.Materials and Methodology

4.3.1. Production of At-211

The At-211 employed in this work was produced by the ARRONAX cyclotron (Nantes, France) through the nuclear reaction ^{207}Bi(α, 2n)^{211}At. Bismuth-209 targets were irradiated for two hours by alpha external beams accelerated at 28 MeV.[16] After irradiation of the target, a dry distillation method was used to isolate At-211 and then recover 10 MBq of At-211 into 200 µL of chloroform.[17] Then At-211 was back-extracted to a 0.1 M $HClO_4$ solution, conditions where At species corresponds to At^+.[13]

4.3.2. Analytic tools

The radioactivity in the two phases were measured with a Packard 2550 TR/AB Liquid Scintillation analyzer with the Ultima Gold LLT scintillation liquid.[13] Quenching caused by the different solvents was considered to determine the ^{211}At activity (A) according to the following equation:

$$A = A_{\text{mes}} \times (8\times10^{-10}\times tSIE^3 - 2\times10^{-6}\times tSIE^2 + 0.0013\times tSIE + 0.7228) \quad (4.1)$$

with A_{mes} being the activity measured by liquid scintillation and $tSIE$ (transformed spectral index of the external standard) a parameter defined by the apparatus for counting efficiency determination.

AtI interaction with Lewis base was studied in cyclohexane. The possible solubility of B in the aqueous phase was systematically checked with a total organic carbon (TOC) meter (Shimadzu TOC V CSH) in the absence of astatine. The distribution coefficient of the organic molecule can be obtained through the fitting of the detected concentration in the aqueous phase as a function of the initial concentration in ligand.

An electrode (Inlab) freshly calibrated with standard pH buffers (pH 4.00 and 7.00, Merck), and a Pt combined redox electrode (Metrohm) calibrated with a redox buffer ($Fe(SCN)_6^{3-}/Fe(SCN)_6^{4-}$, 220 mV/Pt/SCE, Radiometer Analytical), were used to measure the pH and the potential (E) of the aqueous phase at

equilibrium, respectively. Since both the pH and E in the given aqueous solution are essentially controlled by the $HClO_4$ concentration, no significant deviation from the targeted 1 and 0.6 V values, respectively, was observed.

4.3.3. Methodology

4.3.3.1. Experimental system

A liquid/liquid competition method was employed in this work, with one organic and one aqueous phase. This method consists in studying the distribution of ^{211}At between these two phases as a function of initial concentrations in Lewis bases present in the organic phase. The organic phase is composed of cyclohexane with various concentrations of Lewis base. Note that no halogen bond is expected between AtI and the organic solvent, cyclohexane. The aqueous phase is composed of 0.1 M of $HClO_4$ with 0.01/0.1 M of NaI. Considering the pK_a value of HI (−9.5),[18] dissolved NaI salt initially produce 100% of the ionic species I^- given the experimental conditions. The systems were first equilibrated before At-211 (~1000 Bq) addition. After the addition of At, two hours of shaking were done to achieve distribution equilibrium of At between the two phases. Thus the distribution coefficient (D) can be determined as:

$$D = \frac{A_{\mathrm{org}} \times V_{\mathrm{aq}}}{A_{\mathrm{aq}} \times V_{\mathrm{org}}} \tag{4.2}$$

here V_{org} and V_{aq} represent given phase volumes, and A_{org} and A_{aq} are the astatine radioactivity in the organic and aqueous phases at equilibrium, respectively. Uncertainties associated with the D values were calculated according to the following equation:

$$\sigma_D = D \times \sqrt{\frac{\sigma_{A_{org}}^2}{A_{org}} + \frac{\sigma_{A_{aq}}^2}{A_{aq}} + \frac{\sigma_{V_{org}}^2}{V_{org}} + \frac{\sigma_{V_{aq}}^2}{V_{aq}}} \tag{4.3}$$

Experiments were twice repeated with the same experimental conditions and the mean values are given together with 2σ uncertainties (corresponding to a 95% confidence interval).

4.3.3.2. Modeling

The objective is to reproduce the experimental curve displaying *D* variation with the influent parameters considering the equilibria occurring (i) in the aqueous solution (At^+ complexation with I^-), (ii) in the organic phase (interaction between AtI and the Lewis bases) and (iii) between the two phases (extraction/back-extraction of the species). Once the reactions are considered, an analytical expression is derived as a function of the different quantitative parameters. Origin 9.0 was used to fit the experimental data with this equation, to obtain the unknown parameters. The model is considered good when the model can well reproduce the experimental data with a minimum number of "predictable" equilibria and that the parameters of adjustment are not strongly correlated. The uncertainties associated with the determined parameter values were determined by the software (average value and standard deviation were calculated). Note that, all the constants in aqueous solution were calculated at the given ionic strength used in the experiments with the Truncated Davies equation.[19]

4.3.3.3. Quantum mechanical calculations

Relativistic density functional theory (DFT) calculations were performed with the NWChem program, v. 5.1.1.[20] Two-component (2c) B3LYP[21] calculations were performed in conjunction with small-core pseudopotentials (ECP60MDF for At[22] and ECP28MDF for I[23]) and double-zeta basis sets (mAVDZ for At[13,22,24] and aug-cc-pVDZ-PP-2c for I[22–24]). Note that this combination of pseudopotentials and basis sets are referred to as 'AVDZ' in the rest of the text for the sake of simplicity. Geometries were optimized, and the molecular electrostatic potential (MEP) computed at the molecular surfaces.

4.4. Results and discussion

In order to reveal the role that astatine plays in the presence of different Lewis bases, a competition method with two liquid phases was used. In this work, the organic phase consists in cyclohexane (cHex) plus various concentrations of

Lewis bases, and the aqueous phase in 0.1 M $HClO_4$ containing concentrated NaI (0.01 and 0.1 M). According to the Pourbaix diagram (E-pH) of At established by previous researches, the main species in this condition (pH = 1.0 ± 0.2, E = 0.60 ± 0.04 V *vs.* NHE, the Normal Hydrogen Electrode) is At^+, in the absence of any complexing agent.[12,15,25] As described in the previous work, with the presence of I^-, At^+ can form the AtI and AtI_2^- species with the equilibrium constants of $10^{6.1\pm0.2}$ and $10^{8.8\pm0.2}$, respectively (see Chapter 3). Contrary to AtI_2^-, AtI is more affinitive to organic phases. The objective is to observe an increase of astatine extraction following the interaction in the organic phase with the Lewis base, it is therefore important to "start" with conditions where astatine is mainly soluble in the aqueous phase. The experimental conditions were then chosen to get AtI_2^- as the dominant species in the given aqueous phase; as shown in Figure 4.1, AtI_2^- concentration amounts to 98% and 82% for $[I^-]$= 0.1 and 0.01 M, respectively. The hypothesis is that, AtI could act as the halogen bond donor and interact with Lewis bases. Thus, a competition appears between the reaction of AtI with the Lewis base to form halogen bond in the organic phase, and the reaction of AtI with I^- to form AtI_2^- in the aqueous phase. We expect that this competition can be reflected by the change of the D values with varying the Lewis bases concentrations. Furthermore, this change of D value should be different according to the two experimental conditions. Analyzing the radioactivity of astatine in both organic and aqueous phases, the distribution coefficient (D) of At can be achieved. In this work we focused on the equilibrium constant (K_{BAtI}) associated to the following reaction:

$$\overline{AtI} + \overline{B} \rightleftharpoons \overline{BAtI}$$

here $\overline{B}$ represents Lewis base dissolved in the organic phase.

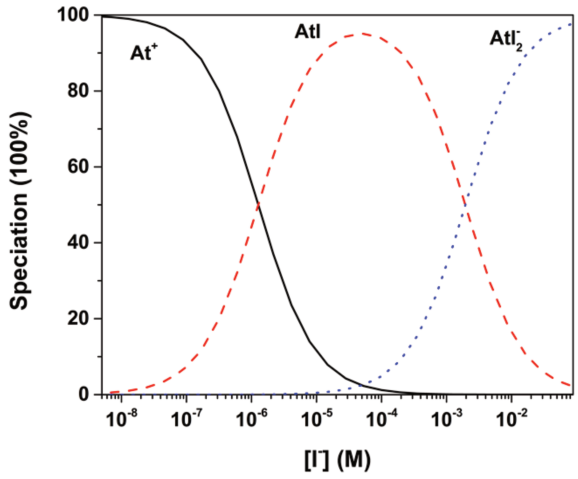

Figure 4.1. Speciation diagram of astatine in 0.1 M $HClO_4$ solution as a function of the I^- concentration, obtained with the equilibrium constants of $10^{6.1\pm0.2}$ and $10^{8.8\pm0.2}$, for AtI and AtI_2^- species, respectively.

Nine commercially available (Sigma-Aldrich) Lewis bases, namely toluene (MePh), hexamethyl benzene (Me_6Ph), diethyl ether (Et_2O), diethyl sulfide (Et_2S), dibutyl sulfoxide (Bu_2SO), ethyl butyrate (Etbutyrate), triphenylphosphane sulfide (Ph_3PS), diethyl methylphosphonate ($Me(EtO)_2PO$), and tributyl phosphate ($(BuO)_3PO$) were employed in this work. Their chemical structures are displayed in Scheme 4.1.

Among these Lewis bases, $Me(EtO)_2PO$ and Bu_2SO appear to be soluble in the aqueous phase, with determined distribution coefficients (D) of $10^{-0.27}$ and $10^{-0.65}$, respectively. Therefore, the Lewis bases used in this work are divided into two groups: the aqueous-insoluble ones, including MePh, Me_6Ph, Et_2O, Et_2S, Etbutyrate, Ph_3PS and $(BuO)_3PO$, and the aqueous-soluble ones that can be "back-extracted" to the aqueous phase, including $Me(EtO)_2PO$ and Bu_2SO.

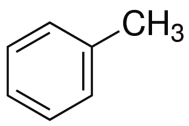

Toluene (MePh)

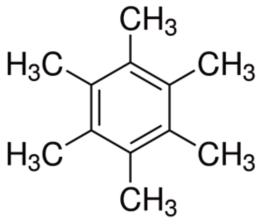

Hexamethyl benzene (Me_6Ph)

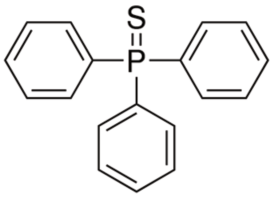

Triphenylphosphane sulfide (Ph_3PS)

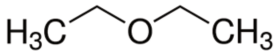

Diethyl ether (Et_2O)

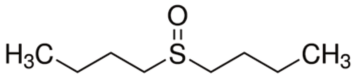

Dibutyl sulfoxide (Bu_2SO)

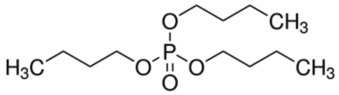

Tributyl phosphate ($(BuO)_3PO$)

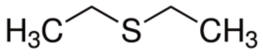

Diethyl sulfide (Et_2S)

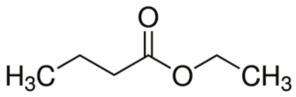

Ethyl butyrate (Etbutyrate)

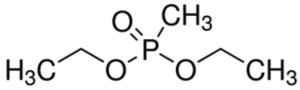

Diethyl methylphosphonate ($Me(EtO)_2PO$)

Scheme 4.1. The chemical structures of the Lewis bases employed in this work.

4.4.1. Interaction of AtI with aqueous-insoluble Lewis bases

The reaction between AtI and aqueous-insoluble Lewis bases is considered to occur solely in the organic phase. Let us discuss $(BuO)_3PO$ as a first example. Figure 4.2 exhibits the *D* value of At as a function of the initial $(BuO)_3PO$ concentration. The data from the system without $(BuO)_3PO$, is displayed in the same figure as well, with star symbols for 0.01 M of I^- and diamond symbols for 0.1 M of I^-. The experimental points obtained with 0.1 M of I^- behave in a "parallel" way of the ones with 0.01 M of I^-. It shows no signature of any speciation change when the initial $(BuO)_3PO$ concentration is below 10^{-4} M. In this concentration range, the *D* value is mainly governed by the extraction of At^+ and AtI to cyclohexane. Then, the *D* value increases with the raising of the $(BuO)_3PO$ concentration, which indicates a competition reaction grabbing At from the aqueous phase into the organic one. The reaction in cyclohexane is

mostly counted by the increasing amount of available $(BuO)_3PO$. For modeling purposes, one must consider the reactions occurring in the aqueous phase between the At^+ and I^- ions:[26]

$$At^+ + I^- \rightleftharpoons AtI \qquad K_1 = \frac{[AtI]}{[At^+][I^-]} \tag{4.4}$$

$$At^+ + 2I^- \rightleftharpoons AtI_2^- \qquad K_2 = \frac{[AtI_2^-]}{[At^+][I^-]^2} \tag{4.5}$$

Then, various equilibria are introduced to describe the extraction of the At^+ and AtI species in the organic phase, the formation of the 1:1 halogen-bonded adducts, and their potential "back-extraction" in the aqueous phase:

$$At^+ \rightleftharpoons \overline{At^+} \qquad D_1 = \frac{[\overline{At^+}]}{[At^+]} \tag{4.6}$$

$$AtI \rightleftharpoons \overline{AtI} \qquad D_2 = \frac{[\overline{AtI}]}{[AtI]} \tag{4.7}$$

$$\overline{AtI} + \overline{B} \rightleftharpoons \overline{BAtI} \qquad K_{BAtI} = \frac{[\overline{BAtI}]}{[\overline{AtI}][\overline{B}]} \tag{4.8}$$

$$BAtI \rightleftharpoons \overline{BAtI} \qquad D_3 = \frac{[\overline{BAtI}]}{[BAtI]} \tag{4.9}$$

where all the overlined species relate to the organic phase. Based on the above reactions, D can be expressed as a function of the initial ligand concentration in the organic phase ($\overline{B}$) as:

$$D = \frac{D_1 + D_2 \times K_1 \times [I^-] + K_{BAtI} \times D_2 \times K_1 \times [I^-] \times [\overline{B}]}{1 + K_1 \times [I^-] + K_2 \times [I^-]^2 + K_{BAtI} \times D_2 \times K_1 \times [I^-] \times [\overline{B}]/D_3} \tag{4.10}$$

D_1 and D_2 are obtained in the range where D value is not affected by the variation of the Lewis base concentration; K_1 and K_2 are fixed values; D_3 and K_{BAtI} should then explain the increase of D when the Lewis base concentration increases. Note that, the parameters used in the model are displayed in the Appendix table. Using Equation (4.10) the experimental data can be satisfactorily and independently fitted with the 0.01 M or 0.1 M initial I^- concentrations. To validate the reproducibility of this method, all the sets of experiments were twice repeated. For each set of data (two for each initial I^- concentration), one equilibrium constant can be obtained. Then, an average value with its associated

standard deviation can be obtained. The investigations with MePh, Et_2S, Etbutyrate, Me_6Ph and Ph_3PS were analyzed with the same process and the related equilibrium constants are presented in Table 4.1.

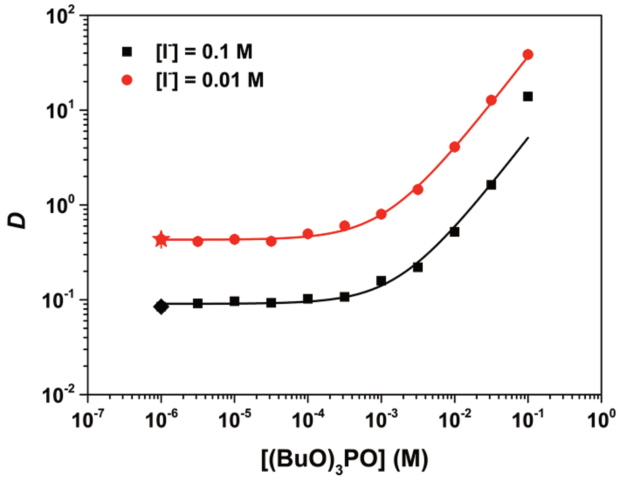

Figure 4.2. Distribution coefficient (*D*) as a function of the initial $(BuO)_3PO$ concentration in cyclohexane, with an aqueous phase of 0.1 M $HClO_4$ solution initially containing 0.01 M (circles) and 0.1 M (squares) of I^-. Star and diamond symbols represent the experimental data obtained with no $(BuO)_3PO$ for initially 0.01 M and 0.1 M of I^-, respectively. Models obtained using Equation (4.10) are displayed with solid lines.

With the purpose of determining the K_{BAtI} values of the reaction between AtI and organic compounds in cyclohexane, one difficulty is that the interactions between At (under various chemical forms) and different organic molecules do not always behave in the same way. Among the aqueous-insoluble Lewis bases, Et_2S shows a different behavior from the others. As seen in Figure 4.3, with the initial presence of 0.1 M of I^- in the aqueous phase, the *D* value increases with an increasing Et_2S concentration and this trend is similar to the ones obtained for the formerly studied organic molecules. The model fitted with Equation (4.10) can still satisfactorily explain the data obtained with 0.1 M of I^- (black dashed line in Figure 4.3a). However, the model defined by these parameters cannot fully explain the data with 0.01 M of I^- (red dashed line in Figure 4.3a), especially

for high initial concentration in Et_2S. This may indicate a transferability problem of the parameter values (which would be very unlikely) or a transferability problem of the model itself. Indeed, a plateau appears when the initial Et_2S concentration is larger than 10^{-3} M, after a sharply increase in the range of 10^{-5} to 10^{-3} M, while the simulation line follow a different trend (monotonous increase of *D*). In order to explain this relative decrease of the *D* value (between the experimental points and the model curve), a further species that can be "back-extracted" into the aqueous phase should be taken into account. Since ionic species are usually soluble in water, we hypothesized the formation of adducts between At^+ and B in the organic phase and its "back-extraction" in the aqueous one, as follows:

$$\overline{At^+} + \overline{B} \rightleftharpoons \overline{BAt^+} \qquad K_3 = \frac{[\overline{BAt^+}]}{[\overline{At^+}][\overline{B}]} \tag{4.11}$$

$$BAt^+ \rightleftharpoons \overline{BAt^+} \qquad D_4 = \frac{[\overline{BAt^+}]}{[BAt^+]} \tag{4.12}$$

D is thus expressed as:

$$D = \frac{D_1 + D_2 \times K_1 \times [I^-] + K_{BAtI} \times D_2 \times K_1 \times [I^-] \times [\overline{B}] + K_3 \times [\overline{B}]}{1 + K_1 \times [I^-] + K_2 \times [I^-]^2 + K_{BAtI} \times D_2 \times K_1 \times [I^-] \times [B]/D_3 + K_3 \times [\overline{B}]/D_4} \tag{4.13}$$

With the new model (Equation (4.13)), the two sets of experimental data can be explained (see solid lines in Figure 4.3b). More importantly, the associated K_{BAtI} values also match the value obtained with the simpler model, based on Equation (4.10), and the 0.1 M of I^- set of data. Therefore, although we do not have direct evidence for the formation of the BAt^+ species, we are confident in the determined log K_{BAtI} value, obtained with the more sophisticated set of equations, that is displayed in Table 4.1.

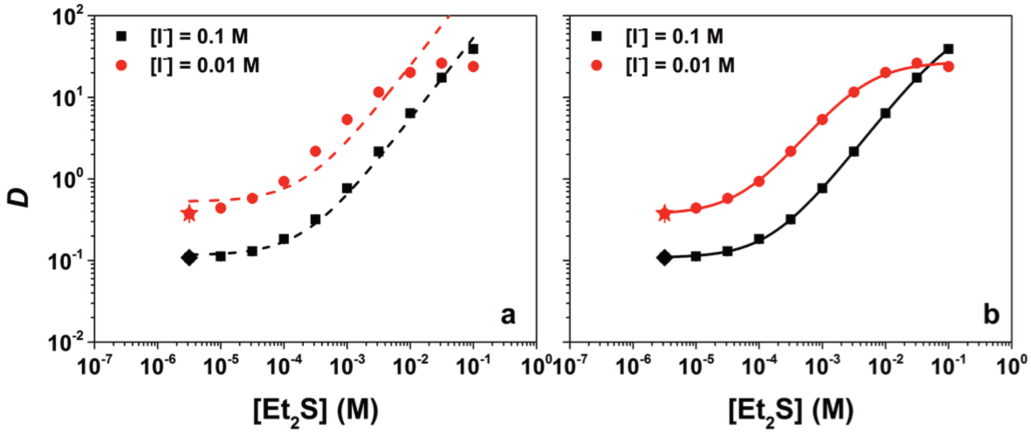

Figure 4.3. Distribution coefficient (*D*) as a function of the initial Et_2S concentration in cyclohexane, with an aqueous phase of 0.1 M HClO4 solution initially containing 0.01 M (circles) and 0.1 M (squares) of I^-. Star and diamond symbols represent the experimental data obtained with no Et_2S for 0.01 M and 0.1 M of I^-, respectively. a. Black dashed line corresponds to the fitted model using Equation (4.10), while the red dashed line is the simulation obtained with these parameters. b. Solid lines represent the fitted models using Equation (4.13). The values used for K_3 and D_4 are displayed in the Appendix table.

4.4.2. Interaction of AtI with aqueous-soluble Lewis bases

Considering that $Me(EtO)_2PO$ and Bu_2SO are soluble in the aqueous phase, the distribution of the organic molecule between the two phases must be accounted for in the model:

$$B \rightleftharpoons \overline{B} \qquad D_5 = \frac{[\overline{B}]}{[B]} \qquad (4.14)$$

The D_5 values for $Me(EtO)_2PO$ and Bu_2SO were fixed to the ones obtained from the TOC measurement in the absence of astatine, *i.e.* $10^{-0.27}$ and $10^{-0.65}$, respectively. As can be seen in Figure 4.4, the distribution of At in the Bu_2SO biphasic system shows a similar trend as the ones obtained with the insoluble ones: the *D* value increases with increasing initial Bu_2SO concentration and the experimental data obtained with 0.01 M and 0.1 M of I^- behave in a "parallel" way. Furthermore, the model, based on Equation (4.10) and the correction of the $\overline{B}$ concentration according to Equation (4.14), satisfactorily explains the

experimental data. The same process was used to analyze the experimental outcomes obtained with $Me(EtO)_2PO$. The K_{BAtI} values obtained with Bu_2SO and $Me(EtO)_2PO$ are thus also displayed in Table 4.1.

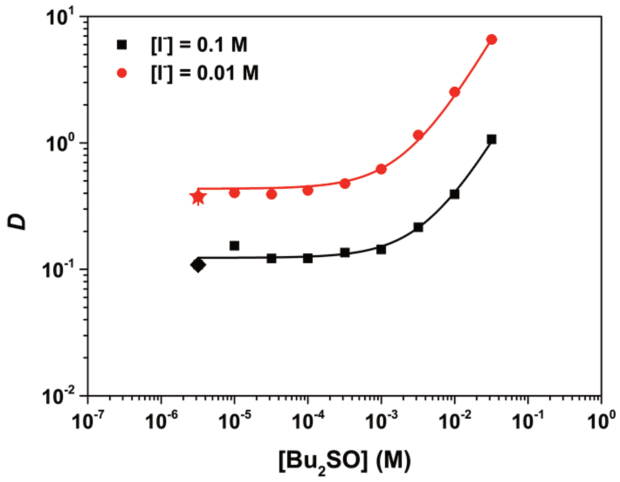

Figure 4.4. Distribution coefficient (D) as a function of the initial Bu_2SO concentration in cyclohexane, with an aqueous phase consisting of a 0.1 M $HClO_4$ solution initially containing 0.01 M (circles) and 0.1 M (squares) of I^-. Star and diamond symbols are used to represent the experimental data obtained with no Bu_2SO for 0.01 M and 0.1 M of I^-, respectively. Solid lines correspond to the fitted models with Equation (4.10).

4.4.3. Discussion

In Table 4.1, the diiodine basicity scale (pK_{BI2}) extracted from the work of Laurence *et al.*[11] is presented, and compared to the one obtained in this work with AtI. Figure 4.5 aims at correlating the log K_{BAtI} to the pK_{BI2} ones. As can be seen in this figure, overall, the log K_{BAtI} values increase with increasing pK_{BI2}. This indicates that the reactions between AtI and these Lewis bases are similar to the ones observed with diiodine. This result shows that the basicity scale obtained with diiodine is indeed transferable to the AtI case. Therefore, we confirm that this scale must be general since it also applies to an interhalogen compound that involves the astatine element. This is also confirming indirectly that the formed adducts must be ruled by halogen bonding. Furthermore, as compared with diiodine, AtI interacts more strongly with Lewis bases. This indicates a stronger

halogen bond donor character for AtI than for diiodine.

Table 4.1. Equilibrium constants of AtI with different Lewis bases (B) obtained in this work, and comparison with the basicity scale obtained with diiodine extracted from the literature.

B	pK_{BI2}[11]	log K_{BAtI}
MePh	-0.44 (Hept)	-0.67 ± 0.24
Et_2O	-0.05 (cHex)	1.54 ± 0.46
Etbutyrate	0.04 (CCl_4)	0.64 ± 0.08
Me_6Ph	0.14 (Hept)	1.15 ± 0.12
$(BuO)_3PO$	1.33 (cHex)	2.83 ± 0.26
$Me(EtO)_2PO$	1.57 (cHex)	1.40 ± 0.28
Bu_2SO	1.93 (cHex)	3.30 ± 0.58
Et_2S	2.29 (Hept)	4.01 ± 0.62
Ph_3PS	2.57 (CCl_4)	3.46 ± 0.62

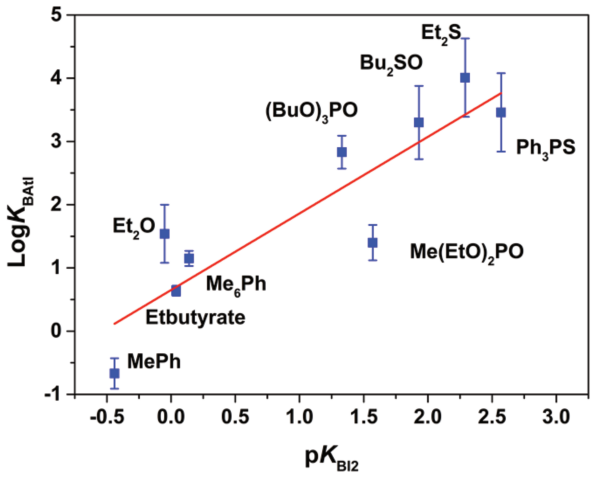

Figure 4.5. LogK_{BAtI} values obtained with a competition method (this work) as a function of the pK_{BI2} values extracted from the literature.[11] The solid line is the tendency curve.

Having experimentally shown that AtI is a stronger XB donor than I_2, we now pursue by giving more insight on the involved chemical bonds. Although one can expect that an XB bond with AtI should directly involve the At atom rather than the I one based on arguments that were provided in the introduction, it is crucial to check this hypothesis by means of appropriate quantum mechanical calculations. One should first recall that relativistic effects (both 'scalar' and spin-dependent) may be of strong influence on the chemical bonds involving heavy atoms such as At.[13,28–30] Therefore, relativistic calculations must be performed to consistently probe such bonds. Here, we have selected the 2c-B3LYP/AVDZ level of theory that proved to be reliable to study astatine chemistry in a wide range of examples[13,15,25,30] (see also Chapter 3). As mentioned in the introduction, the concept of halogen bonding is intimately related to the concept of σ–hole. Therefore, a first view on halogen bonds with AtI consists in computing the molecular electrostatic potential (MEP) at the molecular surface (see Figure 4.6). As can be seen in this figure, a positive region of the MEP clearly appears on the At atom, as well as on the I one (although it is a bit hidden by the perspective).

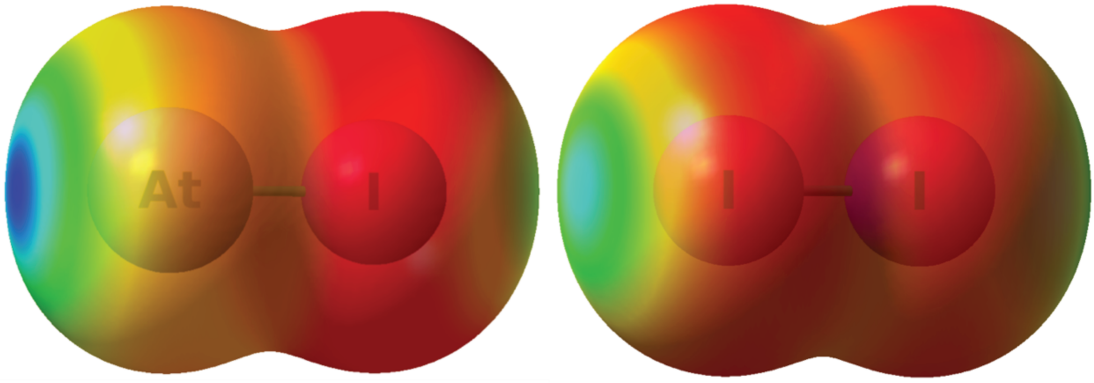

Figure 4.6. Molecular electrostatic potentials (MEPs) obtained at the 2c-B3LYP/AVDZ level of theory at the AtI and I_2 molecular surfaces, defined by isovalues of the electron density of 0.001 e $bohr^{-3}$. Colour code: from red (negative values) to blue (positive values). A positive value of the MEP indicates an electrophilic region.

A quantitative criterion to probe the potential to form XB bonds consists in computing maxima of the MEP at the molecular surface (defined by isovalues of the electron density of 0.001 e $bohr^{-3}$). The $V_{s,max}(X)$ values corresponding to the AtI and I_2 systems (X=At or I) are displayed in Table 4.2. The σ –hole corresponding to the At atom in AtI thus corresponds to a more electrophilic region than the one corresponding to the I atom. Therefore, it is clear at this stage that the reported XB bonds directly involve the At atom of the AtI unit. Also, in order to rationalize the fact that AtI is a stronger XB donor than I_2, it is interesting to compare the maxima values of the MEP of AtI to the ones of the I_2 system (see Table 4.2). Clearly, $V_{s,max}(At)$ in AtI is much larger than $V_{s,max}(I)$ in I_2, which is in line with the previously established experimental trend. Therefore, we conclude that At is a stronger XB donor than I.

One should note that to get further insight on the involved XB bonds, it would be important to also compute the bound species and not only describe the properties of the dissociated XB donor. This is the subject of ongoing researches, aiming at (i) obtaining the geometries of the bound systems and (ii) reproducing the here-obtained experimental trend.

Table 4.2. Maximum values (in kJ mol^{-1}) of the 2c-B3LYP/AVDZ molecular electrostatic potentials obtained at the molecular surfaces (defined by isovalues of the electron density of 0.001 e $bohr^{-3}$).

System	AtI	I_2
$V_{s,max}$(At)	192	N/A[a]
$V_{s,max}$(I)	85	141[b]

[a] N/A denotes not applicable.

[b] $V_{s,max}$(I) is equal for both I atoms by symmetry.

4.5. Conclusion

A competition method was used to explore the interaction between AtI and a series of Lewis bases. The related equilibrium constants were obtained by analyzing the experimental outcomes. We found a similar trend for these constants as the ones obtained for the basicity scale defined with diiodine. This is a first indication that halogen bonding occurs between AtI and the considered Lewis bases. Moreover, we find that AtI is a stronger halogen-bond donor than is diiodine. From the outcomes of quantum mechanical calculations, we showed that At bears a more electrophilic site in AtI than the ones of I in both AtI and I_2. This indicates that (i) the synthesized halogen-bonded adducts directly involve the astatine element and (ii) that At is a stronger halogen-bond donor than I. Since this work reports the first halogen-bonded adducts involving the At element, we hope that it would trigger further researches on halogen bonding and on astatine chemistry. In particular, it would be a long-term perspective to take profit of the halogen bonding properties of At to design novel reagents for nuclear medicine applications.

Appendix table. Related parameters used in the modeling for each Lewis base (B).

B	log D_3	log D_4	log D_5	log K_3
MePh	77	-	-	-
Et_2O	110	-	-	-
Etbutyrate	-0.20	-	-	-
Me_6Ph	0.33	-	-	-
$(BuO)_3PO$	33	-	-	-
$Me(EtO)_2PO$	0.78	-	-0.27	-
Bu_2SO	36	-	-0.65	-
Et_2S	1.75	56	-	-2×10^5
Ph_3PS	30	-	-	-

References

(1) Cavallo, G.; Metrangolo, P.; Milani, R.; Pilati, T.; Priimagi, A.; Resnati, G.; Terraneo, G. *Chem. Rev.* **2016**, *116* (4), 2478.

(2) Kolář, M. H.; Hobza, P. *Chem. Rev.* **2016**, *116* (9), 5155.

(3) Desiraju, G. R.; Ho, P. S.; Kloo, L.; Legon, A. C.; Marquardt, R.; Metrangolo, P.; Politzer, P.; Resnati, G.; Rissanen, K. *Pure Appl. Chem.* **2013**, *85* (8), 1711.

(4) Muller, P. *Pure Appl. Chem.* **1994**, *66* (5), 1077.

(5) Legon, A. C. *Phys. Chem. Chem. Phys.* **2010**, *12* (28), 7736.

(6) Clark, T.; Hennemann, M.; Murray, J. S.; Politzer, P. *J Mol Model* **2007**, *13*, 291.

(7) Politzer, P.; Lane, P.; Concha, M. C.; Ma, Y.; Murray, J. S. *J. Mol. Model.* **2007**, *13* (2), 305.

(8) Maroulis, G. *Atoms, Molecules and Clusters in Electric Fields: Theoretical Approaches to the calculation of electric polarizability*; World Scientific, 2006; Vol. 1.

(9) Alkorta, I.; Blanco, F.; Solimannejad, M.; Elguero, J. *J. Phys. Chem. A* **2008**, *112* (43), 10856.

(10) Hill, J. G.; Hu, X. *Chem. - A Eur. J.* **2013**, *19* (11), 3620.

(11) Laurence, C.; Graton, J.; Berthelot, M.; El Ghomari, M. J. *Chem. - A Eur. J.* **2011**, *17* (37), 10431.

(12) Champion, J.; Alliot, C.; Renault, E.; Mokili, B. M.; Chérel, M.; Galland, N.; Montavon, G. *J. Phys. Chem. A* **2010**, *114* (1), 576.

(13) Champion, J.; Seydou, M.; Sabatié-Gogova, A.; Renault, E.; Montavon, G.; Galland, N. *Phys. Chem. Chem. Phys.* **2011**, *13* (33), 14984.

(14) Ludwig, R.; Fischer, S.; Hussein, H.; Frind, M.; Dreyer, R. *J. Radioanal. Nucl. Chem. Artic.* **1989**, *134*, 141.

(15) Sergentu, D. C.; Teze, D.; Sabatié-Gogova, A.; Alliot, C.; Guo, N.; Bassal, F.; Silva, I. Da; Deniaud, D.; Maurice, R.; Champion, J.; Galland, N.; Montavon, G. *Chem. - A Eur. J.* **2016**, *22* (9), 2964.

(16) Alliot, C.; Cherel, M.; Barbet, J.; Sauvage, T.; Montavon, G. *Radiochim. Acta* **2009**, *97*, 161.

(17) Lindegren, S.; Bäck, T.; Jensen, H. J. *Appl. Radiat. Isot.* **2001**, *55* (2), 157.

(18) Trummal, A.; Lipping, L.; Kaljurand, I.; Koppel, I. A.; Leito, I. *J. Phys. Chem. A* **2016**, *120* (20), 3663.

(19) Colston, B. J.; Robinson, V. J. *J. Environ. Radioact.* **1995**, *29* (2), 121.

(20) Bylaska, E. J.; Jong, W. A.; Govind, N.; Kowalski, K.; Straatsma, T. P.; Valiev, M.; Wang, D.; Apra, E.; Windus, T. L.; Hammond, J.; Nichols, P.; Hirata, S.; Hackler, M. T.; Zhao, Y.; Fan, P.-D.; Harrison, R. J.; Dupuis, M.; Smith, D. M. A.; Nieplocha, J.; Tipparaju, V.; Krishnan, M.; Vaz- quez-Mayagoitia, A.; Wu, Q.; Voorhis, T. V.; Auer, A. A.; Nooijen, M.; Crosby, L. D.; Brown, E.; Cisneros, G.; Fann, G. I.; Fruchtl, H.; Garza, J.; Hirao, K.; Kendall, R.; Nichols, J. A.; Tsemekhman, K.; Wolinski, K.; Anchell, J.; Bern- holdt, D.; Borowski, P.; Clark, T.; Clerc, D.; Dachsel, H.; Deegan, M.; Dyall, K.; Elwood, D.; Glendening, E.; Gutowski, M.; Hess, A.; Jaffe, J.; Johnson, B.; Ju, J.; Kobayashi, R.; Kutteh, R.; Li, Z. Pacific NorthwestNational Laboratory, Richland, WA 2008,.

(21) Stephens, P. J.; Devlin, F. J.; Chabalowski, C. F.; Frisch, M. J. *J. Phys. Chem.* **1994**, *98* (45), 11623.

(22) Peterson, K. A.; Figgen, D.; Goll, E.; Stoll, H.; Dolg, M. *J. Chem. Phys.* **2003**, *119* (21), 11113.

(23) Peterson, K. A.; Shepler, B. C.; Figgen, D.; Stoll, H. *J. Phys. Chem. A* **2006**, *110* (51), 13877.

(24) Armbruster, M. K.; Klopper, W.; Weigend, F. *Phys. Chem. Chem. Phys.* **2006**, *8* (42), 4862.

(25) Champion, J.; Sabatié-Gogova, A.; Bassal, F.; Ayed, T.; Alliot, C.; Galland, N.; Montavon, G. *J. Phys. Chem. A* **2013**, *117* (9), 1983.

(26) Guo, N.; Sergentu, D.-C.; Teze, D.; Champion, J.; Montavon, G.; Galland, N.; Maurice, R. *Angew. Chemie Int. Ed.* **2016**, 1.

(27) Maurice, R.; Réal, F.; Gomes, A. S. P.; Vallet, V.; Montavon, G.; Galland, N. *J. Chem. Phys.* **2015**, *142* (9), 94305.

(28) Pilmé, J.; Renault, E.; Ayed, T.; Montavon, G.; Galland, N. *J. Chem. Theory Comput.* **2012**, *8* (9), 2985.

(29) Pilmé, J.; Renault, E.; Bassal, F.; Amaouch, M.; Montavon, G.; Galland, N. *J.*

Chem. Theory Comput. **2014**, *10* (11), 4830.

(30) Sergentu, D.-C.; David, G.; Montavon, G.; Maurice, R.; Galland, N. *J. Comput. Chem.* **2016**, *37* (15), 1345.

Conclusions and perspectives

Astatine belongs to halogen group and is located under iodine in the periodic table. One of its isotopes, ^{211}At is of great interest as a potential candidate for targeted alpha therapy. The development of labeling strategies is connected to the comprehension of astatine basic chemistry that remains poorly known. In the present work, the behavior of astatine at the oxidation states –I and +I in aqueous solution has been investigated through different methodologies, and the main conclusions are given below.

Astatine is commonly considered as an analog of iodine, and At^- (astatide) species is thought to predominate in reducing condition. However, there is no proof that can confirm the existence of such a species. A homemade electromigration device was established in order to investigate the migration behavior of astatine in acidic reducing medium. The mobility of an ion is a specific character related to its charge and size. The method was first validated with F^- and I^- for which the mobilities are tabulated in the literature. The migration direction of astatine to the positive electrode indicates the presence of an anionic species. An experiment realized in the presence of both I^- and astatine showed that astatine species moved slightly slower than iodide. This result is totally in agreement with recent theoretical calculation and confirm the presence of At^-. The apparent mobilities were corrected from the electroosmotic flow and extrapolated at zero ionic strength using the Onsager-Fuoss model. The first absolute value for the At species is proposed: $(-8.3 \pm 0.8) \times 10^{-4}$ $cm^2V^{-1}s^{-1}$. The trend of absolute mobility as a function of ionic radius is given in Figure 1 for halides.

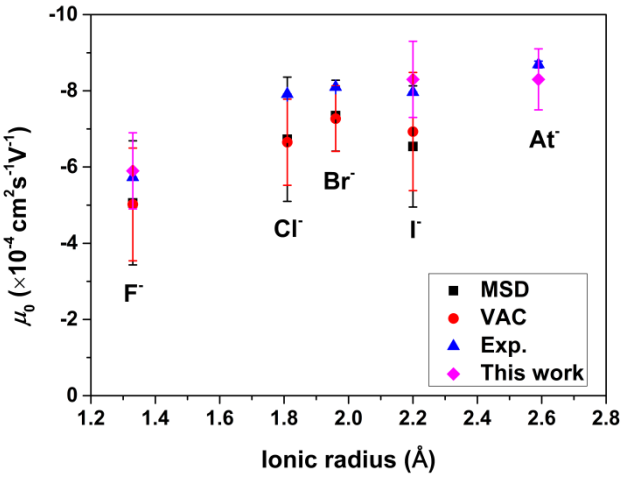

Figure 1. Absolute mobility of halides as a function of their ionic radius. MSD (squares) represents the mean square displacement calculation and VAC (circles) represents the velocity autocorrelation functions;[1] Exp. (triangles) represents the absolute mobilities, which are summarized based on the literature; the diamonds represent the experimental results from this work; and the ionic radii are from literature.[2]

There are numerous studies reporting the existence of binary dihalogens. Only one ternary trihalogen has been reported so far, *i.e.* $IBrCl^-$. We hypothesized that the $IAtBr^-$ analogue would form in aqueous solution. Since it is difficult to experimentally work with astatine, a combined theoretical and competition methodology was employed. Quantum mechanical calculations were used to predict the tiny experimental domain, in which it is possible to detect the presence of the exotic ternary trihalogen anion, $IAtBr^-$. Thus, this theoretical prediction was used to guide a series of experiments. By analyzing the outcomes of competition experiments, it is shown that $IAtBr^-$ exists and can even predominate in aqueous solution (see in Figure 2). The equilibrium constant associated to the $At^+ + I^- + Br^- \rightleftharpoons IAtBr^-$ reaction is determined to be $10^{7.5 \pm 0.2}$, which is in fair agreement with the density functional theory predicted one ($10^{6.9}$). This system not only constitutes the very first example of a ternary trihalogen species that involves the astatine element, but is also the first trihalogen species reported to predominate in solution.

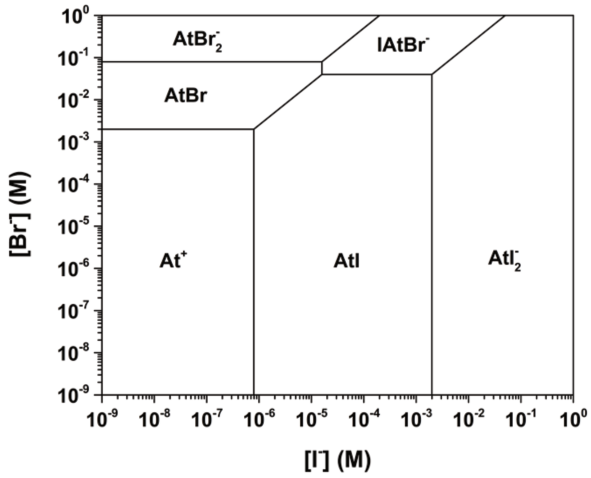

Figure 2. Speciation diagram of At based on experimental data as a function of the initial concentrations of both the Br^- and I^- anions.

A specific property for halogen atoms is that they can form non-covalent halogen bonds with Lewis bases. Such a performance is also expected with astatine, and theoretical calculations predicted the strongest interaction in the halogen series. However, no practical evidence could prove this hypothesis. In this work, a competition method was used to investigate the interaction between AtI and different Lewis bases in cyclohexane. By analyzing the experimental outcomes, an interaction was evidenced and the corresponding equilibrium constants were determined. A good correlation was observed between these constants and the basicity scale defined with diiodine (see in Figure 3). This indicates that halogen bonding occurs between AtI and the considered Lewis bases. The relativistic quantum mechanical calculations showed that At bears a more electrophilic site in AtI than the ones of I in both AtI and I_2. This indicates that the synthesized halogen-bonded adducts directly involve the astatine element and At is a stronger halogen bond donor than I. Therefore, the first halogen-bonded adducts involving At have been revealed, and At is evidenced a stronger halogen bond donor than I.

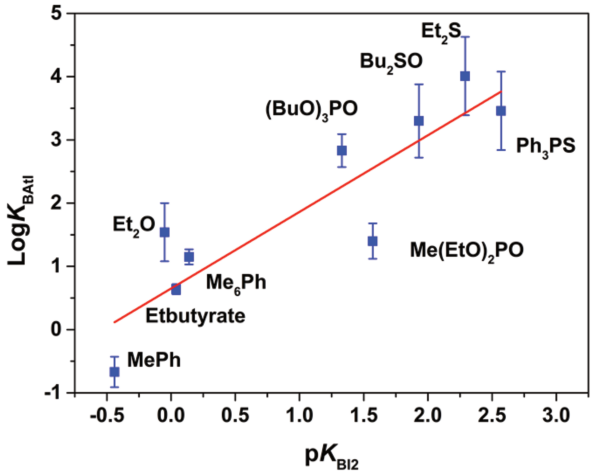

Figure 3. LogK_{BAtI} obtained through competition method as a function of pK_{BI2} extracted from the literature. The solid line is a tendency curve.

There is still a lot of work to do with astatine, and some prospects are itemized below.

1) Except At^- species which predominates in reductive acidic media, another minus charged species of astatine has been proposed in non-reductive basic media, $AtO(OH)_2^-$.[3] This species exists in conditions, in which it was believed to have At^-, such as concentrated NaOH solution. In order to distinguish the two species, At^- and $AtO(OH)_2^-$, electromobility methodology can be employed. The migration behavior of astatine in concentrated NaOH solution can be observed and the absolute mobility of targeted species can be extrapolated at zero ionic strength with the Onsager-Fuoss model. Since the absolute mobility of an ion is not only related to its charge, but also to its size, a difference is expected with the one characterized in this work for At^-. Furthermore, the equilibrium constant quantifying the change from At^- to $AtO(OH)_2^-$ can be determined by investigating astatine mobility as a function of the pH.

2) As mentioned in Chapter 1, according to the Pourbaix diagram established for astatine, two cationic species exist in the acidic oxidizing condition, *i.e.* At^+ and AtO^+. A lot of studies were done on the interaction of At^+ with one or two halides; 1:1 and 1:2 binary dihalogen and even a ternary trihalogen species have been observed. It would be interested to complete the work

with AtO^+. The reactions between AtO^+ and Br^-/Cl^- were already studied by Champion *et al.* and 1:1 and 1:2 complexes were proposed.[4] However, the interaction between AtO^+ and I^- is never reported so far. According to the Pourbaix diagram of iodine, in oxidative acidic aqueous solution, besides I^-, two more species, I_2 and $I_2(OH)^-$, may appear. This makes the system more complicated to investigate. Thus, the experimental condition to study the interaction of AtO^+ with I^- would be extremely restricted. A proper oxidant should be notably found to control the potential of the solution between 0.75-0.80 V *vs* NHE, in order to limit the presence of oxidizing forms of iodine.

3) Since the first halogen-bonded adducts involving the At element has been reported in the previous work, it is important to complete the theoretical calculation on the bound species. This is the subject of ongoing researches, aiming at (i) obtaining the geometries of the adducts and (ii) calculate the equilibrium constants in order to compare them with the experimental ones.

   In the IAt⋯B adduct, Lewis base is expected to interact with astatine atom that presents the strongest "electrophilic interacting site". As shown in Chapter 4, in AtI species, I atom has the halogen-binding possibility as well, with a weaker electrophilic interacting site. One can imagine that when a strong Lewis base is in high concentrations, besides the interaction with At, a second one could occur on the other side with iodine to form a 1:2 B⋯IAt⋯B complex. Such a possibility deserves to be studied/explored.

   Finally, the halogen-bonding between AtX (X=Br and Cl) and Lewis bases is proposed to be stronger than AtI.[5] Thus, the interaction between AtX and Lewis bases can be pursued with X=Br and Cl.

References

(1) Lee, S. H.; Rasaiah, J. C. *J. Phys. Chem.* **1996**, *100* (4), 1420.

(2) Shannon, R. D. *Acta Crystallogr. Sect. A* **1976**, *32* (5), 751.

(3) Sergentu, D. C.; Teze, D.; Sabatié-Gogova, A.; Alliot, C.; Guo, N.; Bassal, F.; Silva, I. Da; Deniaud, D.; Maurice, R.; Champion, J.; Galland, N.; Montavon, G. *Chem. - A Eur. J.* **2016**, *22* (9), 2964.

(4) Champion, J.; Seydou, M.; Sabatié-Gogova, A.; Renault, E.; Montavon, G.; Galland, N. *Phys. Chem. Chem. Phys.* **2011**, *13* (33), 14984.

(5) Hill, J. G.; Hu, X. *Chem. - A Eur. J.* **2013**, *19* (11), 3620.

UNIVERSITE BRETAGNE LOIRE

UNIVERSITÉ DE NANTES

Thèse de Doctorat

Ning GUO

Exploration des propriétés de l'astate aux degrés d'oxydation +I et –I en phase aqueuse

Investigation of the chemical properties of astatine at +I and –I oxydation states in aqueous solution

Résumé

La thérapie alpha ciblée est une technique prometteuse pour le traitement de cancers. L'astate-211, de temps de demi-vie de 7,21 h, est considéré comme un candidat prometteur pour cette application. Une condition pré-requise est de fixer de manière stable l'isotope radioactif sur le vecteur qui va servir à reconnaitre les cellules malades. Ceci demande une connaissance approfondie des propriétés chimiques de l'astate. Compte tenu de sa position dans le tableau périodique des éléments, l'astate peut exister sous la forme At^- en cohérence avec les propriétés chimiques des autres halogènes, et possède aussi un caractère plus métallique qui explique l'existence d'espèces cationiques stables. L'objectif de cette thèse est d'identifier et d'étudier les propriétés des différentes espèces de l'astate en solution aqueuse. La prédominance de l'espèce At^- en milieu acide réducteur a été confirmée au moyen d'une technique d'électromobilité. Une première valeur de mobilité absolue est ainsi proposée. En milieu plus oxydant, l'espèce At^+ domine. La réactivité de cette espèce avec les ions de la série des halogènes a été étudiée/quantifiée. Une espèce exotique $IAtBr^-$ a notamment été mise en évidence grâce à l'aide d'outils de modélisation moléculaire. La particularité du compound AtI à former des liaisons de type halogène a été montrée pour la première fois.

Mots clés
Astate spéciation, liaison halogène

Abstract

Targeted alpha therapy is an appealing method for the treatment of cancer as a complement to the current approaches. Astatine-211, with a half-life of 7.21 h, is considered as an exciting prospective candidate for this application. A pre-required condition is to fix in a stable way the radioactive isotope to the vector that is going to serve to recognize cells. This asks for a thorough knowledge of the chemical properties of astatine. Considering its position in the periodic table, it can exist under the form At^- in coherence with the chemical properties of the other halogens, and also possesses a more metallic character that explains the existence of stable cationic species. The objective in this work is to identify the properties of different At species in aqueous solution. The predominance of the species At^- in reducing acidic conditions was confirmed by means of a technique of electromobility. A first value of absolute mobility is then proposed. In more oxidizing conditions, the species At^+ dominates. The reactivity of this species with the ions of the halogens series was studied/quantified. An exotic species $IAtBr^-$ was highlighted in particular thanks to the help of modeling tools. The peculiarity of the compound AtI to form halogen-type bonds was shown for the first time.

Key Words
Astatine, speciation, halogen bond